Dissertation
submitted to the
Combined Faculties for the Natural Sciences and for Mathematics
of the Ruperto-Carola University of Heidelberg, Germany
for the degree of
Doctor of Natural Sciences

presented by
Aastha Mathur
born in Jaipur, India

Oral examination: 19th of April 2016

Role of cytoskeleton in morphological changes of blood platelets

Referees:

Dr. Péter Lénárt, EMBL Heidelberg

Prof. Dr. Ulrich Schwarz, University of Heidelberg

उद्यमेन हि सिध्यन्ति कार्याणि न मनोरथैः ।
न हि सुप्तस्य सिंहस्य प्रविशन्ति मुखे मृगाः ।।

Acknowledgements

Over a period of four years (plus a month and 18 days), I have had the chance to be surrounded by some extraordinary individuals that have made a huge impact on my scientific research, my scientific aspirations and me.

I would like to start by thanking, François Nédélec, for giving me the opportunity to carry out my research in his lab. He has been a very patient teacher who taught me that doing great science could be great fun. I learnt from him the importance of critical thinking, jokes in a presentation, physicsy stuff and a good red wine (I don't have to mention it because it is obviously French). A critical role in ensuring the timely progress of my research was played by my TAC members: Péter Lénárt, Ulrich Schwarz and Edward Lemke. I would like to thank them for their valuable input at different stages of this project. A special mention to my defense examiners: Ursula Kummer and Darren Gilmour, who have shown interest and support in my scientific progress.

The diverse technologies that went into shaping this project gave me an opportunity to interact with many people who have been a pleasure to work with. I would thank you all: Romain Gibeaux, for data, support and Berkeley tours; Tooba Quidwai and Jonas Ries, for the super super resolution; Sandra "Fairy Godmother" Correia for doing exactly what fairy godmothers do; Serge Dmitrieff aka SergyD for staring at the plots with me; Iana Kalinina, for chips, chats and scientific wisdom; Klaus Schmitt und dem ganzen LAR, einen herzlichen Dank für Sie; Jean-Leon Maître, for advice and sparing some mice; ALMF, with great scopes comes great support. I would also like to thank Karin Sadoul for introducing me to the world of platelets.

This brings me to an amazing bunch of people that I have had a chance to work with over the years in our lab. I would like to thank them for being very supportive: Kasia, for the advice and timely gossips, Karin, for being the cool geek, Celine, Hervé, Julio, Jon, Antonio, and André. I would also like to thank my surrogate lab members: Johanna, for insightful scientific deliberations and cakes; Philippe, for the drugs; Masha, for making sure I have a good morning; Joana, for the daily dose of crazy and elephants; Natalia, for literally everything.

Being at EMBL has been a valuable experience and I have lots of people to thank for that. I would like to thank them for their constant support: Simone and Leo, for homely atmosphere; Thibaut, for being there foamy; Marvin, for food for thought; Eva, for being so cute and awesome; Mie, for the late night company; Gustavo

QGdM, for the brunches; Deepikaaaaa, The Paul, Sarah, Julian, Markus, Thomas. Big thanks for the support from outside EMBL: Ruth and Barbara. Some people are always there when you need, even if they live miles apart. I would like to thank Rounak and Ritika for being that person.

Finally, I would like to thank people without whom none of this would have been possible. Thanks Mom, Dad, Juju and Naren ☺

Zusammenfassung

Thrombozyten sind ein wichtiger Blutbestandteil, durch ihre Rolle in der Aufrechterhaltung der Hämostase. Sie entstehen aus großen, im Knochenmark befindlichen Zellen, sogenannten Megakaryozyten, welche schlauchförmige Fortsätze in die Blutbahn entsenden. Diese Fortsätze fragmentieren und bilden im Ergebnis die 2 bis 3 µm großen, kernfreien diskussförmigen Thrombozyten. Die Aktivierung der Thrombozyten erfolgt durch Signalstoffe, die nach Verletzung des Epithels in die Blutbahn freigesetzt werden, und verursacht eine Reihe spezifischer Formveränderungen der Thrombozyten von diskussförmig zu kugelförmig zu dendritisch und endet in einer ausgebreiteten Form, welche einer Voraussetzung für die Bildung eines Blutgerinsels darstellt. Trotz ihrer einfachen Architektur ist es den Thrombozyten durch ein Repertoire an Zytoskelettproteinen möglich ihre Morphologie drastisch zu verändern. Microtubuli, welche ein Bündel entlang der Thrombozyten-Periphärie bilden, spielen eine entscheidende Rolle in der Erhaltung der ruhenden Diskusform, während Aktin hauptsächlich in den späteren Stadien bei der Adhäsion wichtig ist. Im ersten Schritt der Thromboyztenaktivierung windet sich das aus Mikrotubuli bestehende Randband und es kommt zu einer Formveränderung des Thrombozyten von diskussförmig zu kugelförmig. Sowohl Aktin als auch Mikrotubuli sind in diesem Prozess von Bedeutung, aber die Mechanik der Formveränderung ist nicht gut erforscht.

Das im folgenden beschriebene Projekt wurde durchgeführt, um die Rolle der Mechanik des Zytoskeletts während der Aktivierung der Thrombozyten zu erforschen. Eine Kombination aus experimentellen und analytischen Techniken wurde verwendet, um die mechanischen Eigenschaften des Systems, sowohl im Ruhezustand, als auch während der Aktivierung, durch direkte Vermessung der Morphologie des Randbandes quantitiativ zu ermitteln. Die Struktur und Zusammensetzung des Randbandes wurden mit Hilfe von Elektronentomographie ermittelt, wodurch detailierte Informationen über einzelne Mikrotubuli zugänglich wurden. Hoch auflösende Superresolutionsmikroskopie wurde ebenfalls verwendet um die Gesamtmorphologie und Zusammensetzung des Ranbandes zu erfassen. Mit Hilfe dieser Daten konnten die mechanischen Eigenschaften des ruhenden Randbandes in fixierten Thrombozyten erschlossen werden. Die Dynamik des Windungsprozesses des Randbandes wurde unter Verwendung von Fluoreszenzmikroskopie an lebenden Zellen in einem Mikrofluidik-System analysiert.

Mit diesem System können Veränderung der Form des Randbandes als Folge einer Behandlung mit Agonisten oder Inhibitorien, welche das Zytoskelett in einem Prozess analog zur mechanischen Störung der Thrombozyten beeinflussen, verfolgt werden. Eine große Anzahl von Thrombozyten wurde analysiert um die intrinsische Variabilität der mechanischen Eigenschaften des Randbandes zu ermitteln. Die Software *Cytosim* wurde verwendet um den Windungsprozess des Randbandes zu simulieren.

Durch diese vielseitige Herangehensweise ist es uns möglich neue Erkenntnisse über die Mechanik des Windungsprozess des Randbandes zu gewinnen. Erstens können wir beweisen, dass die Längen der Mikrotubuli eines ruhenden Thrombozyten exponentiell verteilt sind. Die Summe aller Mikrotubuli beträgt 101.84µm ±12.63 je Thrombozyt. Der normale Abstand zwischen zwei Mikrotubuli beträgt im sehr eng gepackten Randband 30 nm. Zweitens können wir durch die Messung der Dynamik des Windungsprozess erschließen, dass sich das Randband bei Aktivierung mit ADP wie ein visco-elestiascher Ring verhält. Diese Reaktion ist von Aktin abhängig, während eine Aktivierung mittels Thrombin aktinunabhängig ist. Die Analyse einer großen Anzahl von Thrombozyten zeigt, dass sich die Intensität des Tubulin-Signales maßstäblich zum Radius des Thrombozyten zur fünften Potenz verhält, was auf eine mögliche Anreicherung von Tubulin in Thrombozyten hinweißt. Schließlich suggerieren unsere Daten das Thrombozyten mit einem längeren Randband eine höhere Tendenz zum Windungsprozess aufweisen.

Obwohl einige unserer Ergebnisse durch weitere Experimente vervollständigt werden müssen, gibt diese Untersuchung einen experimentellen und analytischen Rahmen welcher es uns erlaubt die Morphologie des Thrombozytenzytoskellets quantitativ zu analysieren, mit dem Ziel die Mechanik der Thrombozytenaktivierung in gesunden wie auch im Krankheitszustand zu verstehen.

Table of Contents

Abbreviations

ACD	Acid-citrate-dextrose
ADP	Adenosine Diphosphate
AMP	Adenosine Monophosphate
ATA	Aurintricarboxylic Acid
ATP	Adenosine Triphosphate
DAG	Diacylglycerol
distFit	Error in Fitting
EMBL	European Molecular Biology Laboratory
GA	Glutaraldehyde
GDP	Guanosine Diphosphate
GFP	Green Fluorescence Protein
GPCRs	G-protein coupled receptors
GTP	Guanosine Triphosphate
IP3	Inositol 1,4,5-trisphosphate
Lmb	Length of the Marginal Band
MAPs	Microtubule Associated Proteins
MIP	Maximum Intensity Z-projected
MT	Microtubules
MYH9	Non Muscle Myosin Heavy Chain 9
MYH9-RD	MYH9 related disorders
NA	Numerical Aperture
OOPness	Out of Planeness
PAR	Protease-activated Receptor
PBS	Phosphate-buffered Saline
PCA	Principal Component Analysis
PDMS	Polydimethylsiloxane
PEG	Poly Ethylene Glycol
PI-3-K	Phosphoinositide-3-kinase
PIP2	Phosphatidylinositol 4,5-bisphosphate
PIP3	Phosphatidylinositol 3,4,5-trisphosphate
PKC,	Protein Kinase C
PLC	Phospholipase C
pll	Poly-l-lysine
PRP	Platelet-rich Plasma
nC-TAB	Tyrode's Albumin Buffer without Calcium
TP	Thromboxane Receptor
TxA2	thromboxane A2
P2Y1/P2Y12	Purinergic Receptors
RhoGEF Rho	Guanine Nucleotide Exchange Factor
ROCK	Rho-associated Protein Kinase

Summary

Platelets are an important component of blood that help maintain haemostasis. They are derived from large bone marrow residents, called megakaryocytes, which release tubular processes into the blood stream that fragment and eventually form 2 to 3 μm sized enucleate discoid platelets. Activation of platelets is caused by factors released into the bloodstream upon endothelial damage, to which they respond by undergoing a distinct order of shape transition, from discoid, to spheroid, to dendritic, and finally an extended morphology, required to form a clot. Despite the simple architecture, platelets are able to drastically alter their morphology owing to the repertoire of cytoskeletal proteins they express. Microtubules, which form a bundle running along the platelet periphery, are known to be important for maintaining the resting discoid morphology of a platelet, while actin is heavily implicated in the later stages that require adhesion. During the first step of platelet activation, the microtubule marginal band undergoes coiling, while the platelet changes from a disc to a sphere shape. Both actin and microtubules are implicated in this process but the mechanics of the process are not clearly understood.

The following project has been carried out to explore the role of cytoskeletal mechanics in triggering activation of a platelet. A combination of experimental and analysis techniques was used to quantitatively assess mechanical properties of the system in a resting state, as well as during activation, by direct measurement of the marginal band morphology. The structure and composition of the marginal band was analyzed using electron tomography, which provided detailed information on individual microtubules. Super-resolution microscopy was also used to visualize the overall morphology and composition of the marginal band. With this data we could infer the mechanical properties of the resting marginal band in fixed platelets. To analyze the dynamics of coiling process, live cell fluorescence microscopy was used in combination with a microfluidic system. With this setup, changes in the marginal band shape could be followed in response to treatment with agonists or inhibitors that affect the cytoskeleton, that is, a process analogous to mechanical perturbations of the platelet. A large population of platelets was also analyzed to infer the intrinsic variations mechanical properties of the marginal band. The *Cytosim* software was used to set up simulation of marginal band coiling.

By using a multifaceted approach, we were able to get novel insight into the mechanics of marginal band coiling. Firstly, we showed that length distribution of microtubules in a set of resting platelet marginal bands follows an exponential

distribution. The sum of all polymerized microtubule length was found to be 101.84µm ±12.63 per platelet. The typical distance between two microtubules was found to be 30nm in a tightly packed marginal band. Secondly, by measuring the dynamics of coiling, we could infer that the marginal band behaves like a visco-elastic ring upon activation with ADP. This response was found to be dependent on actin, while thrombin activation elicited a response that manifested in an actin independent manner. Analysis of large population of platelets showed that the tubulin intensity scales as a power of five to the platelet radius, indicating a possible enrichment of tubulin in platelets. Finally, our data suggests that platelets with longer marginal bands have a higher propensity to coil.

Although some of our results need to be followed up with further investigations, this study provides an experimental and analysis framework that allows us to quantitatively analyze platelet cytoskeleton morphology with an aim to understand the mechanics of platelet activation in healthy and disease states.

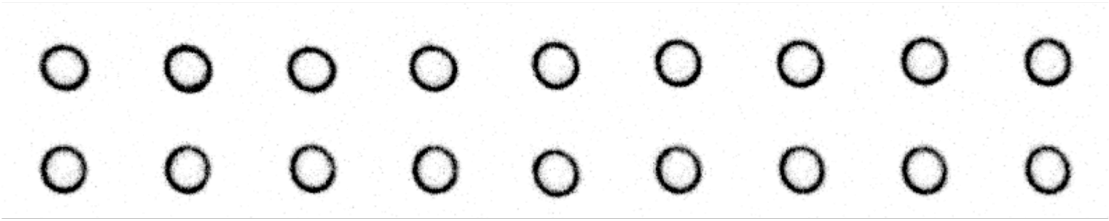

Chapter 1

Introduction

1 Introduction

1.1 Cell morphology and cytoskeleton

In nature, we find cells that differ from each other over an enormous range of shapes and sizes. Already within the bacterial kingdom, while an average spherical bacterium measures around 1µm in diameter, the diversity in size spans over six orders of magnitude. Cells also exhibit an endless variety in terms of shapes. Protista are single celled eukaryotes that show incredibly intricate morphologies and many specialized cellular structures. In multicellular organisms, subsets of cells adopt different morphologies as they undergo differentiation. For example, red blood cells lose their nucleus to adopt a simpler morphology while neurons branch to form complex networks of dendrites.

Morphology of a cell is often found to be its characteristic and is, in many cases, known to provide a functional advantage. It is, however, the mechanical properties of the cell and those of its environment that determine its shape. Bacterial and plant cells have a rigid cell wall that helps them maintain their morphology while the shape of a mammalian cell, bound by a plasma membrane, is often dependent on the mechanical microenvironment. The functional relevance of cell shape leads to the idea that a cell might be able modify its mechanical properties and change its morphology to perform a certain function. Cells undergoing mitosis exemplify this, as they become stiffer by manipulating their osmotic pressure and hence rounding up to facilitate chromosome collection by the spindle (Stewart et al. 2011). Certain cancer cells are also known to exhibit altered stiffness which is correlated with their metastatic potential (Swaminathan et al. 2011). Thus maintenance and modification of cellular mechanical properties can be considered a hallmark of physiological as well as diseased states. Another interesting aspect of morphological changes is the timescale at which they occur. While some cells like neurons, once differentiated can maintain their complex morphology as long as the life span of the organism itself, others like platelets undergo drastic changes in morphology over tens of seconds. Such complex transformations of cells call for a control mechanism that is highly dynamic yet capable of maintaining robust structures.

Cytoskeleton is the critical cellular component for determining the morphology of a cell. It is also one of its most dynamic toolboxes for processes that require change over a large range of time scales. Thus, the structure and properties of the underlying cytoskeleton control various properties of a cell. For example, a frog egg has a contractile cortical cytoskeleton that keeps it in its unique spherical shape. This cellular scaffold also possesses an ability to maintain structures over long time

periods. For example, in human oocytes, the spindle structure is maintained over years, while the individual cytoskeletal components turnover dynamically. On the other hand, fast dynamics of cytoskeleton can also enable it to mediate changes that occur at short time scales, like contraction of a skeletal muscle that occurs over milliseconds time scale or constantly remodeling actin cortex at the leading edge of a migrating cell. The following section will elaborate on the properties of cytoskeleton that enable such diverse functions and will lead into the further section on such morphological changes in platelets.

1.2 Cytoskeleton mechanics

Morphology of a living cell is heavily dependent on its cytoskeleton. Whether a cell is static, migratory, dividing, or undergoing shape transitions, the cytoskeleton maintains and helps mediate the modifications in the cellular morphology to allow cells adapt to a specific task. It is important to note that the cytoskeleton itself is an assembly of polymers, which, even though, is capable of displaying very interesting properties, like self-assembly, nematic ordering etc. *in vitro*, in a biological context it often needs to associate with accessory proteins to form structures that are complex, dynamic and robust. I would like to introduce in detail the two major components of cytoskeleton: microtubules (MTs) and actin. In the following sections, I would glance over their mechanical properties and describe some of the accessory proteins associated with them.

1.2.1 Microtubules

Microtubules are rigid cytoskeletal structures that are often associated with processes like intra-cellular transport, cilia and flagella based cell motility, cell division, etc. These tubular structures have a persistence length of 1.4 ±0.3mm (van Mameren et al. 2009), which makes them effectively a stiff rod over various cellular length scales. Their structure and properties are described below.

1.2.1.1 Microtubule structure and dynamics

Microtubules are non-covalent polymers comprising of repeating heterodimeric subunits of alpha and beta tubulin. These subunits, which measure approximately 8nm longitudinally, bind together in parallel in an alpha to beta tubulin orientation forming a tubular structure of 25nm diameter with around 13 protofilaments (AMOS & Klug 1974). Such composition imparts an inherent polarity to these filaments. In addition to the structural differences, the MT ends show different growth kinetics based on which the more dynamic end is referred to as the plus and less dynamic as the minus end. The tubulin subunit, before incorporation into the polymer, is

attached to a guanosine triphosphate (GTP) molecule that hydrolyzes to guanosine diphosphate (GDP) after addition, making it more likely to disassociate from the filament. At the MT plus end, fast polymerization rates lead to formation of a GTP cap that promotes a growth regime, but loss of which can expose GDP-tubulin causing the MTs to undergo rapid depolymerization through an event called catastrophe. This process where single MTs can experience both a slow growth and a fast shrinkage, is called dynamic instability (figure 1.1) (Mitchison & Kirschner 1984). Stabilization of the plus end with a new GTP cap could, in certain cases, resume a growth regime through an event called rescue. A population of dynamically instable MTs within a bounded growth regime (Dogterom & Leibler 1993), has a steady state length distribution that follows a decaying exponential (Karsenti et al. 2006). The growth kinetics and mechanical properties of MTs can be regulated by various accessory proteins, some of which are described below (figure 1.2).

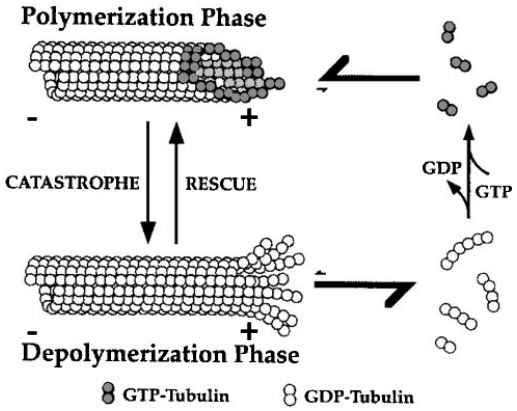

Figure 1.1: Dynamic instability in microtubules. A population characterized by simultaneous presence of growing and shrinking MTs. Tubulin is added to the polymerizing MT in the GTP form, which subsequently hydrolyzes creating a GTP tubulin cap and a GDP tubulin MT lattice. Infrequent loss of GTP cap leads to rapid MT depolymerization (catastrophe). Depolymerizing MTs can reform a GTP cap transitioning back to the polymerization phase by another infrequent process called rescue. Adapted from: **(Desai & Mitchison 1997)**.

1.2.1.2 Microtubule associated proteins

Although tubulin has the ability to self–assemble; spontaneous nucleation of MT assembly is rare *in vivo*. In cells, this process is mediated by nucleator proteins that overcome the lag phase in MT growth enabling fast dynamics. One such example is the gamma-tubulin protein that forms a ring shaped complex (gamma-tubulin ring complex) with other proteins and provides MTs with a template to polymerize on (Zheng et al. 1995) (Kollman et al. 2011). Due to the structural and biochemical differences between the plus end, the minus end, and the lattice, various MT

associated proteins (MAPs) get partitioned along its length and carry out their specific functionalities. Members of a class of proteins called the end binding proteins (EB1, EB2 and EB3) accumulate at the growing plus end of a MT due to its structural features and are known to affect the growth dynamics (Gouveia & Akhmanova 2010). They are often used as a plus end marker. In contrast to the multitude of plus end binding proteins, only very few minus end markers for MTs have been described. Patronin or CAMSAP is one such protein that, first described in 2010 (Goodwin & Vale 2010), has been characterized to stabilize the MT minus end (Yau et al. 2014). Another category of proteins is known to bind MT lattice and carry out functions like stabilization, severing, cross-linking etc. MAP2 and tau are two proteins that induce bundling of MTs (Chen et al. 1992), but result in MT bundles of different architecture. While tau packs MTs in tight bundle with a MT wall-to-wall distance of 26.4±9.5nm, MAP2 results in an average distance of 63.9±10.1nm giving rise to a relatively loosely packed bundle. The nature of packing would have implications on the deformability of a bundle indicating that accessory proteins can affect the mechanical properties of MT structures. Certain proteins, on the other hand, have the ability to affect MT dynamics without directly binding to them. Stathmin is a small protein that binds two tubulin heterodimers reducing the effective tubulin concentration. Such sequestration of tubulin subunits affects the dynamic instability of MTs pushing them towards a shrinking state (Steinmetz et al. 2000). In addition to proteins, small molecules can also affect MT dynamics and are often used to perturb the cytoskeleton. Taxol is a drug that binds along the MT filaments and stabilizes them by preventing depolymerization. It also reduces the stiffness of a MT (Venier et al. 1994). Nocodazole and colchicine are chemicals that induce MT depolymerization by binding the tubulin subunits and capping the MT ends respectively.

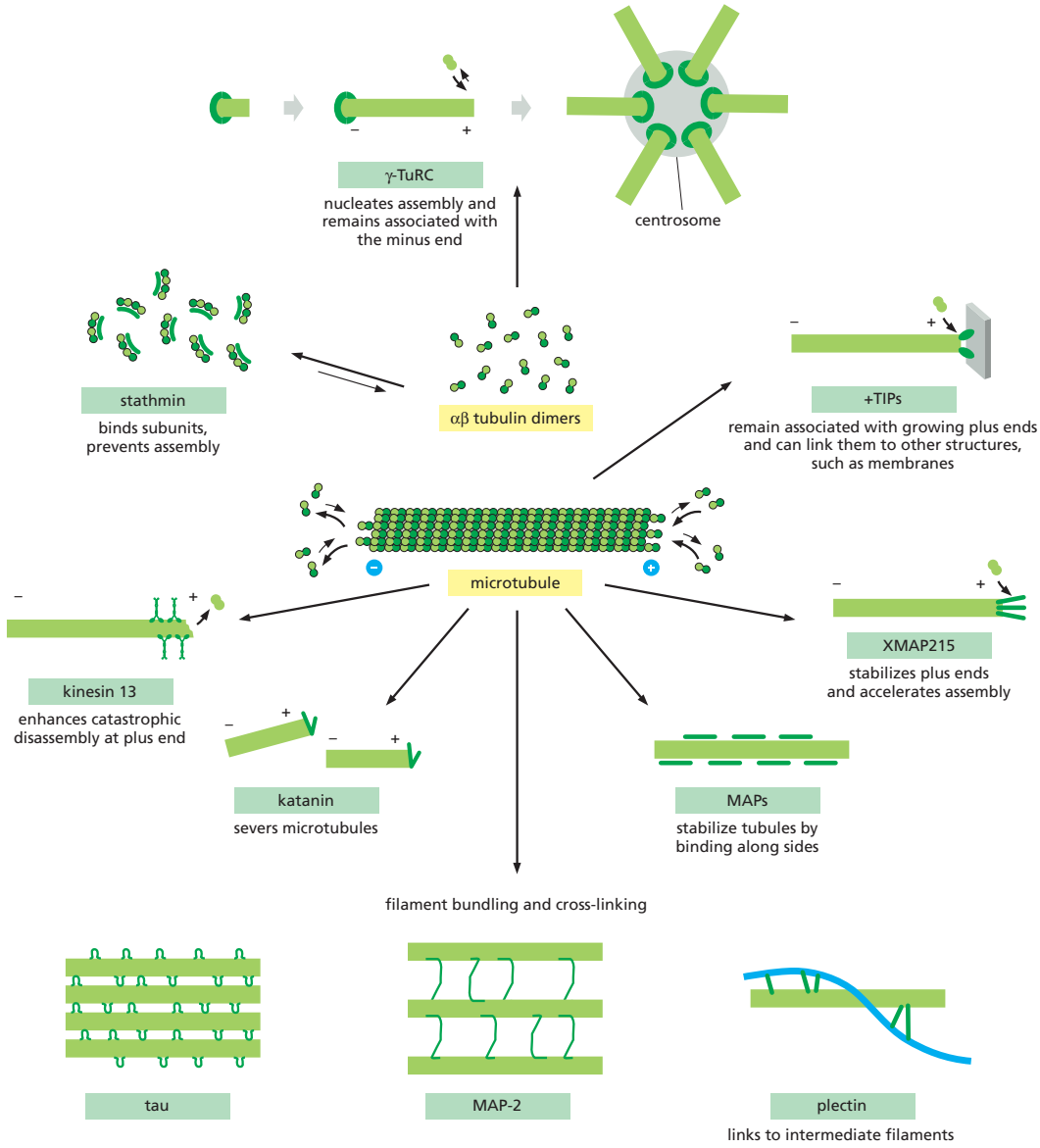

Figure 1.2: Microtubule associated accessory proteins.
Source: Panel 16-3 Molecular Biology of the Cell 5th Ed. (©Garland Science 2008)

1.2.1.3 Microtubule motors

Molecular motors are a class of proteins that can convert chemical energy, usually from hydrolysis of adenosine triphosphate (ATP), to mechanical energy. A variety of these proteins associate with cytoskeleton to help carry out functions like cargo transport, cell locomotion, cell division, etc. The motor proteins associated with MTs can be divided into two main families: kinesin, which are plus-end or minus-end directed motors, and dynein, which are minus end directed motors (Skoufias & Scholey 1993). These motors, which are capable of attaching different kinds of cargos to the MTs, in some cases cross-link two MTs themselves. This property, in presence of an anti-parallel overlap between MTs, allows these motors to slide the

MT relative to each other (figure 1.3 (A)). A tetrameric kinesin 5 motor, Eg5, slides MTs apart during chromosome segregation (Kapitein et al. 2008). Kinesin-1, which has a second MT binding domain, is also capable of sliding MTs apart to drive cell shape changes (Jolly et al. 2010) (figure 1.3 (B)). Sliding motion of opposite directionality can be generated by cytoplasmic dynein, where two motor domains can simultaneously bind two different MTs (Tanenbaum et al. 2013) (figure 1.3 (C)). Such sliding behavior of dynein has recently been implicated in driving active contractions in microtubule networks (Foster et al. 2015).

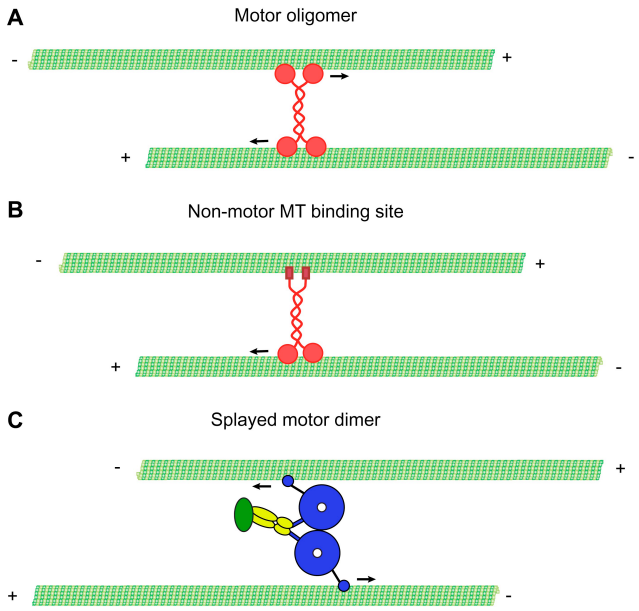

Figure 1.3: Microtubule sliding by molecular motors. Microtubules are arranged in an anti-parallel fashion. **(A)** Tetrameric kinesin-5, plus-end directed, motor cross-linking MTs with opposing motor domains. **(B)** Kinesin-1 or kinesin-14 attaching one MT with an MT binding domain while walking on the other. **(C)** Cytoplasmic dynein splays its motor domains to bind two MTs at the same time. Source: **(Tanenbaum et al. 2013)**.

1.2.2 Actin

Actin is a versatile cytoskeletal protein that is known to play a role in a multitude of cellular processes like muscle contraction, cell motility, maintaining cell morphology, mechanosensing, etc. The persistence length of actin filaments is 17 ±4µm (van Mameren et al. 2009), which makes it pliable at cellular length scales. By association with a plethora of actin binding proteins, it is capable of forming dynamic structures, like filopodia, lamellipodia, cell cortex, stress fibers, etc., that fulfill the diverse functions.

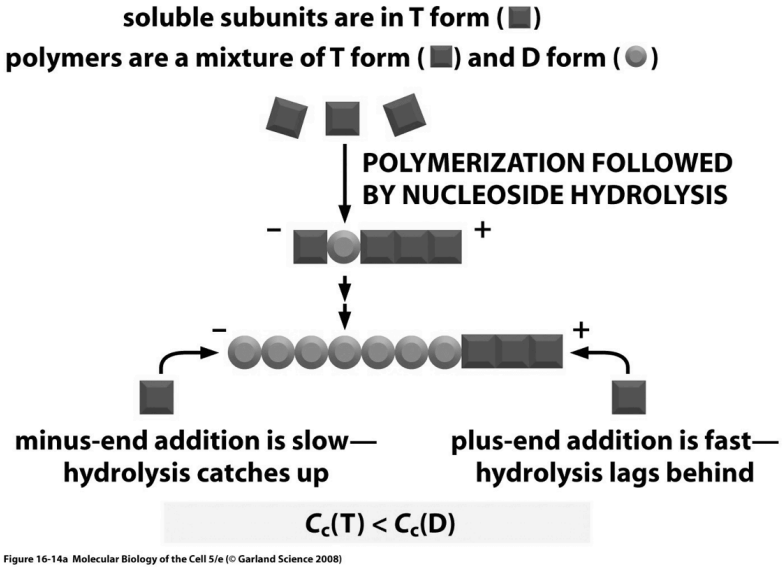

Figure 1.4: Treadmilling of actin. T-form is the ATP bound subunit. D-form is the ADP bound subunit. In this description, filament ends up with a T-form plus end and D-form minus end. $C_c(T)$: critical concentration for T form addition. $C_c(D)$ critical concentration for D form addition. Treadmilling occurs when soluble subunit concentration C is $C_c(T)<C<C_c(D)$. Source: Figure 16-14a Molecular Biology of the Cell 5th Ed. (©Garland Science 2008).

1.2.2.1 Actin structure and dynamics

The polymeric from of actin, called F-actin (filamentous actin), is composed of a single repeating monomeric unit called g-actin (globular actin). The g-actin subunits bind each other in a head-to-tail orientation creating a 7nm thick filament with a helical twist (Holmes et al. 1990) (Kabsch et al. 1990). The structural polarity of actin filament manifests a biochemical difference between the plus end, which undergoes fast kinetics, and the minus ends, which undergoes slower kinetics, in a polymerized filament. From a pool of actin monomers, ATP bound subunits can be added to either of the polymer ends. Once in the filamentous form, the subunits hydrolyze the bound ATP followed by phosphate dissociation, of which the latter is a slow process. Due to the slow kinetics at the minus end, it is usually in the adenosine diphosphate (ADP) form and growth mainly takes place from the plus end causing a disparity in critical concentrations for monomer addition on either ends. If the monomer concentration is more than the critical concentration at the ATP form plus end, and less than the critical concentration at the ADP form minus end, treadmilling ensues, where the plus end grows while the minus end shrinks (figure 1.4) (Wegner 1976) (Pollard 1986). This phenomenon causes apparent filament displacement. In vivo, many actin-associated proteins control dynamics of actin growth and mediate its reorganization.

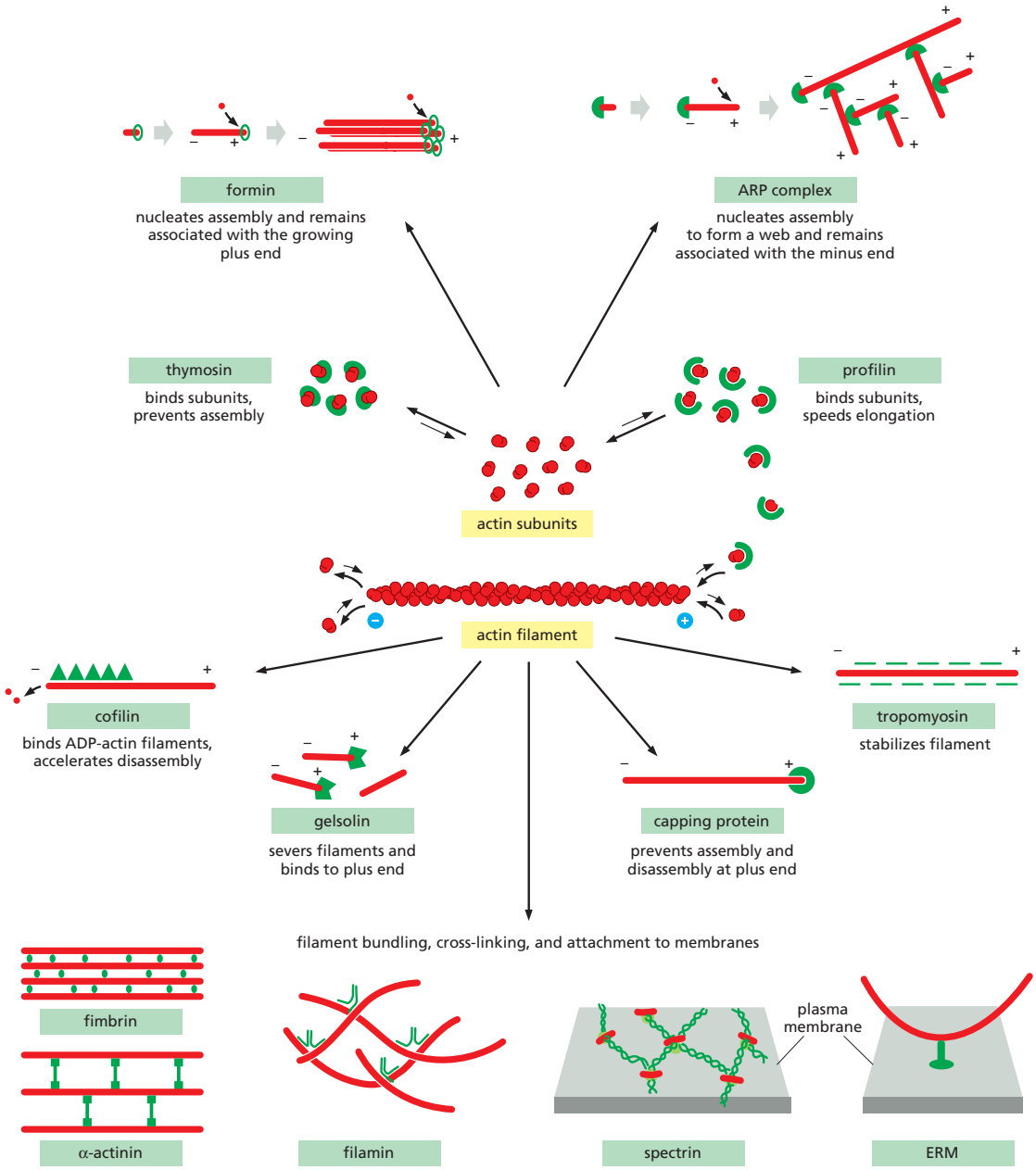

Figure 1.5: Actin associated accessory proteins.
Source: Panel 16-3 Molecular Biology of the Cell 5th Ed. (©Garland Science 2008)

1.2.2.2 Actin associated proteins

An important factor that makes actin a highly versatile cytoskeletal component is the repertoire of accessory proteins it can associate with (figure 1.5). Like for microtubules, nucleation of actin in cells is often regulated by nucleator proteins like Apr2/3, which polymerizes branched actin networks (Heuser & Pollard 1998), and formin, which polymerizes parallel actin bundles from plus end (Pruyne 2002), to generate and maintain fast growing actin filaments. Another method for mediating

growth dynamics is by interacting with unpolymerized monomers. Thymosin sequesters monomers reducing the available poymerizable actin pool, while profilin binds monomers and promotes polymerization in limiting concentrations of soluble actin (Pantaloni & Carlier 1993). Converting one actin rich structure into another requires remodeling of the filaments. The actin severing protein, gelsolin, which is activated in presence of actin, achieves this feat by cutting the existing filaments to free up monomers that can be incorporated into the new structure (Bearer et al. 2002). Certain small molecules also affect actin filament growth and stability. Cytochalasin D is known to prevent actin polymerization by binding monomers, while phalloidin prevents filament depolymerization by preventing monomer dissociation (Cooper 1987) (Wakatsuki et al. 2001). Although a single actin filament is not very sturdy, multiple actin filaments can be packed into networks that have interesting emergent properties. Proteins like alpha-actinin bundle actin filaments in a parallel format, while filamin, often found in cortical cytoplasm, cross-links actin filaments in a three dimensional meshwork. Other proteins like spectrin are able to anchor an actin meshwork to the plasma membrane creating a rigid cortical layer of membrane bound cytoskeleton (Patel-Hett et al. 2011).

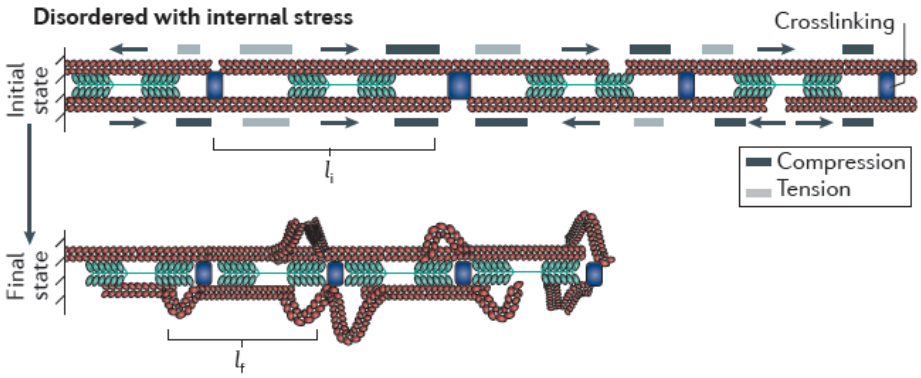

Figure 1.6: Contraction in disordered actomyosin networks. In presence of cross-linking molecules (blue), myosin (green) movement along actin (red) fibers results in regions of compressive and extensile stresses. The compressive stresses are relieved by filament buckling causing an overall compaction, which is dependent on the frequency of cross-linking. Source: **(Murrell et al. 2015)**

1.2.2.3 Actin motors

Actin and its associated motor myosin have long been known to drive muscle contraction in a sarcomeric arrangement (Huxley & Niedergerke 1954) (HUXLEY & HANSON 1954). However, in all the other non-muscle cells that lack the sarcomeric arrangement, a lot of actin functionality is still based on its ability to contract in association with the non-muscle myosin II protein. Actomyosin contractility is known

to drive various processes like cell division, cell migration, tissue morphogenesis, compaction of blood clot, etc., where actin forms a disordered network and is able to exert varying degree of contractile forces (figure 1.6). Even though myosin II is the motor that produces work by walking on the actin filaments and sliding them apart, a combination of proteins that cross-link filaments with each other or with other structures like membranes, are required to exert the contractile forces (Murrell et al. 2015). In certain cases, the disordered actin networks are able to generate forces even higher than striated muscles, as exemplified by platelets (Schwarz Henriques et al. 2012).

1.3 Platelets

After first being observed in early 1840s, platelets remained, for a long time, under much controversy over their identity, being considered as anything from an "organism" (Osler 1873), to developmental stage of red blood cells (Zimmerman, 1846. ref in Osler 1873), to merely an artifact. The presence of material implicated in clotting of blood was already established by T.W. Jones in 1851(Jones 1851), however, it was only several years later, in 1882, that Giulio Bizzozero demonstrated the role of platelets in haemostasis (Bizzozero 1882). Figure 1.7 illustrates his experiment on clotting in guinea pig, showing two clots on either side of an artery. Bizzozero had previously, in 1869, described the presence of megakaryocytes in the bone marrow, but it was only in 1906 that J.H. White made the connection between them by making smart use of what is known as the Wright's stain, which is still used today to distinguish different blood cell types (Coller 2013).

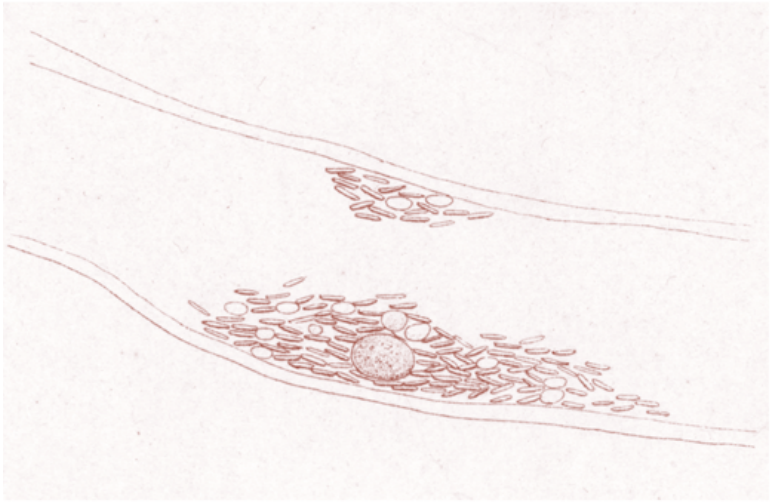

Figure 1.7: Bizzozero's figure of thrombi. Induced in an artery of a guinea pig. A white blood cell is seen among the platelet plaque. (Adapted from **(Mazzarello et al. 2001)**).

With further advances in technology, like the invention of electron microscope in early 1930s (Knoll & Ruska 1932), much was revealed about the structure and morphology of platelets, part of which I will cover under subsequent headings. In this section, I would first like to glance over evolution of platelets and clotting mechanisms. Then I will summarize the process of platelet formation and highlight the role of mechanics in the process. This will be followed by a description of platelet morphology and an introduction on the role cytoskeleton plays in shaping it. Finally I will present the current understanding about the role of cytoskeletal mechanics in first steps of platelet activation.

1.3.1 Evolution of platelets

The mechanism of clotting has existed in some capacity in all blooded organisms from primitive marine invertebrates to modern day mammals. The presence of polyploid megakaryocytes and their progeny of non-nucleated platelets is, however, an exclusively mammalian characteristic. For clarity, the non-mammalian counterparts of platelets are nucleated cells, referred to as thrombocytes. Many have hypothesized on evolution of platelets, but the specific advantage of existence of the megakaryocyte-platelet axis of haemostatic machinery remains to be elucidated.

It is noteworthy, that even though they are mainly associated with haemostasis, platelets exhibit rudimentary bactericidal (Zander & Klinger 2009) and phagocytic (Meseguer et al. 2002) activity, which indicates a possible functional overlap with inflammatory cells. In fact, many invertebrates that do not possess plasma based coagulation machinery, have multifunctional cells that are responsible for haemostasis as well as innate immunity. One such example is the, possibly ancestral, nucleated amoebocyte of *Limulus polyphemus,* or the horse-shoe crab, which fulfills all these functional aspects. More than 400 million years of evolutionary distance away from mammals, this lone surviving merostome has amoebocytes with not just functional, but morphological similarities to mammalian platelets. Figure 1.8 shows the ultrastructure of limulus amoebocyte, which contains different type of secretory granules as well as a marginal band composed of microtubules (figure 1.8(B)). In addition to the functional and morphological aspects, there are similarities in the process of dynamic remodeling of cytoskeletal components during activation of amoebocytes and platelets (Conrad et al. 2004). In both cell types, the marginal microtubule band coils and is retained in the cell interior whereas actin becomes peripheral.

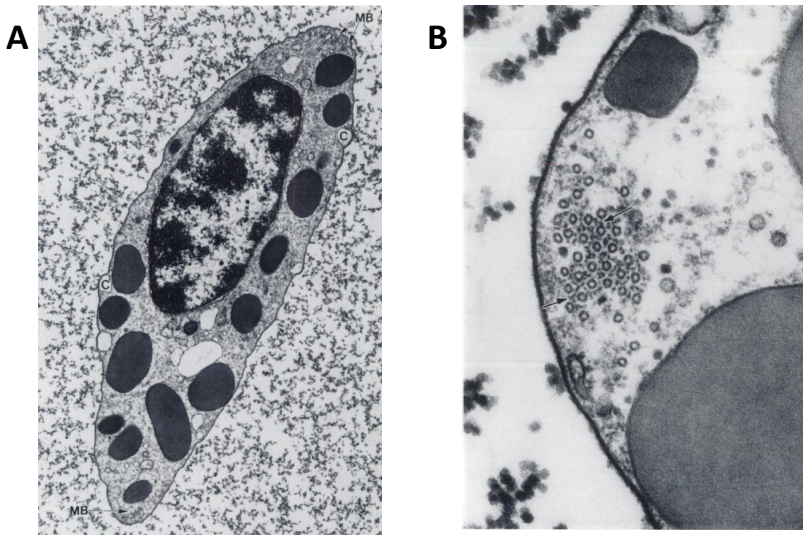

Figure 1.8: Electron micrograph of limulus amoebocyte. (A) Native discoid amoebocyte. **(B)** Higher magnification of marginal band cross-section. Arrows point to electron densities that might be microtubule associated proteins. Source: **(TABLIN & Levin 1988)**

Although they bear a striking parallel in terms of cellular functions, there exists no evolutionary trail linking platelets to their invertebrate equivalents. This could be because the connecting ancestral forms have been lost, or, as has been proposed (Ratcliffe & Millar 1988), a case of convergent evolution. Latter theory is supported by the presence of analogous cell surface receptors between human platelets and avian thrombocytes (Schmaier et al. 2011).

The enigmatic evolutionary appearance of platelets and polyploid megakaryocytes could be explained in the light of certain functional advantages. A major benefit of these cells is the ability of one megakaryocyte to produce thousands of platelets. Such a mechanism of biogenesis can, in case of a pathological challenge, be adapted to produce platelets that are larger (Stenberg & Levin 1989). The platelets produced under these exceptional conditions are also found to be more biologically active than the ones produced at steady state.

Platelets have also been shown to help establish early pregnancy by playing a role in placental attachment. This, however, cannot be considered an evolutionary advantage as both, monotremes (egg-laying mammals) and marsupials, possess platelets and megakaryocytes (Levin 2013). Thus, in absence of illustrative comparative genomic data, the evolution of platelets remains to be explained.

1.3.2 Biogenesis of platelets

Megakaryocytes are large (50-100μm diameter) polyploid cells that reside primarily in the bone marrow. These cells are highly specialized and are capable of undergoing drastic morphological reorganization to give rise to thousands of platelets at once. The unconventional morphology of megakaryocytes and platelets calls for specialized processes for their formation.

Derived from the hematopoietic stem cell lineage, megakaryocytes undergo polyploidization as a result of multiple endomitotic events, where the cellular DNA is duplicated but no physical division of the cell occurs. These cells can achieve between 4N to 64N complements of the genome, while majority of them undergo three endomitotic cycles (16N) (Italiano & Hartwig 2013). The high ploidy is a result of premature termination of mitosis. The cells have normal G1, S and G2 phases and also enter the M phase of cell division. They follow through with prophase, metaphase and anaphase A, but do not enter anaphase B wherein the chromatids are usually separated right before complete division. Cells having higher than 4N complement form a multipolar spherical spindle, which aligns chromosomes half way to the poles, segregates the chromatids but does not completely separate them (Vitrat et al. 1998). Nevertheless, the nuclear envelope reappears resulting in a single but lobbed nucleus. During the 2N to 4N duplication, the cytokinetic furrow is known to form and start ingression, but eventually regress leading to failed mitosis (Geddis et al. 2007). Further maturation of megakaryocytes involves cytoplasmic expansion followed by formation of the demarcation membrane system that provides excess membrane for platelet formation. The cells also accumulate proteins and granules that will be packed into platelets.

The most well supported theory of platelet release from megakaryocytes is the one that includes formation of intermediate proplatelets. These are millimeter long cytoplasmic threads connecting multiple platelet-sized swellings in the middle and similar bulges at the ends. They are said to be derived from the megakaryocyte demarcation membrane system (Schulze et al. 2006) and have been observed *in vitro* (Choi et al. 1995) and *in vivo* (Schmitt et al. 2001) to give rise to platelets (figure 1.9 (A)).

Once mature, the megakaryocytes start to form pseudopods at one end (figure 1.9 (B)). The pseudopods then elongate into to slender cytoplasmic tubes of uniform diameter (2-4μm). In a few hours, the whole cell unravels into thin processes that bend and branch to form an extensive network. These extensions are then released by a sudden retraction of the remaining cell body, giving rise to proplatelets (Italiano

et al. 1999). This morphologically complex process of proplatelet formation is highly dependent on the megakaryocytic cytoskeleton.

Microtubules (MTs) are essential for proplatelet extension (Radley & Hartshorn 1987). In an immature megakaryocyte, dynamic MTs emanate from the centrosome, localized at the cell centre, and end at the cortex. Once the cells form pseudopods, the MTs become cortically arranged and help extend the proplatelets. Depolymerization of MTs by nocodazole abrogates this process and results in retraction of proplatelet (Patel et al. 2005). The force for proplatelet extension is, however, not provided by MT polymerization, as shown by the effect of low doses of nocodazole that prevent MT growth but do not induce depolymerization. The extension is dependent rather on sliding of MTs against each other, a process driven by the molecular motor dynein (Patel et al. 2005) (Bender et al. 2015). In addition to propletelet extension, MTs are also responsible for transport of organelles and granules along the proplatelet shaft to the site of putative platelet formation. The materials are transported bidirectionally along the mixed polarity MT tracks by kinesin motors and get trapped in the bulges where the platelets form (Richardson et al. 2005). Passive mobilization of organelles also occurs due to MT sliding.

Actin, which is the major cytoskeletal constituent of platelets, is responsible for branching amplification of proplatelets. In absence of actin based forces, megakaryocytes only extend straight tubules that have few swellings, while the bending and kinking of proplatelets that leads to end amplification is prevented (Italiano et al. 1999). Furthermore, mutations in non-muscle myosin heavy chain (MYH9) of Myosin II A, an actin related molecular motor, cause a series of platelet disorders (Seri et al. 2000), like May-Hegglin anomaly, Epstein syndrome, or Fechtner syndrome, that result in thrombocytopenia. Spatio-temporally regulated myosin IIA activation is shown to regulate both the size as well as number of platelets (Spinler et al. 2015). During proplatelet extension, myosin IIA inactivation leads to low stiffness of the megakaryocytes as a result of which the released proplatelets are larger. However, once in the flow, these proplatelets need to reactivate their myosin IIA activity by shear stress to ensure a normal size of the final platelet. The latter process is inhibited in patients with MYH9 diseases and as a result, their platelet numbers are not significantly changed but the platelets are larger in size.

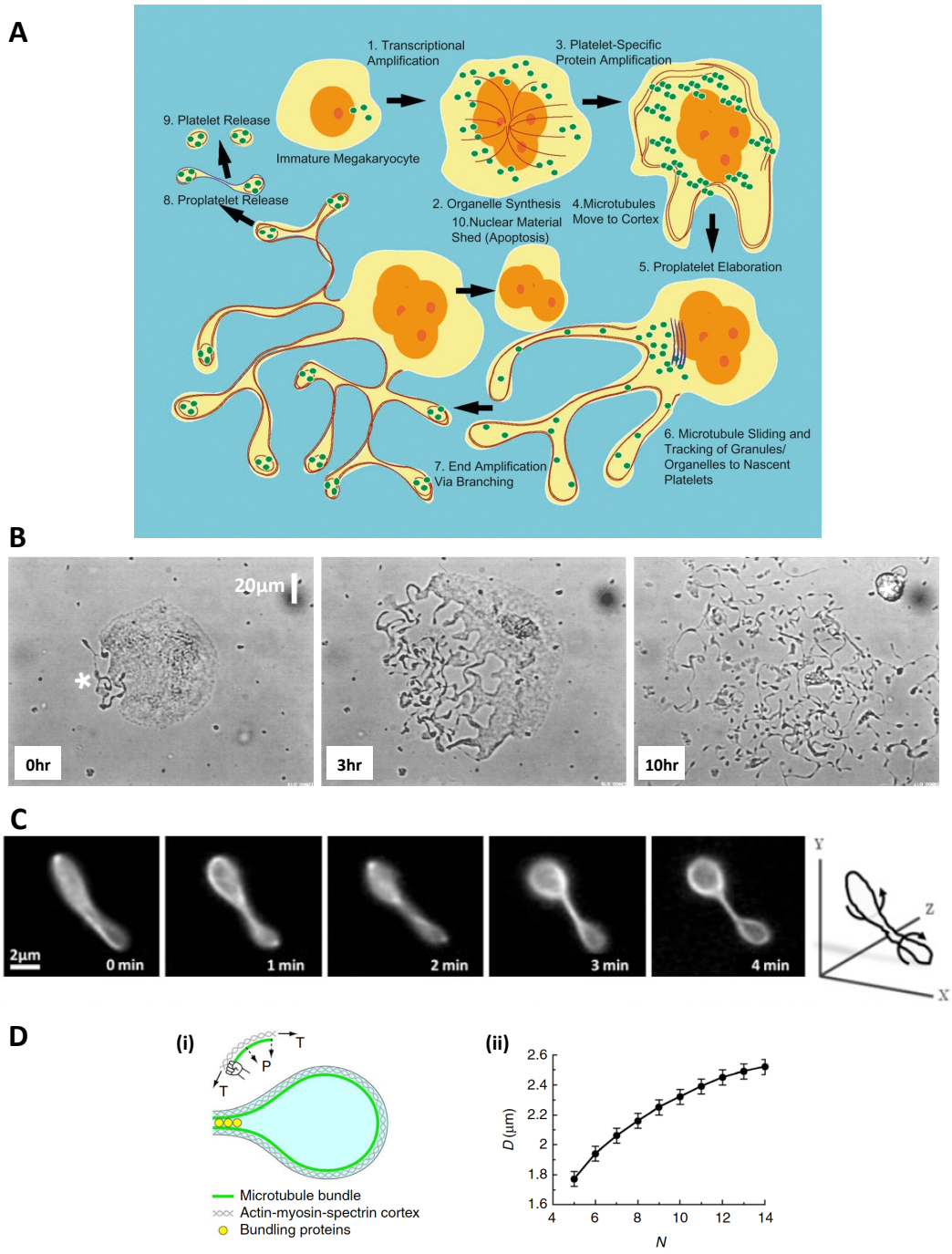

Figure 1.9: Formation of platelets. (A) Schematic representation of megakaryocyte maturation followed by platelet and proplatelet release. Source: **(Hartwig & Italiano 2006)**. **(B)** Formation of proplatelets. Mature mouse megakaryocyte unravels into threadlike proplatelet extensions with platelet bulges at the ends. Adapted from: **(Italiano et al. 1999)**. **(C)** Preplatelet to barbell-proplatelets conversion. Time-lapse of clockwise twisting of marginal band labeled with GFP-β1-tubulin. Adapted from: **(Thon et al. 2010)**. **(D)** Mathematical model for barbell-preplatelet to proplatelet conversion. (i) Schematic of force balance modeled by Laplace's Law (P = pressure, T = cortex tension). (ii) Model prediction of platelet diameter versus number of MTs in the bundle cross-section. Adapted from: **(Thon et al. 2012)**.

Membrane associated cytoskeleton of proplatelets contains spectrin as one of its major components. It is found to uniformly line the membrane from megakaryocyte cell body into the proplatelet projections. Disruption of spectrin markedly reduces proplatelet production (Patel-Hett et al. 2011) and causes blebbing and swelling. Stability of the barbell preplatelet intermediate is also compromised in absence of spectrin cytoskeleton.

The final step of platelet production is the scission of proplatelets that the megakaryocytes extrude in the blood stream, into individual platelets. Shear stress is known to facilitate this process but the final platelet formation can also occur within the blood stream, as often the fragments that are shed are larger than platelets. A mechanical intermediate, circular-preplatelet, in the size range of 3-10µm diameter has been identified which can undergo a reversible transition into barbell shaped proplatelet to finally divide into two individual platelets (figure 1.9 (C)). Thon et. al. (2012) show that the stability of these intermediates, and hence their tendency to divide into two separate platelets, is governed by the biophysical properties, like the diameter and thickness, of the microtubule marginal band. They have described a mathematical model that attributes this conversion to a balance of forces between the cortical cytoskeleton and MT marginal band (figure 1.9 (D)). The critical length of marginal band that would result in barbell transition was predicted to be 10µm. The authors also used the model to predict the final size of a platelet as a function of the number of microtubules contained in the marginal band cross-section. The diameter of a platelet was calculated to vary as a square root of the number of MTs contained in the band cross-section. Predictions about the MT content of the marginal band and the resultant platelet size are in agreement with the aberrant sizes of platelets found in giant-platelet disorders, where platelets are larger in size and have more MTs in the marginal band. Thus, the final size of a platelet can be thought of as a consequence of the mechanical properties of its constituting cytoskeleton.

1.3.3 Resting platelet structure

As described in the pervious sections, morphology of a platelet is the result of its cytoskeletal composition and organization, much of which is reminiscent of its mechanically driven biogenesis process. However, the final resting platelet shape has important functional consequences. When present in the crowded bloodstream, small size and characteristic discoid shape of a platelet allows it to flow in proximity to the vessel wall (Aarts et al. 1988). Such pre-positioning brings it closer to the site of possible injury, facilitating detection and subsequent clot formation. Loss of platelet discoid shape is associated with the onset of activation (White & Burris 1984) and is also known to result from manifestation of certain platelet disorders

(White & Sauk 1984). To demonstrate the mechanical basis of platelet shape determination, I will briefly discuss how the cytoskeletal elements are organized in resting platelets and what are the consequences of some perturbation in their mechanical properties.

1.3.3.1 Microtubule organization and dynamics in resting platelets

Microtubules have long been identified as one of the major cytoskeletal components of platelets. In resting platelets, MTs form a bundle that runs along the periphery (Behnke 1965), constituting what is known as the marginal band. Due to the tight packing of MTs in the marginal band (figure 1.10 (A)), information about single MTs was not available, but estimates based on average number of MTs in the cross-section (approximately 8 to 12) and the average radius of the circular band (approximately 1.5µm), suggested that a platelet contained around 100µm of polymerized tubulin (Behnke & Zelander 1966) (Kenney & Linck 1985). The close packing of MTs in the band also obscured identification of MT ends and it was considered that the marginal band consists of a single MT wound multiple times around the platelet periphery. In 2008, Patel-Hett et. al. provided hard evidence that the platelet marginal band contained multiple dynamic MTs that are organized in a bundle of mixed polarity. They transfected megakaryocytes with green fluorescence protein (GFP) labeled EB3 (MT associated protein that marks a growing plus end) and characterized MT growth in platelets produced by these megakaryocytes. They found the average MT growth speed to be 7.7±3.1 µm/min, within a range of 2.4µm/min to 12.2µm/min. They also observed the EB3 spots moving in parallel and anti-parallel directions, suggesting that the marginal band contains both parallel and anti-parallel MT overlaps, which could provide a site for binding of specific cross-linkers. Additionally, they characterized the marginal band composition in terms of the number of growing MTs (8.66 ±2.11), by counting the number of EB1 (MT associated protein that marks a growing plus end) spots, and the total number of MTs (9.06 ±1.61), by looking at the number of gamma-tubulin (MT associated protein that marks the stabilized minus end) localizations, in the marginal band (Patel-Hett et al. 2008).

Considering the diameter of a platelet (2-3µm) and the persistence length of a MT (1.4mm; (van Mameren et al. 2009)), a bundle composed of curved MTs running along the platelet circumference suggests that the marginal band is likely under tension (proposed (Behnke 1965)) and could possibly maintain the lentiform shape of the platelet. This was confirmed, in 1998, by White and Rao who showed that depolymerization of MTs, by cold treatment or tubulin monomer sequestration with vincristine, led to loss of the discoid shape. Without MTs, platelets became spherical

and extended filipodia-like projections that were dependent on actin polymerization as these structures were lost upon Cytochalasin B treatment. Rewarming the chilled platelets caused reassembly of MTs and restoration of the discoid shape, reiterating the importance of MTs in determining the resting platelet morphology (White & Rao 1998). The importance of MTs in establishing platelet morphology, and possibly activity, was further confirmed by Schwer et. al. in 2001. They showed that mice lacking β1-tubulin, the megakaryocytic lineage specific beta-tubulin isoform, have thrombocytopenia owing to defects in porplatelet generation. Importantly, the platelets that were formed showed a spherical morphology and had only 2 to 3 MTs in the marginal band cross-section. Mice with these mutations also displayed prolonged bleeding times (Schwer et al. 2001). These and many other studies together demonstrate that the microtubule marginal band is essential for proper activity of platelets.

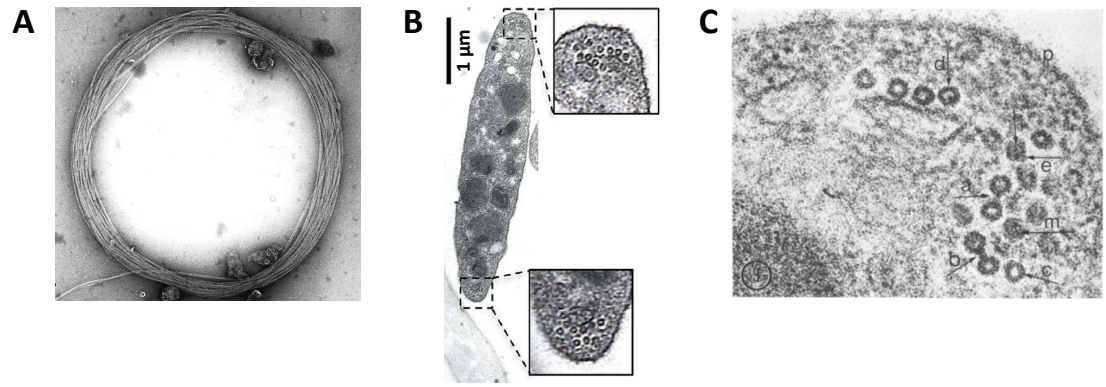

Figure 1.10: Microtubules in resting platelets. (A) Detergent extracted platelet marginal band. MTs form a tightly packed circular bundle. Source: **(White 2013)**. **(B)** Cross-section of a discoid platelet. Marginal band MTs cluster at opposite ends. Adapted from: **(Bender et al. 2014)**. **(C)** Close up of marginal band cross-section. Some MTs are observed to be connected by bridges. Source: **(Behnke 1967)**.

The compact packing of multiple dynamic MTs in the marginal band very likely requires them to be held together by means of cross-linkers to form a stable structure. With the earliest studies of the marginal band structure, it was demonstrated that an electron-lucid clearance zone is present around the individual as well as bundled MTs (Behnke 1965), which meant that the MTs were close enough to exclude electron dense cytoplasmic material from within the bundle, yet far enough to never come into direct contact with each other. Availability of higher resolution electron microscopy data (Behnke 1967), revealed that the MTs could be connected to each other by electron dense structures (figure 1.10 (C)). In 1985, Kenney and Linck showed that MTs in extracted marginal band were coated with

amorphous granular material (Kenney & Linck 1985), which was later discovered to connect two microtubules or a microtubule to F-actin (Nakata 1987). Such connections among MTs and with other cytoskeletal elements would have important implications for mechanical properties of the marginal band.

It has been suggested that the MTs in the platelet marginal band are held together by means of cross-linking molecules (Italiano et al. 2003) which would determine the mechanical properties of the band and its response to forces applied to it. The nature of the cross-linking molecules is of great importance in controlling the properties of the marginal band. An MT cross-linking protein from MAP4 family has been found in platelets (Tablin et al. 1988). This protein is related to MAP2 and Tau, which are known MT cross-linking molecules (MacRae 1992). In addition to the passive bundling molecules, marginal band MTs are know to be associated with motor proteins that might also have cross-linking properties. Rothwell and Calvert, in 1997, showed that platelets contain both kinesin (plus-end directed) and dynein (minus-end directed) motors. They also showed that the dynein motors partition differentially between platelet soluble and insoluble fractions before and after stimulation with different agonist molecules. Activation also affects the phosphorylation state of the motor, as the molecules recovered from the soluble fraction showed a transient phosphorylation after activation, while the ones in the particulate fraction showed only a reduced degree of phosphorylation (Rothwell & Calvert 1997). Such complex behavior of dynein recruitment and phosphorylation state indicates the importance of this motor in platelet activation. Diagouraga et. al. , in 2014, demonstrated the effect of MT motor inhibition on resting platelet marginal band morphology. Though treatment of platelets with dynein inhibitor (erythro-9-[3-2-(hydroxynonyl)]adenine; EHNA) did not change the band morphology, inhibition of kinesin motor (by aurintricarboxylic acid; ATA) caused a reduction in marginal band size, indicating that a balance of kinesin and dynein motor activity could be required to maintain resting marginal band morphology. Additionally, MT sliding by dynein has been demonstrated to be crucial for normal platelet biogenesis (Bender et al. 2015). Role of cytoskeleton associated molecular motors has also been determined in platelet activation (Diagouraga et al. 2014) and will be discussed in one of the following sections.

1.3.3.2 Actin organization and dynamics in resting platelets

The ability of platelets to undergo rapid morphological changes is highly dependent on the cytoskeletal proteins that comprise more than half of the platelet proteome (P Holly et al. 2011) (Burkhart et al. 2012). Actin itself amounts to 15-20% (0.5mM)

of total platelet proteins (Fox 1993) suggesting its likely importance in platelet functionality.

In a resting platelet, 30-40% of its actin content is present in the form of filaments that make a cross-linked network spanning the platelet cytoplasm (figure 1.11(A)). A part of the polymerized actin, along with spectrin, is also known to form the membrane associated cytoskeleton (Zucker-Franklin 1969) (White & Rao 1998). Resting platelets also contain monomeric actin (300-350µM) (Fox & Phillips 1981) in concentrations much above the known critical concentrations for actin barbed (0.2µM) and pointed ends (1µM) (Pollard & Cooper 1986), suggesting the presence of mechanisms that might inhibit actin polymerization in resting state. Presence of such mechanisms provides means to control actin polymerization, which is required for platelet activation (Bearer et al. 2002). However, depolymerization of actin in resting state, by treatment with cytochalasin D, does not disrupt the discoid morphology (Casella et al. 1981), which seems to be determined by the microtubule marginal band (White & Rao 1998).

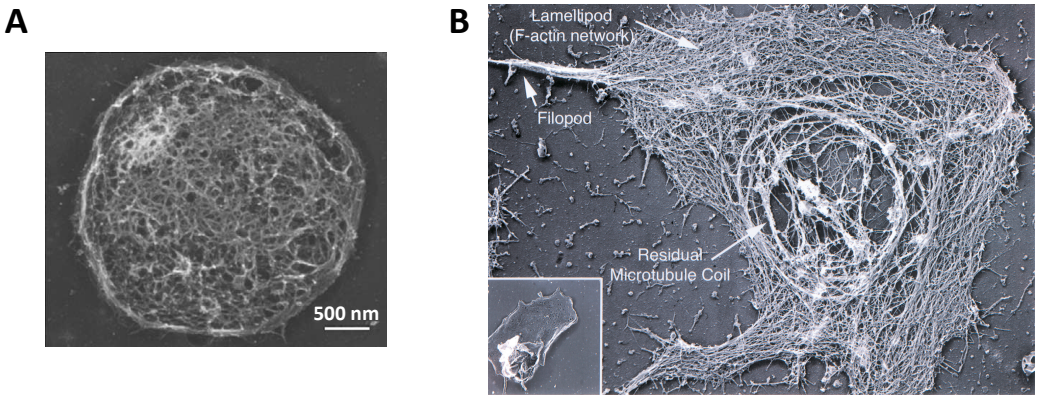

Figure 1.11: Cytoskeleton in extracted platelets. (A) An extracted discoid platelet cytoskeleton. Actin seems to be distributed in the middle of the platelet. Source: **(Bender et al. 2014)**. **(B)** An extracted adherent platelet. Actin is enriched in the lamellipodia. Remnants of MT marginal band present in the centre. Inset shows an adherent un-extracted platelet. Source: **(Hartwig 2013)**.

Platelets also contain large copy numbers (96900 per platelet; (Burkhart et al. 2014)) of non-muscle myosin II A, which is a molecular motor associated with actin and is responsible for generating contractile forces outside striated muscle fibers (Morano et al. 2000). Mutations in the non-muscle myosin II-A gene, Myh9, cause a whole range of platelet disorders called the giant platelet syndrome or the MYH9-related diseases, which are associated with macrothrombocytopaenia. However, the large

size of platelets in these disorders is mainly due to problems with platelet biogenesis, as blocking myosin activity with blebbistatin (small molecule inhibitor of myosin) does not affect resting platelet morphology (Séverin et al. 2012) (Diagouraga et al. 2014). Although it is dispensable for resting platelet shape determination, acto-myosin activity is important for other platelet functionality like shear sensing (Spinler et al. 2015), granule secretion (Sakurai et al. 2015) (Oury et al. 2004) etc.

1.3.3.3 Other elements of membrane associated cytoskeleton

In addition to actin and microtubules, spectrin is another cytoskeletal element that is important for platelet morphology. Spectrin is an integral part of the platelet membrane cytoskeleton (Boyles et al. 1985) (Fox 1988). Platelets contain both erythroid and non-erythroid subunits of sepctrin that are very closely associated with actin, forming virtually a single continuous structure underlining the plasma membrane (Fox et al. 1987). The role of spectrin-based membrane associated cytoskeleton is demonstrated in stabilizing megakaryocytic membrane system and proplatelets, eventually facilitating platelet formation. Dissociation of spectrin into dimers in platelets and proplatelets destabilizes the membrane cytoskeleton resulting in swelling and blebbing (Fox 1988).

1.3.4 Platelet activation mechanics

To carry out their physiological function, platelets undergo a drastic morphological change. The first step involves the discoid platelets to convert into a sphere with filopodia. This transition can occur while the platelets are still in solution. The second step takes place when the platelets come in contact with a surface on which they can adhere and take up a dendritic morphology. In the last step, platelets spread out by extending a lamellipodium. Figure 1.12 shows typical morphologies of platelets during the activation process. Cytoskeletal mechanics play a crucial role in all of these morphological changes.

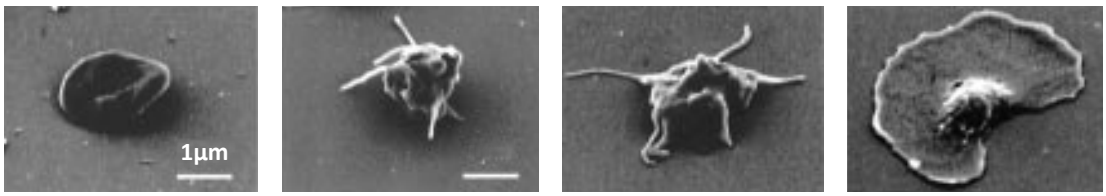

Figure 1.12: Morphological changes during platelet activation. Scanning electron microscopy images of different morphologies adopted by a platelet. Source: **(Kuwahara et al. 2002)**

The resting morphology of a platelet is governed by the presence of a marginal band that pushes on the membrane associated cytoskeleton resulting in the discoid shape. Upon activation, platelets first undergo a disc-to-sphere transition, which has been shown to require polymerized actin (Casella et al. 1981). In 2014, Diagouraga et. al. described the morphology of the marginal band during this change in platelet shape. They found that the marginal band undergoes a coiling transition upon onset of platelet activation (figure 1.13(A)) either with transient activation due to blood extraction procedure or by treatment with various agonists like ADP, thrombin and arachidonic acid (figure 1.13 (B)). Coiling of the marginal band was also reported to occur in response to addition of kinesin motor inhibitor ATA, suggesting that perturbation in composition of marginal band could induce coiling. The authors also observed a correlation between the degree of coiling (figure 1.13 (D)) of a marginal band and its length, where longer bands were found to be more coiled. This data was acquired on a population of fixed platelets. During later stages of activation, authors observed a rearrangement of MTs in the marginal band, where growing MTs short-circuited the coiled marginal band resulting in a smaller band of shorter length (figure 1.13 (C)). They saw no effect of myosin inhibition with blebbistatin on the initial morphology of coiling, while the final states were found to be less compact than controls. Based on these observations, they proposed a model, where the marginal band coiling is triggered by dissociation of kinesin from the marginal band causing it to lengthen due to dynein activity and coil as a consequence of pushing against the membrane cytoskeleton. Actin was proposed to be responsible for the later stage of irreversible coiling induced by contraction (figure 1.13 (E)). A key point to note is that in the model proposed by Diagouraga et. al., the elongation of the marginal band is causing the coiling.

The adherent stages of platelet activation are highly dependent on both actin polymerization and myosin-based contractility while MTs are deemed dispensable for this process (Italiano et al. 2003). With the onset of activation, platelets experience a rise in the amount of polymerized actin from between 30% and 40% in resting platelets to about 70% in activated ones (Fox 1993). This process is known to be concomitant with the rise in calcium levels from 10-20nM to 3-5µM, which could affect actin dynamics in many ways (Davies et al. 1989), one of which utilizes the actin severing protein: Gelsolin. In presence of calcium, gelsolin cuts the actin filaments, providing uncapped ends and increasing the soluble actin pool that can then be polymerized into new actin structures like filipodia and lamellipodia. Due to the need to recreate new actin structures, these steps are also dependent on Arp2/3 complex, an actin nucleator, and the corresponding increase in polymerization (Li et al. 2002). A fully spread platelet extends a symmetric lamellipodium allowing it to

generate isotropic contraction, and to bring about compaction of a blood clot. Owing to their specialized design and composition, platelets have a higher contractility than smooth and even striated muscle cells, while simply making use of the disordered acto-myosin network and non-muscle myosin IIA (Schwarz Henriques et al. 2012) (Murrell et al. 2015). This underlines the importance of myosin in platelet functionality (CALAMINUS et al. 2007).

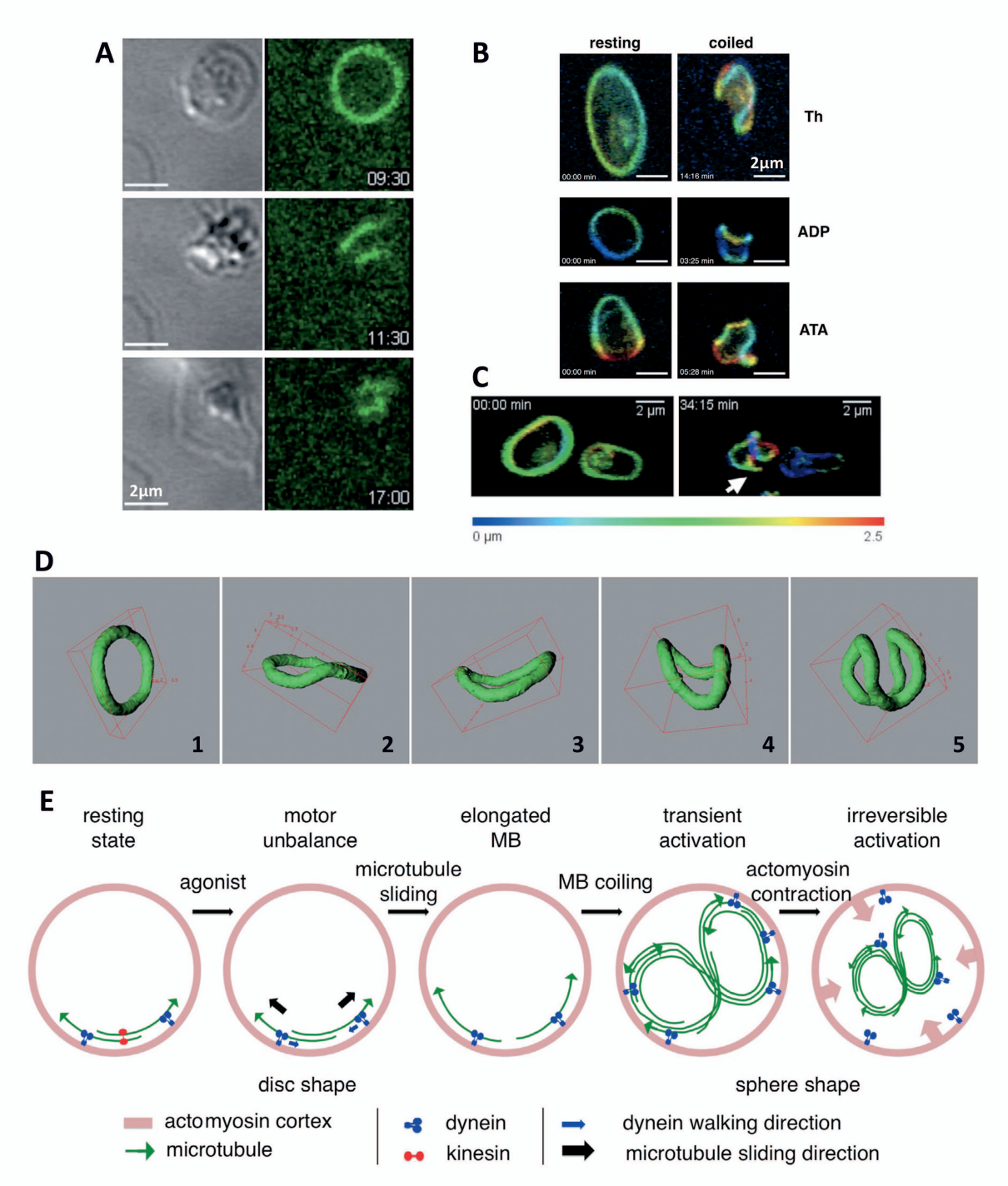

Figure 1.13: Role of molecular motors in marginal band coiling. Coiling observed in live platelet marginal bands labeled with TubulinTracker. **(A)** Platelet spreading on glass accompanied by marginal band coiling. **(B)** Uncoiled and coiled states of platelets treated with thrombin (0.017U/ml) and ADP (135nM) or treated with ATA (6.7µM). **(C)** Marginal band rearrangement in platelets stimulated with ADP (270nM). Arrow marks MTs that are short-circuiting the coiled marginal band. **(D)** 3D representation of marginal bands at each of the five discrete stages of coiling. **(E)** Length extension based model for marginal band coiling. Source: **(Diagouraga et al. 2014)**

1.4 Signaling through ADP and thrombin receptors

Platelet activation in response to agonists like ADP and thrombin is triggered by ligand binding to their specific cell surface receptors, which transduce signaling downstream via a number of G-proteins. Belonging to a family of GTPases, G-proteins are often associated with the G-protein coupled receptors (GPCRs) that together help transducing signals from cell exterior to interior (Offermanns 2006) (Wettschureck 2005). Platelets express different classes of GPCRs and G-proteins, which make use of second messengers to amplify signal and elicit responses while providing multiple steps at which this process could be biochemically regulated (Brass et al. 2013).

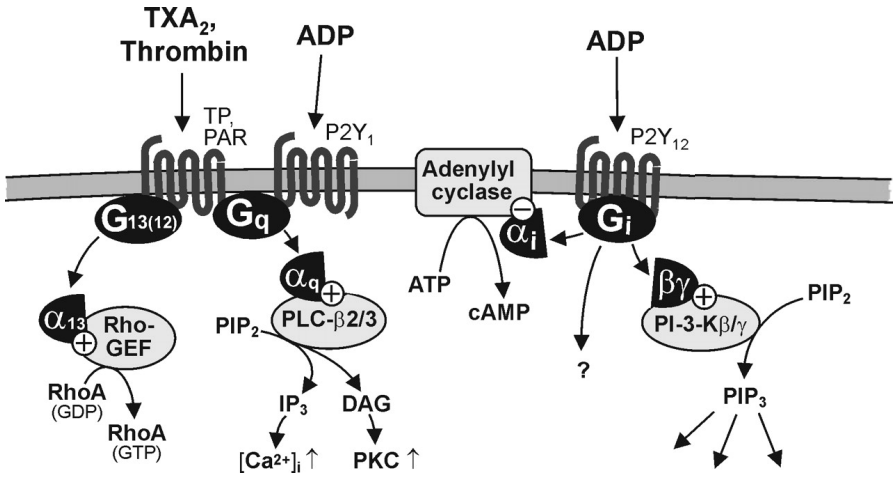

Figure 1.14: ADP and thrombin signalling in platelets. Components: TxA2, thromboxane A2; TP, TxA2 receptor; PAR, protease-activated receptor; P2Y1/P2Y12, purinergic receptors; RhoGEF, Rho guanine nucleotide exchange factor; PLC-β2/3, phospholipase C-β2/3; PI-3-K, phosphoinositide-3-kinase; PIP2, phosphatidylinositol 4,5-bisphosphate; IP3, inositol 1,4,5-trisphosphate; DAG, diacylglycerol; PKC, protein kinase C; PIP3, phosphatidylinositol 3,4,5-trisphosphate. Adapted from: **(Wettschureck 2005)**

At the site of vascular injury, ADP is released, by the damaged epithelium. Platelets themselves store ADP in dense granules that can be released upon activation making it a paracrine as well as an autocrine signal. Studies have shown that addition of ADP increases the effectiveness of other agonists, but on its own, ADP is considered a weak platelet activator. This can be attributed to difference in signaling downstream ADP receptors. Platelets express two types of purinergic receptors for sensing ADP: the $P2Y_1$ and the $P2Y_{12}$ receptors. ADP signaling through $P2Y_1$ receptor, which is coupled to the G-protein, G_q, is responsible for ADP dependent shape change as loss of this protein abrogates the morphological response. Rise in calcium level is

important for platelet activation which is why calcium levels in resting platelets is maintained at a low concentration of 0.1μM at the expense of utilizing ATP to pump calcium outside the cell or in the dense tubular system. Activation of phospholipase C (PLC; figure 1.14), which is downstream of the G_q protein, hydrolyzes the membrane bound PIP2 to IP3 and DAG which are second messengers that raise the cytosolic calcium concentration. The increase in calcium levels signals the myosin light chain kinase causing activation of myosin, which is responsible for platelet shape change. Additionally, APD signaling through the $P2Y_{12}$ receptor and G_i protein is responsible for inhibiting cyclic adenosine monophosphate (AMP) second messenger release, which turns off signaling in platelets (Brass et al. 2013) (Woulfe et al. 2001).

Thrombin is considered one of the most potent activators of platelets. Its activity is triggered by binding to the protease activated receptors (PAR) family of GPCRs. Human platelets contain three PAR proteins, PAR1, PAR3 and PAR4, while mouse platelets lack PAR1. By efficient activation of the PLC though PAR and G_q coupling, thrombin provides strong signal for PIP2 hydrolysis and as a result, causes the fastest and highest increase in cytosolic calcium levels. On a population level, calcium response is uniform and strong in response to thrombin and less so for ADP. Single platelets, however, show heterogeneity and spiking behavior. In addition to signaling through G_q, PAR proteins also signal through G_{13} protein, which directly mediates cytoskeletal changes by activating RhoA and Rho-associated protein kinase (ROCK; figure 1.14) (Wettschureck 2005). This eventually signals to cofilin, and myosin light chain kinase affecting both actin and myosin(Brass et al. 2013). Thus thrombin elicits very strong signaling towards platelet shape change using Rho-ROCK pathway and calcium increase, in contrast to ADP, which only depends on calcium increase.

1.5 Cytoskeleton related platelet disorders

The integrity of cytoskeletal elements is essential for normal biogenesis and physiological function of platelets. The discoid morphology of resting platelets is important in order for them to partition along the vessel wall while in flow. A characteristic feature of many platelet disorders is the altered resting platelet morphology, where platelets lose their discoid shape and become spherical. These diseases have been studied in human patients and mouse models to deduce that such morphological alterations can occur due to alterations in the cytoskeleton.

A class of inherited macrothrombocytopaenia, or disorders related to large platelet size, are caused due to mutations in the MYH9 gene, and hence called MYH9-RD (MYH9 related disorders) (Seri et al. 2000). These include autosomal disorders like

May-Hegglin anomaly, Fechtner syndrome, Sebastian syndrome, etc. In May-Hegglin anomaly, the MYH9 mutation prevents myosin from assembling into filaments (Kelley et al. 2000). A disruption in normal myosin function has been demonstrated to cause pro-platelets to have larger swellings at the ends leading to release of larger platelets that are more spherical (Spinler et al. 2015) (figure 1.15 (C)). Activity of myosin was deemed dispensable for ADP dependent platelet shape change in solution while essential for adhesion and contraction (Léon et al. 2007). These platelets also had higher number of MTs in the marginal band cross-section (White & Sauk 1984).

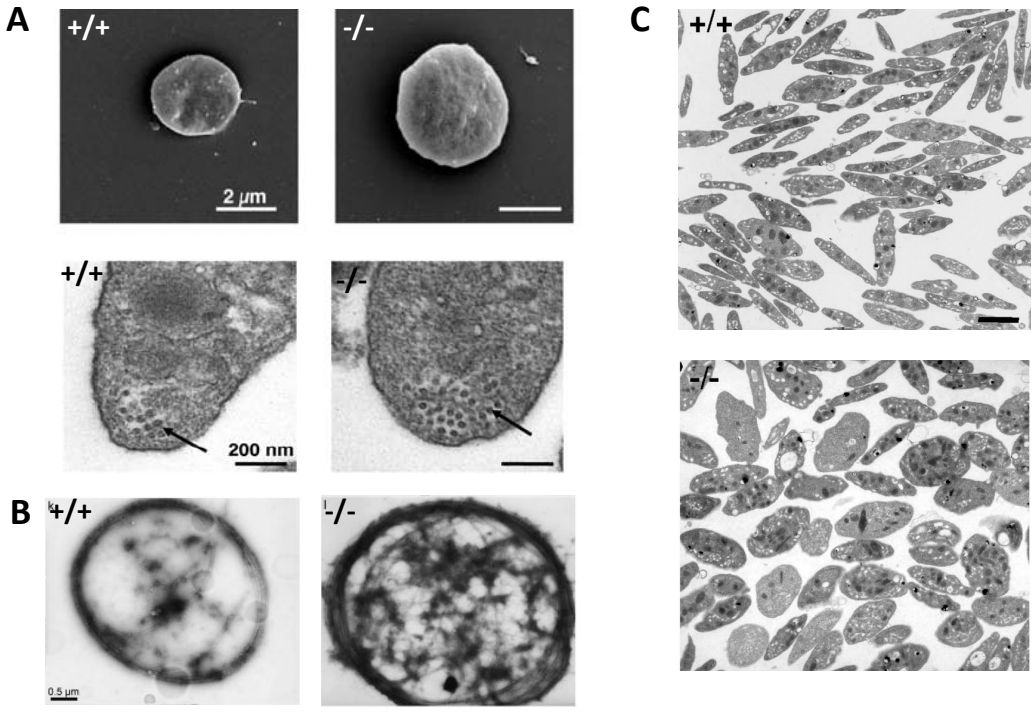

Figure 1.14: Platelet morphology in cytoskeleton related disorders. (A) Scanning electron microscopy images of platelets from Bernard Soulier Syndrome mouse model. Cross-section of platelets showing MTs in the marginal band. Knockout platelets are larger and have more mTs in the marginal band cross-section. Source: **(Strassel et al. 2009)**. **(B)** Extracted marginal band of filamin (FLN-a) knockout platelets is larger and thicker than control. **(Jurak Begonja et al. 2011)**. **(C)** Transmission electron microscopy image of platelet population with MYH9 deletion. Platelets lose their discoid shape becoming more spherical **(Léon et al. 2007)**.

The Bernard Soulier syndrome is a well-known example of a hereditary cytoskeleton related platelet disorder which is caused by mutations leading to deficiency in von Willebrand factor receptor (or glycoprotein complex GPIb-V-IX). This cell surface receptor is known to link actin to the membrane by means of filamin molecules resulting in a rigid membrane cytoskeleton. Loss of either the receptor (figure 1.15

(A)) (Strassel et al. 2009) or filamin (figure 1.15 (B)) (Jurak Begonja et al. 2011) causes platelets to be larger in size and have more number of MTs in the marginal band. This defect arises from faulty proplatelet morphology where the shaft becomes lose and MT bundles in proplatelet get thicker. These platelets are also easier to deform as shown by micropipette aspiration (White et al. 1984), which causes them to be fragile.

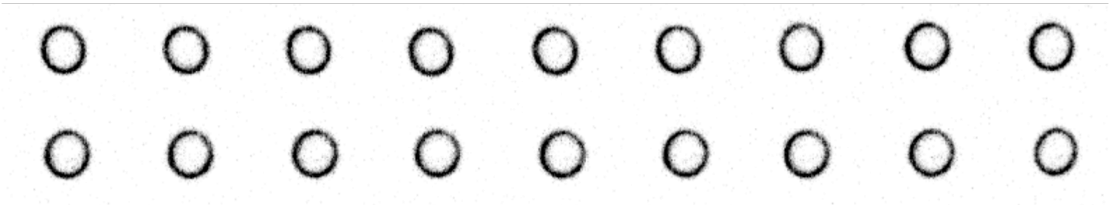

Chapter 2

Objectives

2 Objectives

Platelets are small cytoplasmic fragments specialized to undergo rapid changes in morphology to fulfill their physiological function. The resting discoid shape of a platelet is determined by cytoskeletal mechanics during the process of platelet biogenesis. Activated platelets are known to utilize cytoskeletal structures, like filopodia and lamellipodia, to increase their surface area and adopt an extended morphology. Much is known about platelet mechanics before they take up the discoid morphology and after they get activated and spread. There is, however, little known about mechanics of platelet disc-to-sphere transition, which is the first natural response of a platelet when stimulated by any chemical agonist. The elongation of marginal band based on microtubule motor activity has been proposed as a possible mechanism to drive this shape change (Diagouraga et al. 2014), but the role of actin as a trigger to induce coiling has not been sufficiently addressed. The simple architecture and specialized cytoskeleton make the platelet an interesting model system to study morphological changes. Hence, I decided to carry out my doctoral research elucidating the role of cytoskeletal mechanics in platelet activation with a focus on the disc-to-sphere transition. The goal of my research was addressed by using different techniques for which various collaborations were established.

The first objective of this study was to understand the implications of resting platelet marginal band structure on its mechanical properties. The marginal band is known to be composed of multiple MTs, but quantitative data was not available on their length distributions, spatial arrangement, etc. To this end, electron tomography was used to study the detailed structure of the marginal band. Additionally, we decided to make use of data from super-resolution microscopy, which has a lower resolution but higher throughput, to quantify the overall morphology of the marginal band. It also provided an added advantage of allowing visualization of multiple proteins at the same time.

During the platelet disc-to-sphere conversion, the MT marginal band has been shown to undergo a coiling transition. Following this mechanical change could provide interesting insights into the properties of the marginal band as they respond to various stimuli. To understand the physical principles that govern this transition, a simulation of the marginal band coiling process was set up for which information was derived from literature and supplemented with the structural data obtained with electron tomography. The motivation behind simulating the coiling process was to identify necessary and sufficient processes that can cause such changes in

marginal band morphology. The predictions for the model could then be tested by designing suitable experiments to perturb the system.

To further the understanding of marginal band coiling process, we decided to carry out characterization of dynamics of this morphological change, where the challenge was to visualize coiling in live cells. Due to their small size, high sensitivity to the chemical and physical environment, and lack of genetic amenability, platelets are difficult to image, especially in a solution state. To overcome these restrictions, we labeled platelet MT cytoskeleton with a small molecule probe and used a microfluidic setup to observe platelets change shape in response to drugs while they are still in solution. The setup also allowed me to carry out perturbations in cytoskeletal properties by treating platelets with chemical inhibitors. These dynamic changes in morphology were imaged and quantitatively analyzed to yield parameters that describe the physical properties of the marginal band and how these changed over time with platelet activation.

If mechanics of cytoskeleton were at play to trigger coiling of the marginal band, size of the platelet would have profound effects on its propensity to get activated, as often seen in platelet related bleeding disorders. Since there is a pre-existing natural variation in platelet sizes, due to the fragmentation process responsible for their biogenesis, we decided to make use of it to understand how mechanical properties of the marginal band change with size. First the variations observed in a resting population were characterized, and then the activating platelets were analyzed to understand the implications of having different starting characteristics on the ability of marginal band to coil.

A combination of experimental techniques and quantitative analysis was used to understand the role of cytoskeletal mechanics in the process of platelet activation. A detailed description of the methods and results can be found in the following sections.

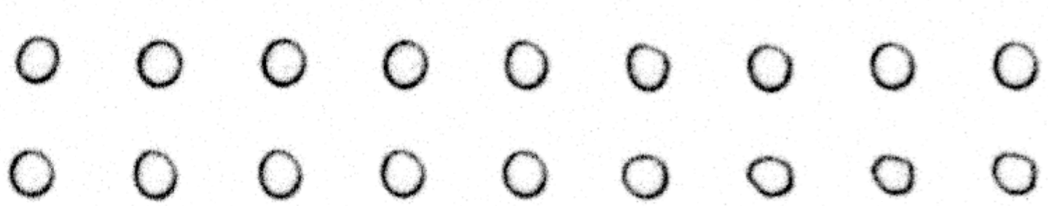

Chapter 3

Methods

3 Materials and Methods

3.1 Mouse lines

All animal work was performed in the animal facility at the European Molecular Biology Laboratory (EMBL), which is operating according to the guidelines and recommendations of the Federation for Laboratory Animal Science Associations. Mice were housed in a temperature-controlled room with proper 12/12 darkness-light cycles and fed with a regular *ad libitum* diet.

The experiments were performed on platelets extracted from mouse blood. We made use of three mouse lines. C57BL/6 is a common inbred laboratory mouse strain that was the control line as the transgenics were based on this strain. The eGFP tubulin labeled reporter line (Abe et al. 2011) was obtained from Dr. Jan Ellenberg's lab at EMBL. We also queried an actin reporter line with GFP Lifeact label. These mice were a kind gift from Dr. Takashi Hiiragi's lab.

3.2 Blood collection

2ml syringes with 25-gauge needles were preloaded with 200µl of acid-citrate-dextrose (ACD; in mM: 85 trisodium citrate dihydrate, 66.6 citric acid monohydrate, and 111 anhydrous D(+)glucose) solution (Cazenave et al. 2004) to prevent coagulation during the collection process. The animals were anaesthetized by exposure to isoflurane vapours. Blood was collected from adult (between 8 to 45 weeks of age) mice by cardiac puncture. Once obtained, the blood was immediately used for Platelet-rich Plasma (PRP) separation and was always processed in polypropylene tubes at room temperature.

3.3 Platelet isolation

Blood was centrifuged for 4 minutes at 200g without breaks. The upper phase, or PRP, was carefully removed with a wide-bore plastic Pasteur pipette. The PRP was then centrifuged at 2000g for 2 minutes. The plasma was discarded and the platelet pellet was resuspended in Tyrode's Albumin Buffer without Calcium (nC-TAB) (Cazenave et al. 2004).

3.4 Electron tomography

The data for electron tomography was generated and modeled by Dr. Romain Gibeaux.

Freshly extracted PRP was cryo-immobilized by high-pressure freezing. This was followed by freeze substitution in a solution containing 0.2% uranyl acetate which

provides negative staining to cellular structures. The samples were then resin embedded and polymerized by exposure to UV. The sample block was then cut into 300nm thick serial sections. The sections were then post stained with 2% uranyl acetate to generate contrast. Digital images of the sections were taken from -60˚ to +60˚ tilt. The axis of acquisition was then rotated by 90˚ and a second tilt series was acquired. Tomograms were generated for each rotation and section, which were then joined in z to reconstruct full platelets. The joined tomograms were finally modeled and analyzed using IMOD software (Kremer et al. 1996).

3.5 Super resolution microscopy

Localization based 3D super-resolution microscopy was performed on fixed platelets to elucidate structural composition of the marginal band. These experiments were done by Tooba Quidwai from Dr. Jonas Riess' Lab.

Platelets were fixed in cytoskeleton buffer (in mM: 10 MES or 2-(N-morpholino) ethanesulfonic acid at pH 6.1, 150 NaCl, 5 EGTA, 5 glucose, 5 mM $MgCl_2$) containing 2% glutaraldehyde (GA) for 15 minutes. The fixation solution was then spun down on poly-l-lysine (pll) coated coverslips at 600g for 5 minutes. The coverslips were washed with PBS to remove fixative. Auto-fluorescence due to GA was quenched by treating samples with 0.01mg/ml solution of sodium borohydride in phosphate-buffered saline (PBS; in mM: 137 sodium chloride, 2.7 potassium chloride, 10 disodium hydrogen phospate, and 1.8 potassium dihydrogen phosphate; pH 7.4) for 7 minutes. The samples were thoroughly washed with PBS. Unspecific binding of antibodies was blocked simultaneously during premeabilization process by incubating coverslips for 1 hour with a solution of 50% Image-iT® (Thermo Scientific) and 0.25% TritonX-100 in PBS. After a wash with PBS, the samples were labeled with primary antibodies against the desired epitope (table 1) in 3% bovine serum albumin (BSA) for 2 hours. Following another brief wash with PBS, the samples were labeled with the corresponding secondary antibody (table 1) for 2 hours. To ensure continuous labeling of marginal band, a second round of labeling with the secondary antibody was performed after which the coverslips were washed and imaged.

Table 1 - List of primary and secondary antibodies used for immunofluorescence labeling

	Host	Dilution	Supplier (catalog number)
Primary Antibodies			
α-Tubulin	Mouse	1:500	Thermo Scientific (MS581)
Y-Tubulin	Rabbit	1:500	Sigma (T5192)
Secondary Antibodies			
Alexa Fluor 647 Anti-mouse IgG	Goat	1:200	Thermo Scientific (A-21236)
CF 680 Anti-rabbit IgG	Goat	1:200	Sigma (SAB4600362)
Alexa Fluor 488 Anti-mouse IgG	Goat	1:200	Thermo Scientific (A-11001)

3.6 Live platelet imaging

3.6.1 Platelet labeling

In addition to visualizing the inherent fluorescence of platelets from GFP-tubulin and GFP-Lifeact mice, live cell markers were also used to label platelet membrane and microtubules. For demarcating the membranes, platelets were incubated in 1µg/ml solution of CellMask deep red (Thermo Scientific) and incubated for 30 minutes at room temperature. For labeling microtubules, we used 50nM solution of SiR tubulin (Spirochrome) and incubated the cells for at least 45 minutes before imaging. Very low concentration of SiR tubulin was used to ensure the probe itself, which is based on docetaxel, does not affect mechanical properties of microtubules.

3.6.2 Microfluidic chip

The mould for the microfluidic device (Fig. 3.1(A)) was designed and made in SU8 photoresist by Dr. Iana Kalinina. It was then used to cast polydimethylsiloxane (PDMS) devices. One part of PDMS base was mixed with ten parts of the curing agent and stirred thoroughly. After degassing, the PDMS mixture was poured over the mould and baked in the oven at 65˚C for at least 12 hours. The devices were then cut out and 0.75mm holes were punched through to make the inlets and outlets (Fig. 3.1(A), 1 to 8). Glass coverslips (25x50mm #1.5) were sonicated in a 50% ethanol in water solution for 30 minutes and dried at 37˚C overnight. Clean devices (channel-side up) and coverslips were exposed to oxygen plasma for 1 minute and immediately bound together. The chips were further baked at 65˚C for 2minutes to strengthen the binding. To prevent activation of platelets due to negatively charged glass surface, a 0.1mg/ml solution of poly-l-lysine – Poly Ethylene Glycol (pll-PEG) in 10mM HEPES buffer was introduced into the channels, incubated for 1 hour and

then washed off thoroughly with water. The pll chains bind to glass exposing the hydrophobic PEG chains towards the solution. This passivates surface, which prevents platelets from coming in direct contact with the glass. The chips were stored under water until used for imaging.

3.6.3 Imaging setup

Platelets are present in our blood stream and stay suspended in fluid during their lifecycle unless they are activated. In order to replicate such environment, we developed an imaging setup such that platelets could be kept in suspension while imaging. This setup could also be used to visualize dynamics of platelet activation as it allowed imaging of the suspension cells during treatment with chemicals (Fig. 3.1(A)).

Isolated platelets were diluted in 0.2% methylcellulose solution prepared in nC-TAB. This increased the viscosity of the medium and prevented thermal movements of platelets during 3D imaging. The cell suspension was then applied to the side channels C1 and C2 of the microfluidic chip (Fig. 3.1(A); Chip dimension: C1=C2=CC = 85µm; F1 = F2 = 3µm) and the channels were sealed with plugs. The central channel CC was connected to a reservoir on one side and to a sink on the other by means of flexible microfluidic tubing creating a vertical fluid column. A gravity flow could be created in the central channel by elevating the reservoir with respect to the sink. The molecules of interest were introduced in the reservoir and released into the central channel when required. Subsequent treatment was based on diffusion of the molecules from the central to side chambers through the filters, F1 and F2.

The timing of chemical treatment of platelets was analyzed by tracking diffusion of a fluorescent molecule through the microfluidic chip. We used fluorescein (332.31g/mol) at a concentration of 1µg/ml in imaging medium and imaged the field of interest (Fig. 3.1(A); red square) at the usual frame rate of 1 frame per 5 seconds over 10 minutes. The length scale of diffusion of fluorescein, given the diffusion coefficient (D) 0.64x10-9 m^2/s (Galambos & Forster 1998), was calculated using Einstein's theory:

$$x^2 = 2Dt$$

where, x is the length scale and t is the timescale of diffusion. Thus, for a time period of 5 seconds the fluorescein molecule can be expected to cover a distance of 80µm. This value is around 20% smaller than our field of view, which is 104µm by 104µm in size.

The effect of diffusion can be seen in the quantification of images (Fig. 3.1(B)). The field of view (1000x1000 pixels) was not evenly illuminated (Fig. 3.1(B) Grayscale image) due to which the analysis was performed on the central region (500x500 pixels) marked in black. The plots (Fig. 3.1(B)) show mean intensity, I_X, calculated along the horizontal (X) and, I_Y, along the vertical (Y) dimensions. These are formalized as

$$I_X(t) = \frac{\sum_{Y=1}^{N_Y} I_{XY}(t)}{\sum_{Y=1}^{N_Y} Y} \qquad I_Y(t) = \frac{\sum_{X=1}^{N_X} I_{XY}(t)}{\sum_{X=1}^{N_X} X}$$

where, I_{XY} is the image matrix with X and Y pixels over time t. In the plot along Y dimension, after around 200 sec, a slight gradient is visible from top to bottom. This was investigated further by weighting the positions X and Y of every frame by the line intensity means I_X and I_Y as

$$\bar{X}_X(t) = \frac{\sum_{X=1}^{N_X} X.I_X(t)}{\sum_{X=1}^{N_X} I_X(t)} \qquad \bar{Y}_Y(t) = \frac{\sum_{Y=1}^{N_Y} Y.I_Y(t)}{\sum_{Y=1}^{N_Y} I_Y(t)}$$

A shift of around 15 pixels in mean position along the Y dimension towards lower pixel positions (Fig. 3.1(C), inset) is observed over time which coincides with the fact that the fluorescence source is present along the Y = 0 position. This fluorescence shift equilibrates within 150 seconds as the mean position returns to center of frame. The shift corresponds to a distance of 1.56µm showing concentration asymmetry of fluorescein. However, this distance is fairly small with respect to the 104µm field of view (Fig. 3.1(C)). Additionally, when compared to asymmetry along the orthogonal dimension, this shift is not significant. The plot in Fig. 3.1(D) shows an increase in mean intensity of the whole frame over time. This gives us a timeframe over which the chemicals would diffuse through the filter and reach the imaging chamber.

Imaging was performed using a spinning disk microscopy setup (Perkin Elmer Ultraview VoX). Live platelets were imaged using a 63x (1.4NA) Oil objective, which produced images with a lateral pixel size of 0.104µm. The axial dimension was imaged with a spacing of 0.4µm. An image stack was acquired every 5 seconds over 10 minutes or every 15 seconds over 30 minutes for different treatments.

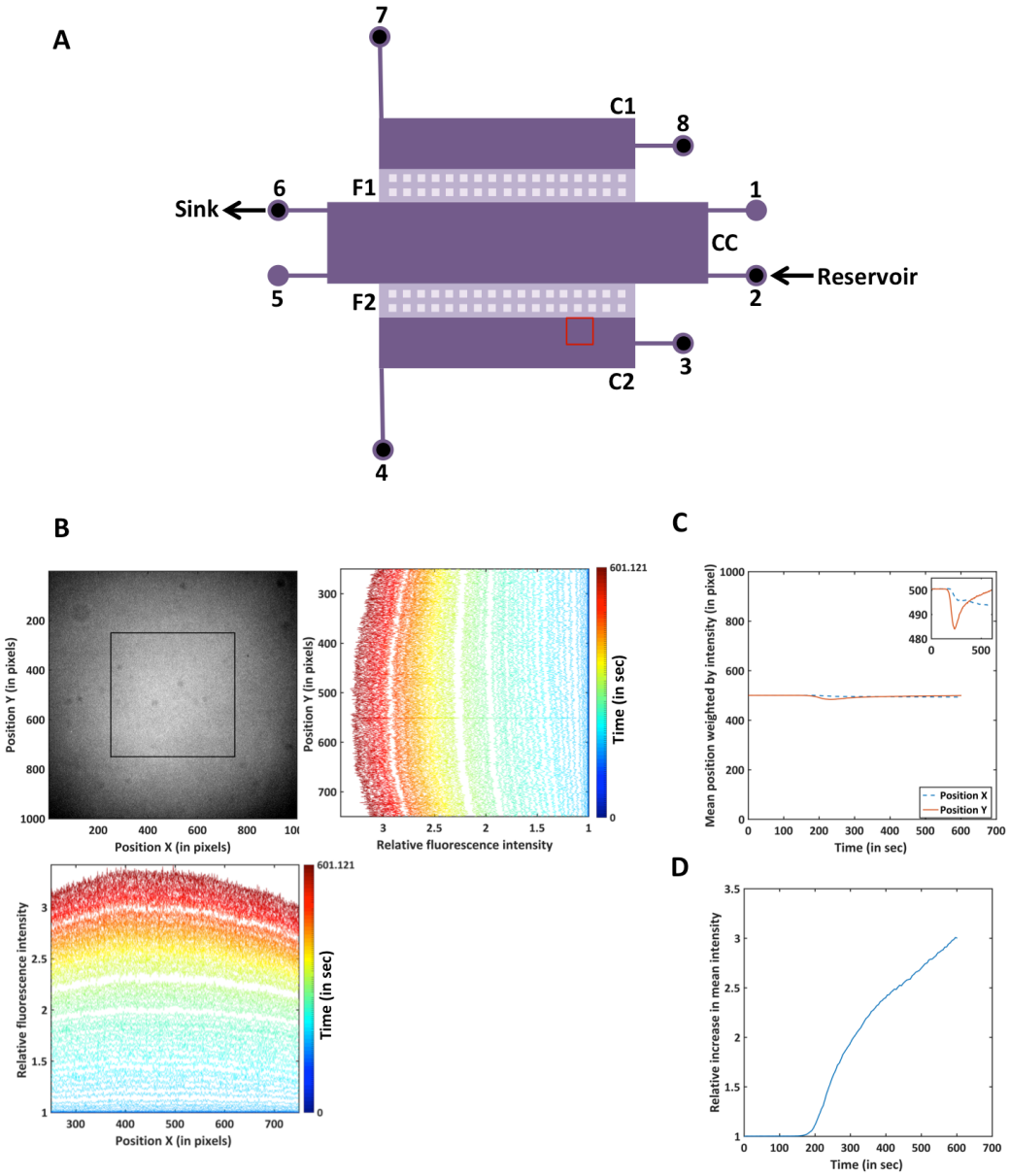

Figure 3.1: Live cell imaging setup. (A) A two level microfluidic chip used for imaging platelets. Chip height: CC = C1 = C2; F1 = F2. Channel inlets (1 to 8). Black inlets have punched hole of 0.75mm diameter. Red square depicts an imaging region. **(B)** Maximum intensity projected image of fluorescein over time. Region bound by black square used for plotting. Plots along X and Y axes showing mean fluorescence along Y and X axes respectively, color-coded in time. **(C)** Mean position of fluorescence along X and Y dimension. Inset: Zoomed y-axis. **(D)** Mean fluorescence intensity of the full frame over time.

3.7 Volume measurement by fluorescence exclusion

The technique used to measure platelet volume was adapted from previous work by Bottier et.al. (Bottier et al. 2011). This method is based on estimation of volume by fluorescence exclusion and is shown, subsequently, to work on multicellular aggregates(Woolley et al. 2013) and (Monnier et al. 2015).

3.7.1 Principle

The intensity (I) recorded in an image of a region with fluorescent molecules is proportional to the number of fluorescent molecules (N_{fl}) contained in that region.

$$I \propto N_{fl}$$

The number of molecules contained in a region is equal to concentration of the molecules (C_{fl}) times the volume (V_{fl}) of the region.

$$N_{fl} = C_{fl} \times V_{fl}$$

The volume, in turn, can be written as

$$V_{fl} = Ar \times H$$

where Ar is the area and H is the height. Assuming a homogenous solution of fluorescent molecules, the concentration (C_{fl}) is constant. Owing to the setup, the imaged area (Ar) is constant too. This leads to the intensity being directly proportional to the height of the fluorescent solution.

$$I \propto H$$

In presence of a transparent object, excluded of fluorescence, within the imaging volume, a loss in intensity would be recorded which would correspond to the number of fluorescent molecules displaced. This in turn corresponds to the volume of the object. Using the relation between intensity and height, we can calculate the height of the object at any point in the image as

$$I - I_0 = H$$

where, I_0 is the intensity value corresponding to zero height (H_0 = 0) or no fluorescent molecules, while I is the intensity which would correspond to an object of height H (Fig. 3.2(B)).

This relation would hold if the height of the object of interest were within the height of the fluorescent solution that can be imaged at once (Fig. 3.2(A)). This distance is formally defined as the depth of field and can be calculated for a high magnification objective as

$$F_d = \frac{\lambda n}{NA^2}$$

where, λ is the wavelength of light, n is the refractive index and NA is the numerical aperture of the objective. The intensity I_1 related to the maximum height (F_d)

imaged at once, depicted in Fig. 3.2(B), is the upper limit of the intensity for the given height.

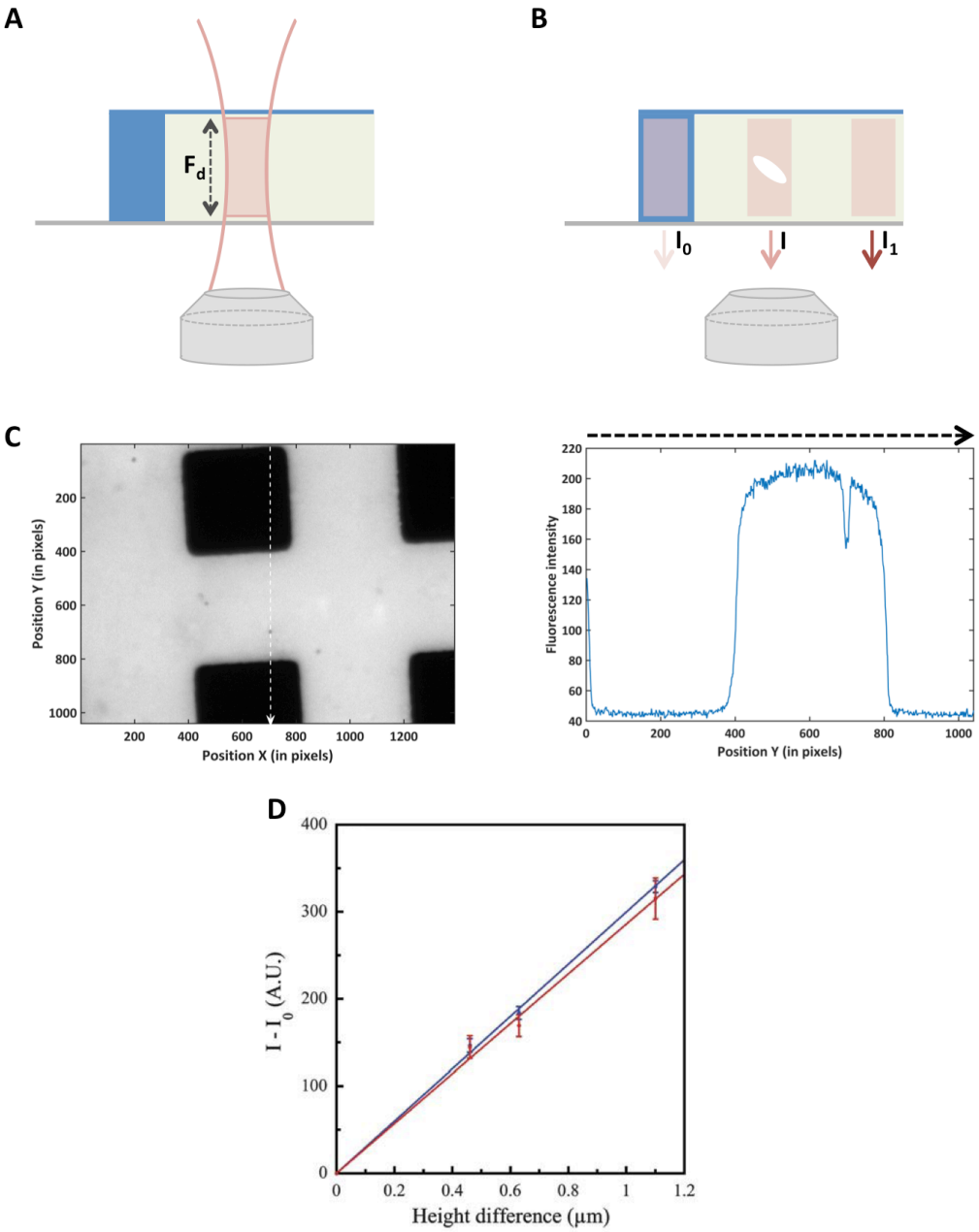

Figure 3.2: Volume measurement by fluorescence exclusion. (A) Microfluidic chamber, made of PDMS (blue) bound to glass coverslip (gray), filled with fluorescent solution (green). Red shaded area with a height of F_d is imaged with the low NA objective (gray) at the bottom of the chamber. **(B)** Presence of fluorescence excluded object (white) gives an intensity I which lies between minimum I_0 and maximum I_1. **(C)** Single plane image of a region with platelets (small round shadows) and pillars (dark squares). Intensity along the white dashed arrow is plotted on the right. **(D)** Calibration plot for difference in intensity versus height. From Bottier et. al. (Bottier et al. 2011).

3.7.2 Setup

To ensure that the platelets do not exit the volume being imaged, we implemented a setup were the height of the imaging channel was approximately the same size as the depth of field of the objective. This also ensures that the measurements are not affected by light coming from beyond the F_d region (Fig. 3.2(A)). Chips of the same design as Fig. 3.1(A) were cast in different heights (1.5µm, 1.8µm and 3µm) of the filter regions F1 and F2 which restricted the movement of platelets in axial dimension. The depth of field was maximized by using a widefield epifluorescence microscope (Zeiss Cell Observer) with a 40x (NA 0.6) objective that gives an F_d of 1.44µm to 1.87µm depending on the wavelength of the emission 512nm to 667nm respectively. Platelets in imaging medium were mixed with fluorescein (final concentration of 50µg/ml), introduced into the chip and imaged. Figure 3.2(C) shows such a typical field of view along with fluorescence intensity measurement along the dashed line. The line passes through pillars, corresponding to H_0, and a platelet. The calibration of intensity difference and height of object shown in figure 3.2(D) is adapted from the publication by Bottier et. al. (Bottier et al. 2011).

3.8 Image analysis

All the image analysis was done using MATLAB (http://www.mathworks.com/), including the image analysis toolbox, and Fiji (http://fiji.sc/Fiji/). Statistical tests were performed using MATLAB statistics and bioinformatics tool box. A software pipeline was developed in MATLAB to perform automated image analysis. The pipeline comprised of functionally diverse and compatible modules implemented as functions. These could be combined to quantify and systematically record parameters that were subjected to further analyses. Scripts were contributed by Dr. François Nédélec and Dr. Serge Dmitrieff.

An example of data analysis with the pipeline is shown in figure 3.3 where marginal band length is calculated over time using images of platelets labeled with SiR tubulin. Image files containing 4D (z-stacks of 2D images in time) data were read into the pipeline using *tiffread.m* (written by Dr. François Nédélec) or bio-formats importer (http://www.openmicroscopy.org/). These raw images were stored as 3D matrices. Figure 3.3 (blue module) shows such a maximum intensity z-projected (MIP) stack.

The images were then processed to identify individual platelets. To identify platelet boundary a large sized median filter was used to blur the labeled marginal band. The background was then flattened for uneven illumination by quadratic fitting and a threshold value for background was determined. The shape was identified and the estimated background threshold was subtracted from intensity values taken from

the raw data. Figure 3.3 (red module) shows a MIP of the segmented platelets. With the segmented images, we were able to identify platelet parameters like, summed fluorescence intensity (I_{plt}) (figure 3.4 (A) (i)). The 2D projected shape of the segmented platelet was used to identify the outer boundary pixels (modified convex hull using MATLAB image analysis toolbox) which were then used calculated the mean platelet radius using ellipse fitting (figure 3.4 (A) (ii)).

Individual platelets were then subjected to further processing (Figure 3.3; green module) to identify the marginal band. First, a small sized median pixel was used to eliminate speckle noise. Then the platelets were registered over time using the tracking algorithm, *Matlab Particle Tracking Code,* developed by Daniel Blair and Eric Dufresne (http://site.physics.georgetown.edu/matlab/index.html). A second threshold for each of the tracked platelets was then determined, which was smoothed over the track by linear regression to reduce noise in the data due to thresholding. With this we were able to identify pixels corresponding to the marginal band (figure 3.4 (B)), the summed intensity of which was recorded as the parameter I_{mt}. Once the pixels comprising the marginal band were identified, the 3D matrix (I), of dimensions X by Y by Z, was converted to a point cloud (P).

$$I = \begin{bmatrix} I_{111} & \cdots & I_{1y1} \\ \vdots & \ddots & \vdots \\ I_{x11} & \cdots & I_{xy1} \end{bmatrix} \cdots \begin{bmatrix} I_{11z} & \cdots & I_{1yz} \\ \vdots & \ddots & \vdots \\ I_{x1z} & \cdots & I_{xyz} \end{bmatrix}$$

with, $1 \leq x \leq X; 1 \leq y \leq Y; 1 \leq z \leq Z$. While, $I_{xyz} \geq 0$

$$P = \begin{bmatrix} x & y & z & I_{xyz} \\ \vdots & \vdots & \vdots & \vdots \end{bmatrix}$$

This creates a 2D list with coordinates to each non-zero pixel and their corresponding intensity values. Such a point cloud is plotted in Figure 3.3 (green module).

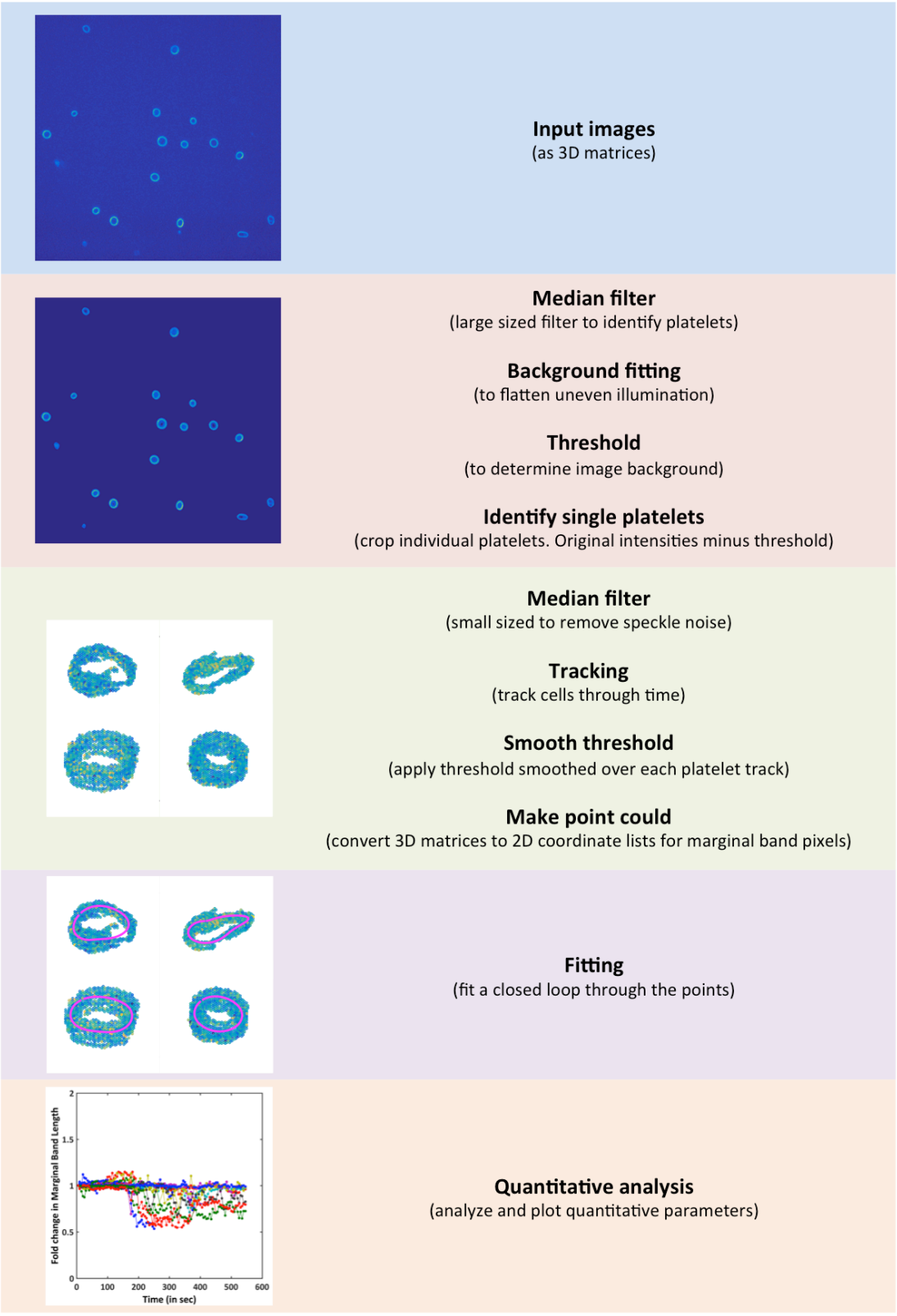

Figure 3.3: Schematic of the image analysis pipeline. An example describing processing during measurement of MB length. Different modules (coloured boxes) detail the steps implemented in each of them with an example of the output after each step.

To quantitatively determine the marginal band morphology, a mean plane was fit through the weighted data points, such that it minimizes the distance from all the points. A similar plane could be identified by performing principal component analysis (PCA) on the three dimensional data points (figure 3.4 (C)). This detects any tilts in marginal band orientation that can be straightened out. A closed loop was then fit through the data points by spline averaging (Figure 3.3; purple module). The fitting was scripted by Dr. Serge Dmitrieff. Many quantitative parameters, like marginal band length (Lmb), degree of coiling or out of planeness (OOPness), compactness (distFit), etc. were obtained upon fitting. The OOPness was determined as the average distance of the points on the curve from the fitted plane, normalized to their radial distance. distFit was the error of the fitting calculated as the least square distance of marginal band points from the fitted curve.

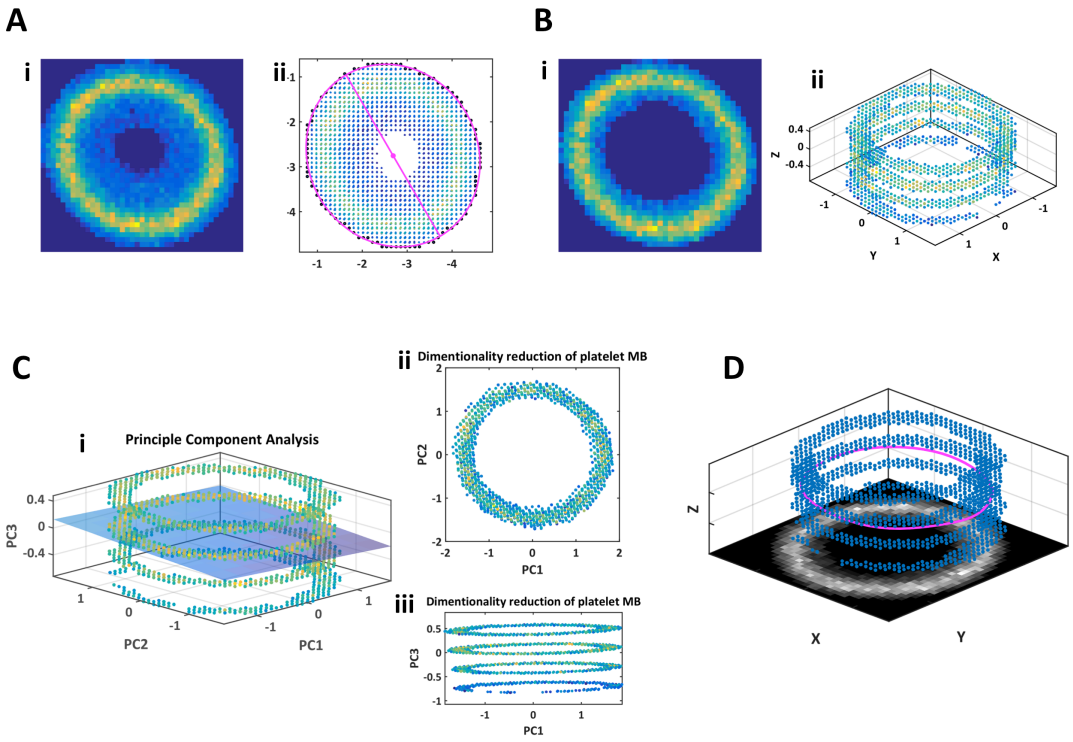

Figure 3.4: Quantitative parameters and how to find them. Illustration of the quantitative parameters used to describe properties of the platelet and the marginal band. **(A)** Parameters from cropped platelet after background subtraction. (i) Summed pixel values give summed intensity of platelet (I_{plt}). (ii) Platelet boundary pixels used to fit an ellipse (magenta) to get mean platelet radius. **(B)** Marginal band parameters obtained after second thresholding. (i) Summed pixel values give summed intensity of marginal band (I_{mt}). (ii) 3D representation of marginal band pixels. Average distance pixels from centre gives mean marginal band radius. **(C)** Identifying the plane of the marginal band using minimization of least squares or principal component analysis. (i) Marginal band with plane described by first and second principal components (PCs). (ii) Data projected along PC1 and PC2. (iii) Data projected along PC1 and PC3. **(D)** Closed curve (magenta) fitted to the marginal band points (blue). Maximum intensity projection of the image at the base of the axis.

After quantification of individual tracked platelets, any of the quantitative parameter could be analyzed over time. The plot in figure 3.3 (orange module) shows changes in marginal band length over time upon platelet activation with ADP. The analyzed data was stored in the form of a MATLAB structure array.

This method of data analysis was also applied to the data we had from experiments other than just light microscopy, i.e. electron tomography, super-resolution microscopy as well as simulations. As a result, the quantitative parameters were directly comparable.

3.9 Simulations

To understand the physical implications of our hypothesis for marginal band coiling, we used the software *Cytosim* (http://www.cytosim.org) to simulate this process. Cytosim uses a Brownian dynamics approach, specialized to simulate cytoskeleton.

Our simulations of the platelet disc-to-sphere transition consisted of a space containing dynamic microtubules and cross-linking motors. Actin was not explicitly simulated as individual fibers, but the effect of increase in actin contractility was implemented by using a contractile simulation space. This was implemented by Dr. Serge Dmitrieff, where the simulation space had a term associated with it representing surface tension. An increase in the surface tension caused the space to geometrically transform to a shape that minimizes surface area for a conserved volume. The cross-linking motors had a specificity for walking towards the plus or the minus end, mimicking the behavior of kinesin or dynein motors.

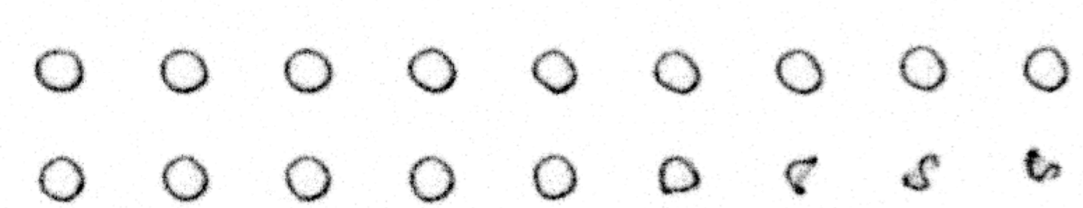

Chapter 4

Results

4 Results

The objective of my research was to understand the role of cytoskeletal mechanics in platelet function. Specifically, I wanted to address how mechanical properties of the cytoskeleton determine resting platelet size and explore their role in shape changes that occur during the first step of activation. To this end I, with multiple collaborations, made use of different experimental techniques to query the structural as well as dynamic aspects of platelet morphology. Our approach was based on directly measuring the organization and dynamics of the microtubule (MT) cytoskeleton, and inferring the mechanical state of the platelet based on it.

We made use of electron tomography to explore the detailed spatial organization of platelet MT cytoskeleton. Additional structural information, regarding the number and arrangement of MTs was obtained by using super-resolution microscopy. The aforementioned techniques required platelets to be fixed, so to analyze platelets in a more native form, we used live cell light microscopy. Coupled with quantitative analysis methods, this allowed us to assess large platelet populations and quantify the natural variation in the parameters that determine their mechanical properties. Based on the structural insights from our data in combination with existing knowledge in the field, we established a simulation of the marginal band coiling process that made predictions about the role of cortical cytoskeleton in this process. To address these predictions, we used live cell microscopy together with microfluidic devices, which enabled us to visualize the activation process and quantify the dynamic changes in MT marginal band properties. Design of the imaging setup also allowed us to carry out perturbations in platelet mechanical properties and analyze their effects on marginal band morphology during activation process. Quantitative assessment of the observed platelet behavior enabled us to uncover possible mechanisms by which cytoskeletal mechanics could determine the morphology of platelets and drive the shape changes during activation. Based on our data, we have proposed a model for mechanics of platelet MT marginal band coiling during activation. Attempts were made to quantify volume of platelets during activation to test the underlying assumption of volume conservation in the model. Preliminary results are stated below while the work remains in progress.

4.1 Platelet marginal band structure

Morphology of a cell is highly dependent on the organization of underlying cytoskeleton. In the case of platelets, their discoid resting shape is a result of balance of forces applied by the marginal band composed of microtubules (MTs) and the membrane cytoskeleton comprising of actin-spectrin network. This discoid shape is

lost upon depolymerization of MTs (White & Rao 1998). To get a better understanding of the mechanical properties of the marginal band, we decided to characterize its structure and composition by making use of electron tomography and super-resolution microscopy. The experiments were performed on fixed, resting platelets. Our results are described below.

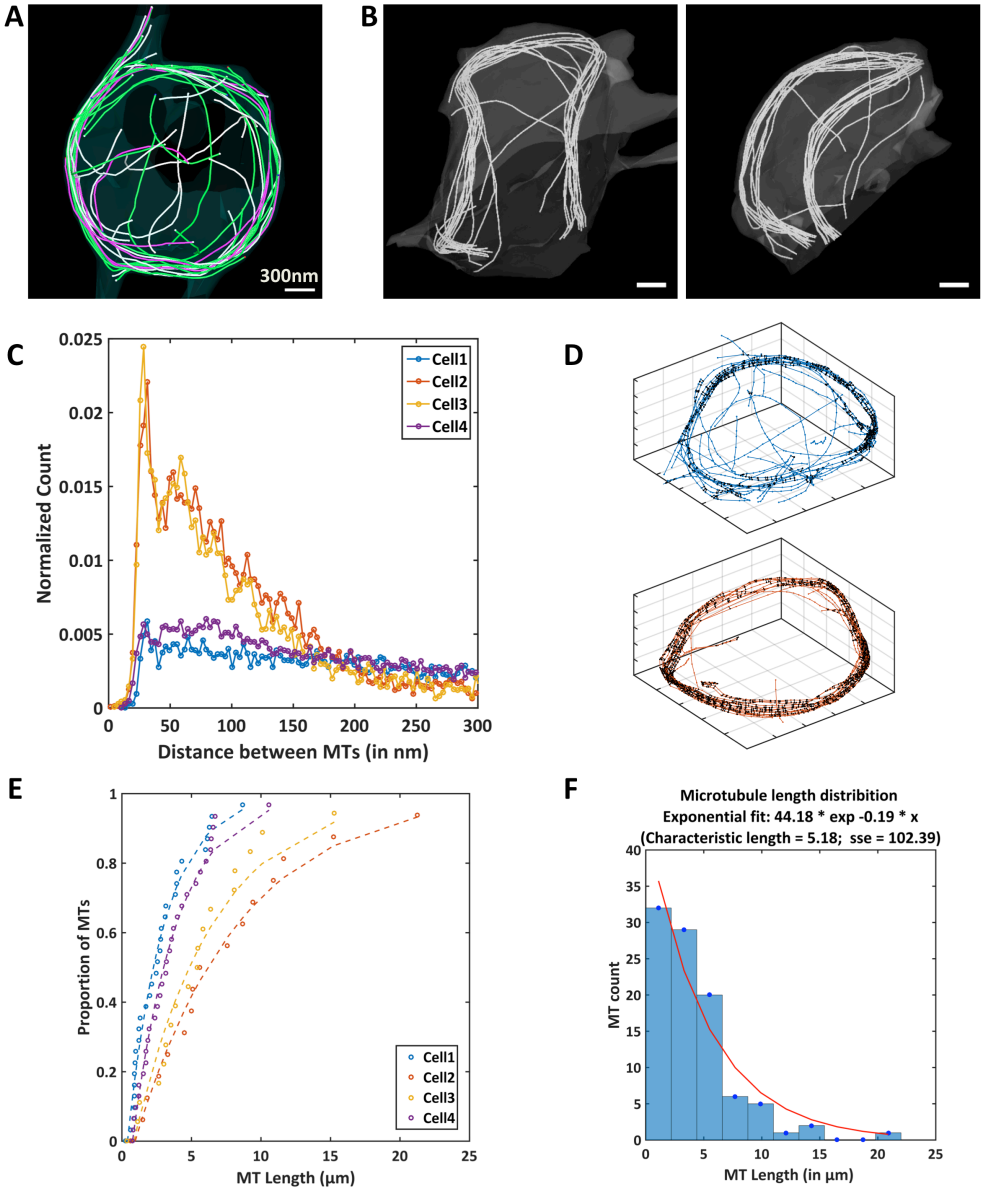

Figure 4.1: Structural organization of MTs with electron tomography. (A) 3D modeled tomogram of a platelet showing MTs running clockwise in green, counter-clockwise in magenta, and of unknown polarity in white. Membrane profile shown in semi-transparent green. **(B)** Two views of a partially coiled platelet with MTs in white. Scale bar: 300nm. Membrane profile shown in semi-transparent white. **(C)** Histogram of pairwise distances between MTs. Distances cut off at 300nm. Counts normalized to total number of distances calculated. **(D)** Two example platelets, Cell1 and Cell2, showing pairwise distances cut off at 40nm. **(E)** Cumulative MT length distribution with corresponding exponential fits as dashed lines. **(F)** Histogram of lengths of all (n=96) MTs from four platelets.

4.1.1 Electron tomography reveals organization of individual microtubules in the marginal band

Mechanical properties of a composite material are the resultant of the properties of its individual components and the interactions between them. The marginal band could be thought of as a similar material comprising of multiple MTs and cross-linking molecules that hold them together. In order to infer its properties, we decided to quantify the structure and organization of its major constituent: the MTs. Electron tomography enabled us to visualize individual microtubules within the marginal band. The transmission electron microscopy images were acquired at a pixel size of 1.5nm. This combined with serial sectioning and tomographic reconstruction gave us highly detailed 3D dataset, which was further analyzed to yield quantitative parameters. Acquisition of electron microscopy data and 3D reconstruction was done by Dr. Romain Gibeaux.

A total of four resting platelets were reconstructed, of which, one is shown in figure 4.1(A). Most of the MTs in these platelets were found bundled in the marginal band. However, some MTs do appear to bend either towards the center, mostly isolated, or in the outward projections, mostly as bundles (top of the image in figure 4.1(A)). Based on their morphology, plus-ends of MT, which are flared (Höög et al. 2011) (Gibeaux et al. 2012), and minus-ends, which are blunt (O'Toole et al. 2003), could be identified. Neither the plus nor the minus ends were found to be clustered together indicating absence of a localized nucleation, assembly or disassembly center for MTs. The marginal band was found to be a bundle of MTs with mixed polarity, as shown previously (Patel-Hett et al. 2008). In addition, we directly observed the presence of antiparallel overlaps within the marginal band, which could serve as sites for generation of forces by MT associated molecular motors like kinesin (Kapitein et al. 2005) and dynein (Tanenbaum et al. 2013). Coiled marginal band have already been shown to occur in freshly extracted blood due to activation of platelets (Diagouraga et al. 2014). We were also able to visualize such a coiled state of the marginal band in our electron tomography data (figure 4.1(B)). Due to the loss of a serial section, the marginal band was not complete and could not be used for quantification.

It has been previously estimated that platelet marginal band contains a total length of approximately 100µm of polymerized MTs. This estimate is based on average MT numbers in marginal band cross-section (≈10) multiplied by the average platelet circumference ($2\pi r$; $r \approx 1.75\mu m$) (Kenney & Linck 1985). It is also known that 56.7±2.8% of total tubulin content of a resting platelet is found in polymerized form, which amounts to 31.86 fg per platelet (Steiner & Ikeda 1979). This corresponds to

an equivalent length of approximately 112.4µm of polymerized MTs. Our electron tomography data, where MTs can be individually followed, is in agreement with this estimate as the total MT length adds up to 101.84µm ±12.63 (figure 4.2). However, the average number of MTs in the platelets (24 ±8.1; figure 4.2), though variable, is much larger than that estimated from marginal band cross-section, or localization of MT plus end (EB1: 8.7±2) or minus end (Gamma tubulin: 9.06±1.6) markers (Patel-Hett et al. 2008).

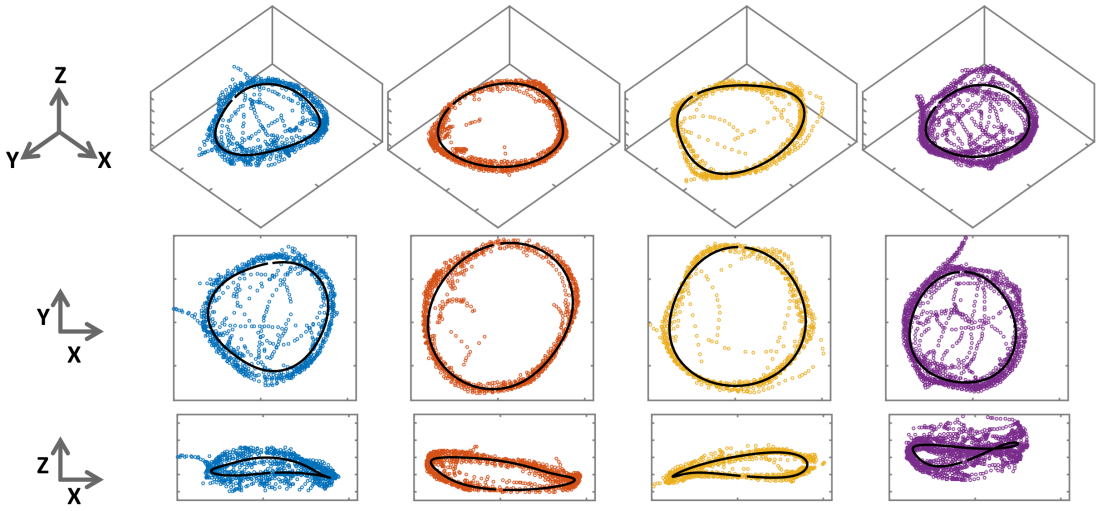

Number of MTs	31	16	18	31
Mean MT length (µm)	2.78	7.16	5.42	3.52
Total MT length (µm)	86.19	114.64	97.53	109.0
Lmb (µm)	6.14	7.83	7.39	5.94
OOPness	3.1×10^{-3}	0.98×10^{-3}	3.2×10^{-3}	7.8×10^{-3}
distFit (µm)	0.241	0.136	0.156	0.272

Figure 4.2: Quantitative parameters from electron tomography data. The plots show MT contours (dotted and coloured) from different views with the fitted curve in black. The table contains measured parameters in black (number, mean and sum of length of MTs) and fitted parameters in gray. Lmb: length of curve fitted to marginal band, OOPness: Average distance of points from fitted plane of maximum variance, distFit: Average distance of points from the fitted curve.

The previously inaccessible parameter that our data allows us to explore is the length of individual MTs that make up the marginal band. Figure 4.1(E) shows the cumulative distribution of MT lengths in each of the platelets with the corresponding exponential fits. Cell2 and cell3, which have fewer yet longer MTs, better match an exponential curve. Since there is only a small number of MTs in each platelet, we pooled all the MTs from the four platelets to get a better grasp on MT length distribution in the population. The histogram in figure 4.1(F) shows the distribution with an exponential fit. The characteristic length was found to be 5.18µm. An exponential distribution of MT lengths in a population is indicative of dynamic instability model of MT growth (Mitchison & Kirschner 1984) (Karsenti et al. 2006). This hypothesis was previously proposed for MTs in platelet marginal band based on MT growth speeds and regimes coupled to an exhaustive pool of free tubulin monomers (Patel-Hett et al. 2008). The distribution of MT lengths from our data supports this hypothesis.

With the 3D spatial organization of MTs at our hands, we can measure the distances between them. This allows us to explore the mechanical properties of the marginal band by looking at the arrangement of MTs and possible interactions between them. Figure 4.1(C) shows a histogram of the pairwise distances between splined MTs. The counts are normalized to the total number of pairwise distances that were calculated per platelet. From the histograms, we can observe high level of similarity between the cells 1 and 4, and cells 2 and 3. A peak in the histogram is found to occur at around 30nm in all four platelets but is more evident in cells 2 and 3, and less so in cells 1 and 4. This peak is followed by a dip around 40nm in all platelets. The pairwise distances of up to 40nm have been marked in the figure 4.1(D) for cells 1 and 2 to compare the MT organization in the morphologically different marginal bands. Here, cell 2 which has four to five times as many short, 30nm, distances seems to have a more compactly packed marginal band. Cell 2 also has fewer and longer MTs, which suggests that, as in cell 1, shortening of MT length and increase in their number is concomitant with loosening of the marginal band. In addition, preference for a certain distance between MTs could be a range set by cross-linkers that hold them together. It could also be suggestive of the band's propensity to expand or contract dependent on the nature of motors and cross linkers that can bind the parallel and anti-parallel MT overlaps (Ward et al. 2014). In the distance histogram, cells 2 and 3 also show a second peak between 50 to 60 nm after which the distances rapidly decay. In cells 1 and 4, on the other hand, the proportion of longer distances plateaus and the decay is gradual.

The MT coordinates from electron tomography data, shown as scatter plots in figure 4.2, were also analyzed using our data analysis pipeline. This yielded quantitative parameters and made our data generated with different techniques directly comparable. As shown in figure 4.2, the shape of the marginal band is well recapitulated by the fitted curve (in black). By comparing the parameters like length of the marginal band (Lmb), degree of coiling of the band (OOPness) and distance of points from the fitted curve (distFit), we can conclude that cells 2 and 3 are likely to be in a resting state, while cells 1 and 4 seem to be getting activated. This is based on the fact that the marginal bands in cells 2 and 3 are flatter and more compact. Marginal bands with tightly packed MTs are known to occur in resting platelets. In cells 1 and 4, shortening of Lmb is accompanied by a higher degree of coiling and less compactness. Loosely packed MTs are associated with platelets that have started to get activated (Nachmias 1980).

The differences in the morphologies of the marginal band can be traced back to the preparation of sample for tomography. Cells 1 and 4 were from the same batch while cells 2 and 3 belonged to another. Since platelets are very sensitive to changes in their chemical and physical environment, variations in the extraction phase can be very important as they might affect the marginal band morphology. Due to the extremely low throughput of electron tomography, no repetitions were made and other techniques were adapted to get more information.

4.1.2 Quantifying microtubule numbers and organization with super-resolution microscopy

Localization based super-resolution microscopy provides a gain in resolution over light microscopy by algorithmically locating the point source of light with very high precision. This technique can yield a resolution of 30 nm laterally and 50nm axially. Sample preparation for super-resolution microscopy is based on immunofluorescence, which provides an opportunity to visualize proteins other than tubulin. This technique also provides a higher throughput as compared to electron tomography, but the resolution is around an order of magnitude lower. As a consequence, the direct visualization of individual MTs packed in a marginal band was not possible. Thus, we adapted this method to get information about the number of MTs in the platelet by labeling a MT minus-end marker, gamma tubulin. These experiments were performed in collaboration with Dr. Jonas Ries' lab. Sample fixation, labeling and image acquisition was done by Tooba Quidwai.

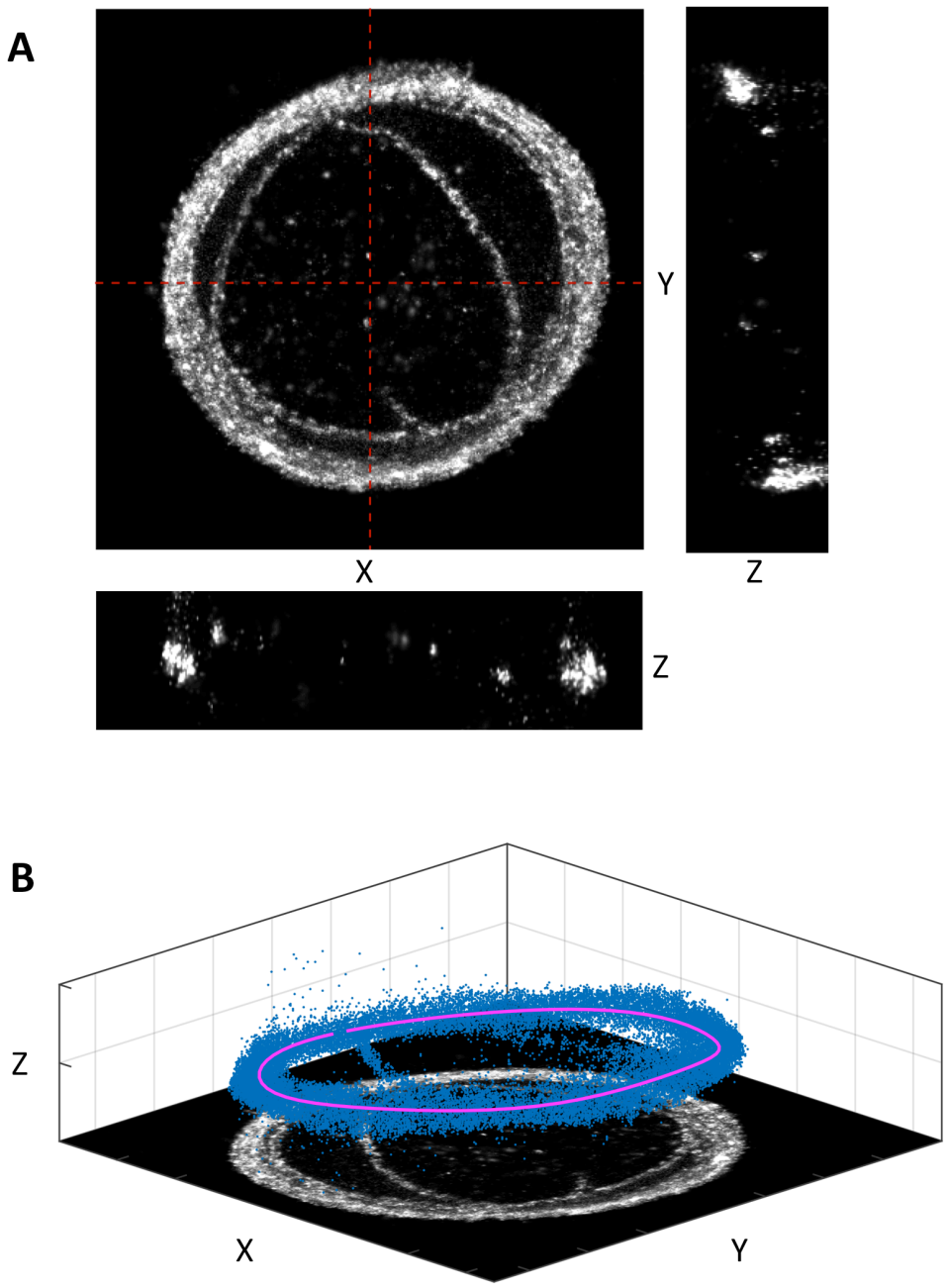

Figure 4.3: Super resolution imaging of platelet marginal band. (A) Maximum intensity projection along the axial dimension of a platelet labeled for alpha-tubulin. Image on the right shows intensities along the axial dimension and the vertical dashed red line. Image at the bottom shows intensities along the axial dimension and the horizontal dashed red line. **(B)** A 3D-plot of pixels isolated (blue) from the image projected at the base of the axes. The fitted curve is shown in magenta.

4.1.2.1 Assessing marginal band structure by alpha tubulin labeling

Using super-resolution microscopy, our first objective was to resolve individual MTs in the platelet marginal band. To this end, platelets were fixed and labeled with anti-α-tubulin primary antibody followed by a secondary antibody coupled to a dye molecule. A representative image is shown in figure 4.3(A), where single MTs running into the center of the platelet can be easily identified. However, most of the MTs that are confined to the marginal band are too closely packed to be followed individually. The widths of single MTs in platelet center were measured by fitting Gaussian curves to line profiles across the MTs and recording the full width half maximum (FWHM) of the curve. Recorded widths were found to vary between 30nm to 50nm with high standard deviations of 10nm to 20nm. The use of a primary followed by a secondary antibody for protein labeling, displaces the dye molecule (carried by the secondary antibody) from the site of protein localization by approximately 10nm (Ries et al. 2012), introducing a linkage error. Considering the known width of a MT (25nm (AMOS & Klug 1974)), we expect an additional error of around 20nm. From our electron tomography data, we could observe a peak in centre-to-centre pairwise distances at 30nm in resting platelet marginal bands. This implies that the MTs could be down to 5nm apart in the marginal band. Thus, with our current method, we do not expect to be able to identify individual MTs in the platelet marginal band.

The images with labeled marginal bands were run through the data analysis pipeline and the fitted curve followed the marginal band very well (figure 4.3(B)). A total of 20 platelets were analyzed. Figure 4.4(A) shows a gallery of the isolated marginal band pixels and a curve fitted through it. Since imaging was performed on resting platelet samples, the isolated marginal bands were flat and circular. This is shown in the figure 4.4(B), where the mean distance of marginal band pixels from platelet centre, or the average radius of the marginal band, when plotted against the length of the marginal band, or the perimeter, falls on the $y = 2\pi*x$ line. Other quantitative parameters, like marginal band intensity (I_{mt}; figure 4.4(C)), band intensity per unit length (figure 4.4(D)), compactness of band (figure 4.4(E)) and degree of coiling (figure 4.4(F)) were calculated but correlation between these parameters and the length of the marginal band was not observed. Very low values of OOPness show that the marginal band is not in a coiled state.

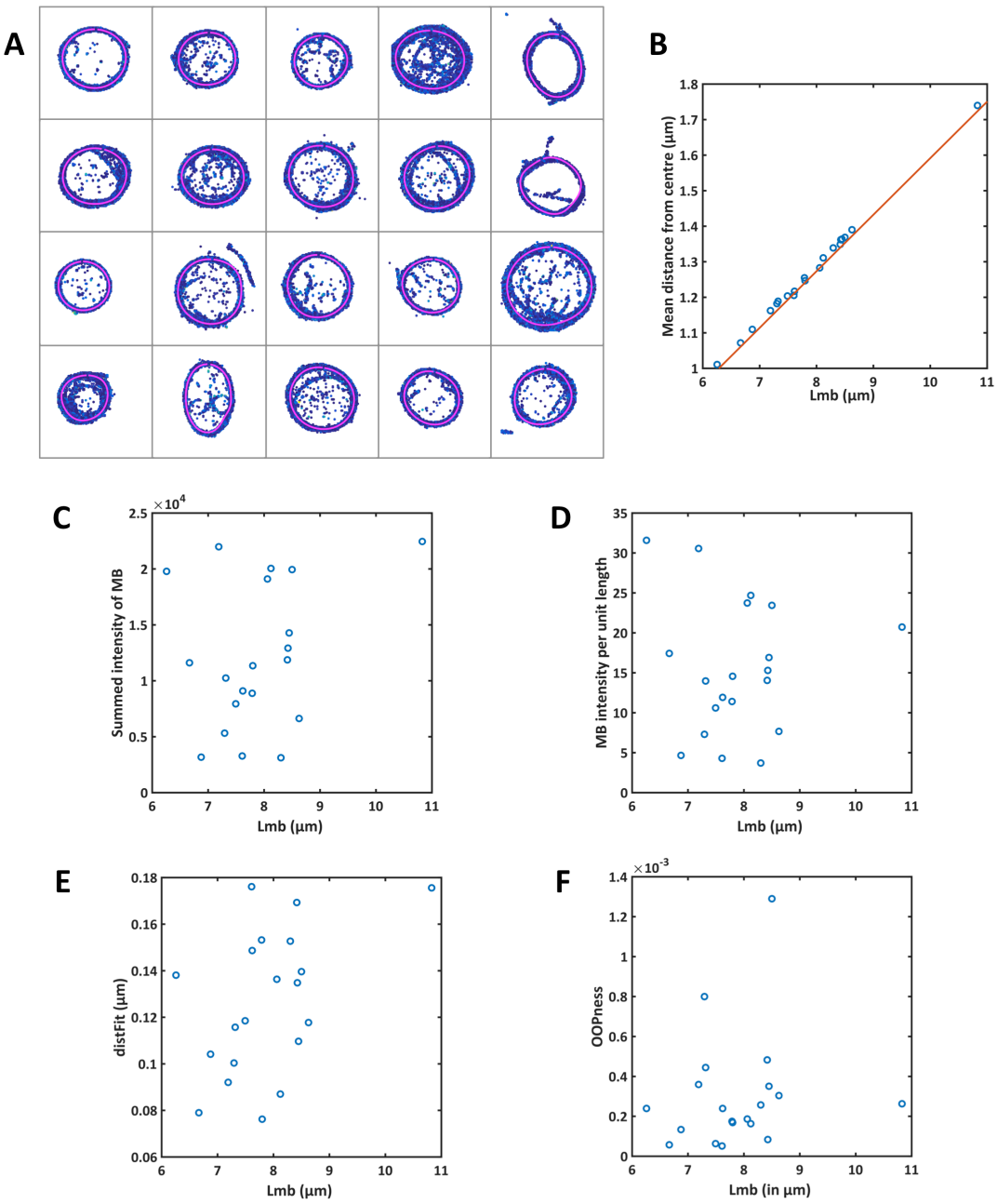

Figure 4.4: Quantitative parameters from super-resolution imaging data. (A) Gallery of platelet marginal bands (blue points weighted to intensities) with fitted curves in magenta. **(B)** Plot showing circularity of marginal band as the data points (blue circles) fall on the y = 2π*x line in red. (C, D, E, F) Plots showing variation in the values of quantitative parameters with length of marginal band.

4.1.2.2 Gamma tubulin as readout for microtubule numbers scales with marginal band length

The compact packing of MTs in the marginal band prevented us from directly measuring the numbers and length of individual MT with super-resolution microscopy. However, this technique allowed us to tag other proteins of interest in addition to alpha-tubulin. Gamma-tubulin is known to often associate and stabilize the negative end of a MT. We made use of gamma-tubulin to mark the relatively stable minus end (in contrast to the dynamic plus end (Patel-Hett et al. 2008)) of the MT and used the number of gamma-tubulin foci as a proxy for the number of microtubules in the marginal band. Figure 4.5(A) shows a diffraction-limited image of gamma-tubulin foci over alpha-tubulin marginal band. A total of 113 platelet marginal bands were analyzed over four separate experiments. We observed an average of 8.26 ±2.6 gamma-tubulin localizations with diffraction-limited microscopy. This number is in agreement with what has been previously reported (Patel-Hett et al. 2008). However, upon subjecting the samples to 3D super-resolution microscopy, many of the diffraction-limited foci could be further resolved into multiple localizations (figure 4.5(B)). As a result, we obtained a different distribution for the number of gamma tubulin foci (figure 4.5(C)) with an average of 25.18 ±6 foci per platelet. This number is much larger than reported in literature, but falls within the range that we measured on our electron tomography data (24 ±8.12).

With the ability to label multiple proteins at the same time, we tagged alpha and gamma tubulin in the same population to find the correlation between number of MTs in a platelet and the length of the marginal band. The gamma-tubulin foci were counted in the super-resolution images, whereas alpha-tubulin was acquired in 2D diffraction-limited format. The projected marginal band length was calculated by fitting an ellipse to the thresholded 2D alpha-tubulin signal. The plot in figure 4.5(D) shows how the length of the marginal band changes with the number of MTs. The data has high variability, but when we perform an orthogonal fit using principal component analysis (PCA) on log values of the data, we find that the marginal band length scales as the square of the number of MTs.

$$L_{MB} \propto (N_{MT})^2$$

where, L_{MB} is the length of the marginal band and N_{MT} is the number of MTs based on the number of gamma-tubulin foci. The foci are, however, not always associated with the marginal band. As evident in the image (figure 4.5(B)), some gamma tubulin foci are present in the centre of the platelet. The fidelity of these localizations is being further investigated by double label super-resolution microscopy for co-labeling alpha-tubulin or other minus end markers like CAMSAP with gamma-tubulin. The information regarding scaling of number of MTs with the marginal band length

would tell us about the changes in mechanical stability of the marginal band as it gets longer. A marginal band composed of more numerous and shorter MTs can be expected to be harder to deform.

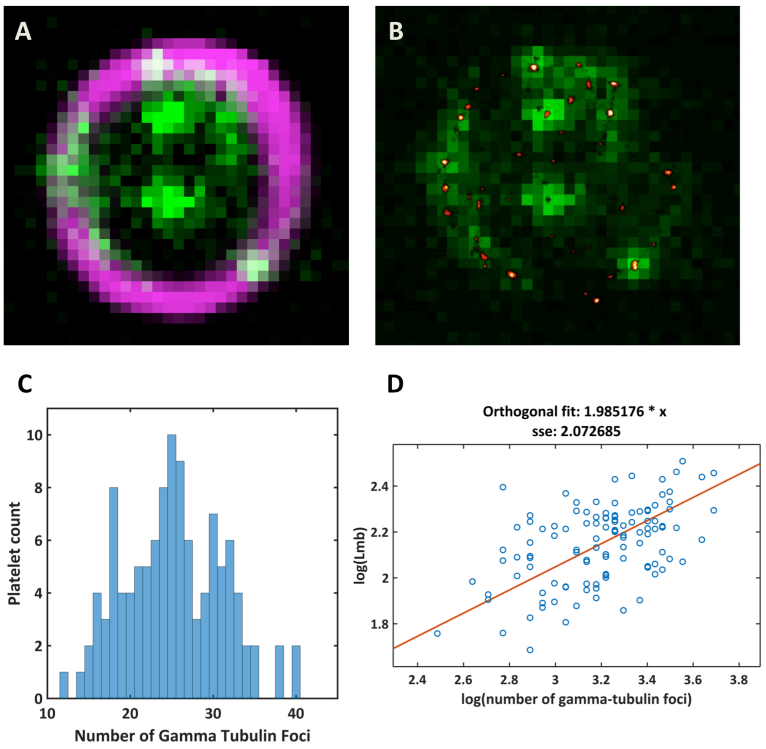

Figure 4.5: Quantification of number of microtubules in marginal band. Estimation of number of microtubules in marginal band by counting gamma-tubulin localizations in resting platelets **(A)** Diffraction limited imaging. Magenta: alpha-tubulin, Green: gamma-tubulin. **(B)** Red: Super resolved gamma-tubulin, Green: Diffraction limited gamma-tubulin. **(C)** Histogram of number of gamma-tubulin foci. **(D)** Dependence of length of the marginal band on number of MTs. Data is plotted as log values. Orange line shows an orthogonal fit.

4.2 Quantification of live platelet marginal bands reveals intrinsic population variations

The physiological function of a platelet is dependent on the changes in morphology this highly specialized cell is able to undergo. These changes are known to be brought about by the mechanical interaction of cytoskeletal structures, which also determine the platelet shape and size (Thon & Italiano 2012). Our approach was to quantify marginal band morphology in platelet population with the aim to infer its mechanical properties. However, the high intrinsic variation in the quantitative aspects of platelets often obscure the dependencies between these parameters and make it difficult to uncover their mechanical behavior. Thus, to infer the parameter dependencies, we analyzed large populations of live platelets, which helped us

discover such correlations even in populations with high variability. Additionally, examining live platelets in a microfluidic setup mimicked a, close to, physiological state that reduced the chances of additional artifacts. Thus, to understand the mechanical implications of platelet shape, we used light microscopy with sophisticated analysis methods to quantitatively assess the role cytoskeletal elements play in this process. The morphology was recorded by visualizing the microtubule marginal band in live platelets. The experiments, in part, were performed by Sandra Correia.

4.2.1 Microtubule label SiR tubulin does not perturb resting marginal band structure

To get an accurate measure of platelet sizes in near physiological settings, quantification was done on live resting platelets in suspension. The platelets were extracted from transgenic GFP tubulin mice, which gave a fluorescent signal that was mainly localized to the platelet marginal band (Figure 4.6). However, tubulin GFP is also present in soluble form, which is evident with the high fluorescence intensity inside the platelet compared to outside. This resulted in low signal to noise ratio and an eventual loss of accuracy during segmentation of the marginal band. To improve the visibility of the marginal band, we used SiR tubulin, which is a bright silicon rhodamine derived dye coupled to a taxol based probe. Since SiR tubulin selectively binds polymerized MTs (Lukinavičius et al. 2014), the signal to noise ratio for the marginal band improved (Figure 4.6), which enabled us to more precisely analyze the marginal band.

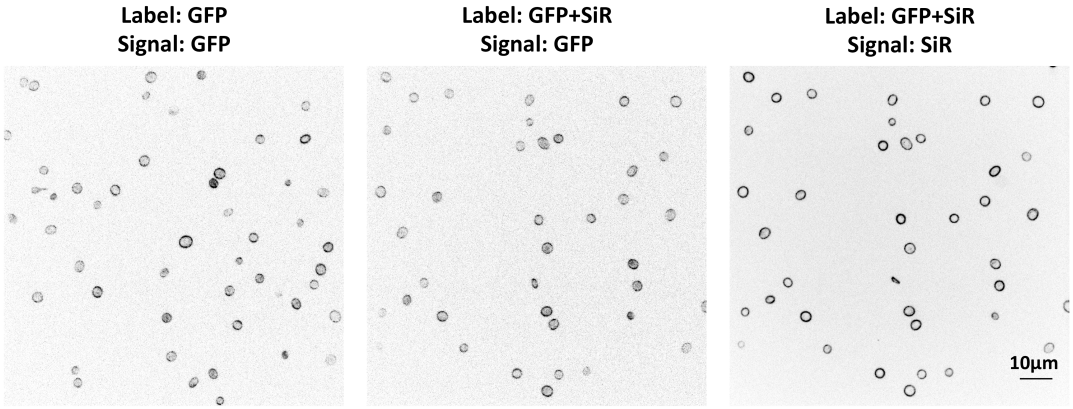

Figure 4.6: Imaging of live platelet marginal band. Representative images (maximum intensity projections of 3D acquisitions) of live resting platelets from GFP tubulin mice. Marginal band is visualized using GFP tubulin fluorescence (left and central panel) or SiR tubulin (right panel). Note the high signal to noise ratio with SiR tubulin signal due to labeling of only polymerized tubulin.

Taxol has long been known as an MT stabilizing molecule (Schiff & Horwitz 1980). Addition of taxol decreases the rigidity of MTs (Mickey & Howard 1995) and hence the MT response to forces applied on them is changed. SiR tubulin probe binds MTs via doxytacel, a taxol based compound. The high affinity and brightness of the probe allows us to use it at very low concentrations of 100nM to 50nM. A concentration of 100nM was reported to not significantly affect cell viability upon long term imaging (Lukinavičius et al. 2014). To ensure that addition of SiR tubulin does not significantly perturb platelet properties, we compared GFP tubulin platelets with and without SiR tubulin. Figure 4.7 (A) shows a comparison of distribution of platelet radius for the two treatments. The two populations are found not to be significantly different from each other based on a two-sample t-test (p-value 0.0143). The GFP only population had a mean radius of 1.6µm ±0.27 and the GFP with SiR platelets had a mean radius of 1.6µm ±0.26. No significant difference is observed in the distribution of total GFP tubulin intensity between either of the populations (t-test, p-value: 0.7371). It is noteworthy that the population shows a fairly narrow distribution for platelet radius with a variability of around 30% (GFP only: 32.5%; GFP+SiR: 33.75%). Given a fragmentation based formation process, one could expect to see higher variation in platelet size. The observed distribution is indicative of additional mechanisms that keep the size distribution in check.

The parameter I_{plt} (summed intensity of platelet) for a GFP tubulin platelet should correspond to the total amount of tubulin present in a platelet. We wanted to investigate how this parameter would scale with the size of the platelet. Figure 4.7(C) shows a plot of I_{plt} against mean platelet radius. To uncover the power law underlying the dependence of intensity on platelet radius, we performed log transformation of the data (figure 4.7(D)), followed by orthogonal linear regression. The slope of the fitted line gives the power of the x-axis variable, with which the y-axis variable varies. Our data shows that the tubulin intensity (I_{plt}) scales as a power of 5.44 (GFP+SiR) or 4.9 (GFP) to the radius (R).

$$I_{plt} \propto R^n$$

n = 4.9 (GFP only)
n = 5.44 (GFP+SiR)

For soluble proteins, one can expect the number of molecules (or its indirect readout, intensity) to vary as a power of three of length scale (correspondingly, the radius). This would derive from the fact that at a given concentration, the total number of molecules changes proportionately with the volume, which is a power three of the length scale. A platelet can be considered as an oblate spheroid, that is,

a sphere with equatorial radius larger than the polar radius. For such a shape, we can expect the volume to vary as a power *n* of the radius, such that 2< *n* <3. The unexpected scaling behavior of our data implies that considering platelet radius alone is not sufficient to explain the observed variation in tubulin intensity. Higher power dependence, as we observe in our data, indicates that there is preferential enrichment of tubulin in platelets and it is not just a volume dependent partitioning of a homogenous soluble protein. Similar analysis when performed on platelets labeled with SiR tubulin (figure 4.7 (E) and (F)) yields an even higher power dependence (*n* = 6.6) of intensity on radius. The key difference between GFP tubulin and SiR tubulin signals is that the latter labels only polymerized MTs. Thus the summed intensity for SiR tubulin signal would correspond to the volume of the marginal band only and not of the whole platelet. Thus, a higher value of *n* in this case is expected.

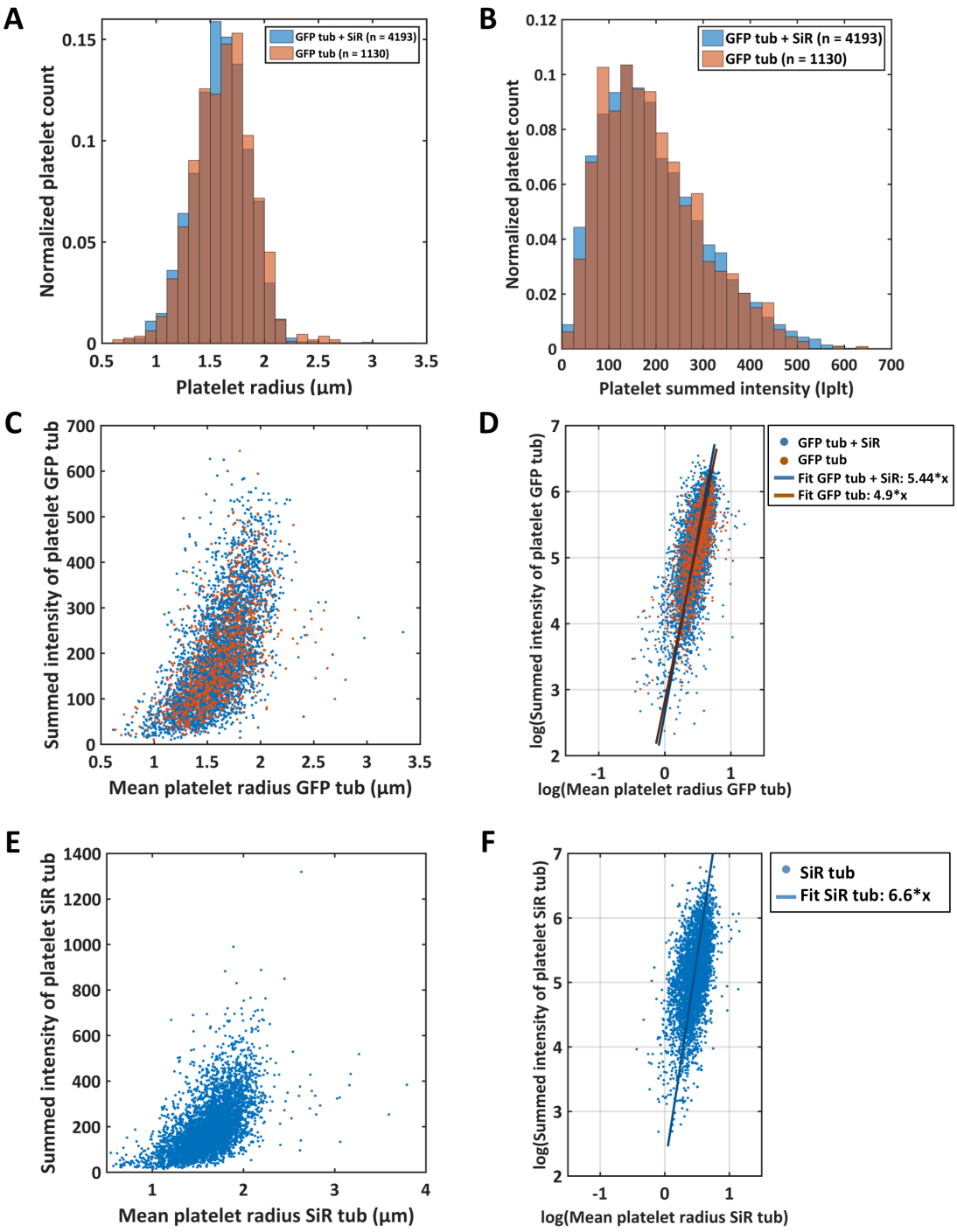

Figure 4.7: Effect of SiR tubulin on resting platelets. Comparison of GFP tubulin platelets with (blue) or without (orange) 50nM of SiR tubulin based on GFP signal. **(A)** Normalized histogram of mean platelet radius. **(B)** Normalized histogram of summed platelet intensity. **(C)** Changes in summed platelet intensity with mean platelet radius. **(D)** Orthogonal linear fit to log transformation of data in plot (C). The intensity changes as the power of 5.44 (GFP+SiR) or 4.9(GFP) to the radius. **(E)** Changes in summed platelet intensity of SiR tubulin with mean platelet radius. **(F)** Orthogonal linear fit to log transformation of data in plot (E). The intensity changes as the power of 6.6 to the radius.

4.2.2 SiR tubulin signal allows precise quantification of marginal band properties

Our results show that, in resting platelets, addition of SiR tubulin does not seem to affect platelet sizes. However, our methods of quantification are based on fluorescence intensity, which is different in case of GFP and SiR. Hence, we need to analyze how comparable our quantification is depending on which fluorescence method is used. To do this, we imaged GFP tubulin platelets labeled with SiR tubulin in their corresponding channels. After the analysis we compared measurements for the same platelets in both the channels. The plot in figure 4.8(A) shows the mean platelet radius measured in GFP and SiR channels. High degree of equivalence can be seen in both measurements, as evident from the linear regression of slope 1 and an r-squared value of 0.93. A two-sample Kolmogorov-Smirnov test was also performed on the data, which deemed that the populations were not significantly different (p-value: 0.97). When comparing the length of the marginal band (Lmb), we do not see a one-to-one correspondence in the measured values and a linear regression is meaningless given the negative r-squared value (figure 4.8(B)). Majority of data points lie above the x=y line (in gray) indicating that Lmb for GFP signal is underestimated compared to SiR signal. To pin down the reason of discrepancy in measurements, we plotted mean platelet radius (the equivalent measurement) against Lmb (the non-equivalent measurement) for both the channels (figure 4.8 (C) and (D)). For SiR tubulin signal, the two measurements correspond to each other. The data points fall below the diagonal indicating that the radius of marginal band is systematically shorter than platelet radius. For GFP tubulin signal, the data is much more variable and noisy, however, the overall trend is similar.

The reason for this mismatch is the difference in signal quality. Isolation of platelets to get parameters like mean platelet radius and platelet intensity is based on distinguishing platelet pixels from background pixels, which works well for both signals resulting in parameters that are more comparable. Calculation of platelet radius is also less dependent on the pixel values, which are different for GFP and SiR channels. Identification of the marginal band, however, is based on an additional step of automated thresholding, which needs to distinguish platelet central pixels from marginal band pixels. This difference is much smaller than in case of GFP signal where the central pixels are also fluorescent due to the presence of soluble protein. As a result, the marginal band fitting, which is sensitive to pixel values, is underestimated (figure 4.8 (D)) for GFP signal. Due to the difference in quantification of the two channels, only platelet based measures were calculated for GFP signal. Since SiR tubulin signal was brighter and more robustly quantifiable, we used it for both platelet and marginal band measurements.

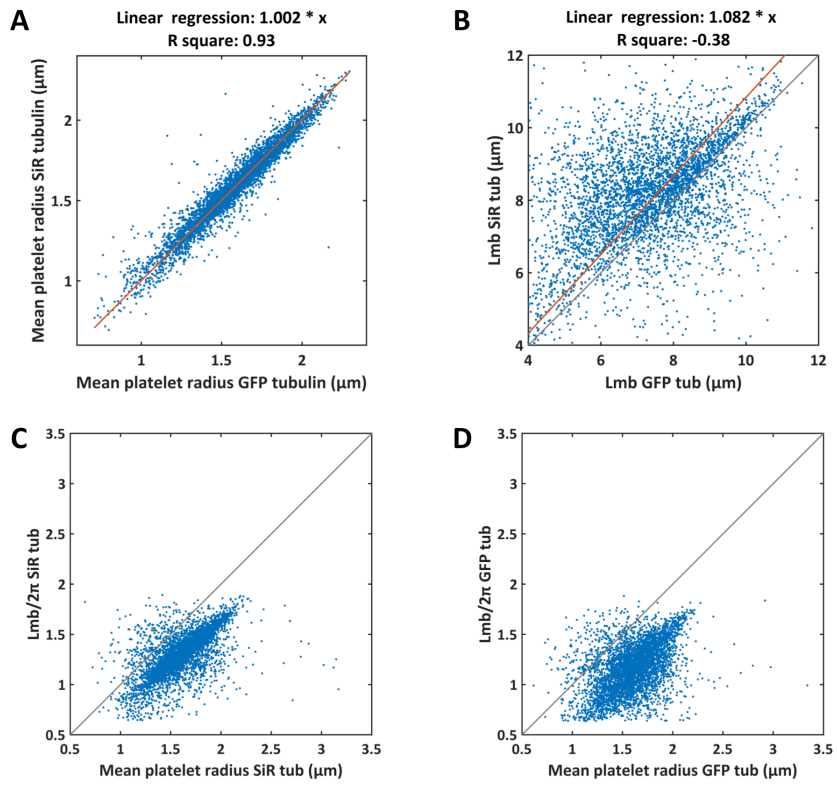

Figure 4.8: Quantification of GFP and SiR tubulin signal. Comparison of GFP and SiR tubulin signal for a set of GFP tubulin platelets (n = 4193) labeled with 50nM SiR tubulin. **(A)** Mean platelet radius analyzed using GFP and SiR tubulin signal. Red line with a slope of 1 shows linear regression. **(B)** Length of the marginal band for GFP and SiR tubulin signals. Regression (red) shows a slope of 1 but r-squared is negative. Gray line: x=y. **(C)** SiR tubulin and **(D)** GFP tubulin data comparing mean platelet radius to radius of marginal band (Lmb/2π). Marginal band radius is usually shorter than platelet radius.

4.2.3 Population variation of quantitative parameters of marginal band

The formation of platelets is a mechanically driven fragmentation process where pro- and pre- platelets break and divide to give rise to stable fragments. As a result, we expect to see a variation in their sizes. In addition, changes in properties of the cytoskeleton like actin (Bender et al. 2010) (Bender et al. 2014) and microtubules (Bender et al. 2015) (Thon et al. 2010) during their biogenesis leads to variations in the final platelet size. Our objective was to exploit this natural variation in platelet size and see how this affects the platelet propensity for activation. As a first step towards this goal, we decided to characterize the extent to which the platelet quantitative parameters vary.

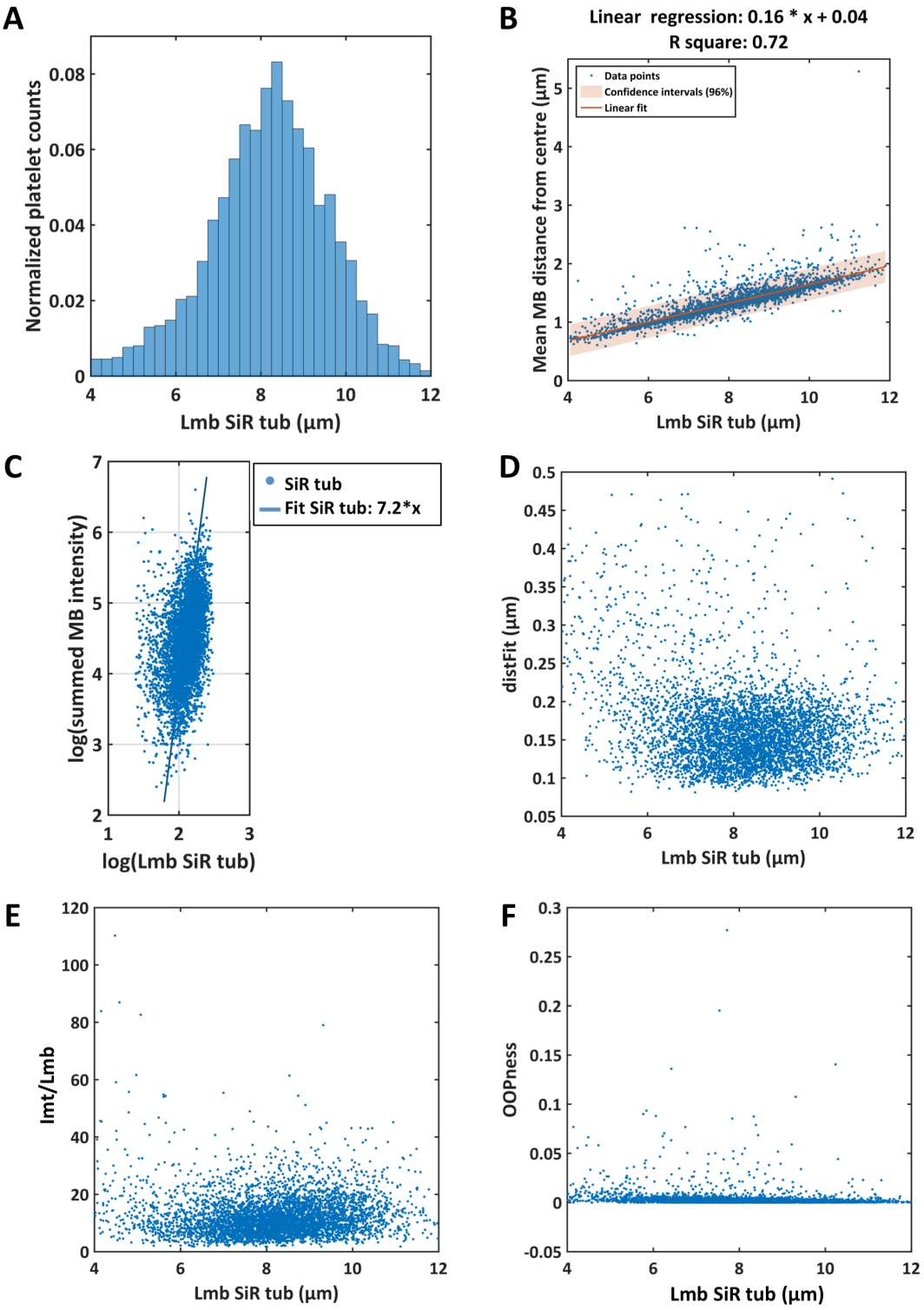

Figure 4.9: Quantification of marginal band in resting platelets. Analysis of platelets (n = 4867) labeled with 50nM SiR tubulin. **(A)** Histogram of marginal band length (Lmb). **(B)** Plot of marginal band (MB) radius versus Lmb to show MB circularity as the slope of linear regression in 1/2π. **(C)** Orthogonal linear fit to log transformation of summed marginal band intensity (I_{mt}) and Lmb. The intensity changes as the power of 7.2 of the Lmb. **(D, E, F)** Variation in quantitative parameters with Lmb.

The marginal band is the mechanical support structure that keeps the platelet in a resting morphology. As we have observed over a two-fold variation in resting platelet radius, we can also expect to see a corresponding variation in marginal band lengths. Variability in length could imply a variation in mechanical properties of the band as a function of length. Analyzing parameters of the marginal band that vary with its length can help us predict the changes in its mechanical properties. Figure 4.9 (A) shows a histogram of Lmb. The population mean was found to be 8.19µm with a standard deviation of 1.4µm. Based on expected platelet sizes, the lengths less than 4µm and more than 12µm were filtered out as either of the extremes were often caused by limited accuracy of thresholding and fitting of the marginal band. In resting platelets, the marginal band was found to be circular as seen in figure 4.9(B), where a linear regression of the marginal band radius against length gives a line of slope $1/2\pi$. The summed intensity of the marginal band seems to scale with its length (figure 4.9 (C)) as a power of 7.2, as compared to a power of 6.6, which was earlier derived from summed platelet intensity and platelet radius (figure 4.7(F)). These exponents can be expected to be the same as both summed intensities are a measure of the marginal band intensity and the length scales are either radius or perimeter. The difference in the factor for these dependencies could be attributed to an extra step of thresholding from summed platelet to marginal band intensity. However, the values are comparable as second thresholding does not drastically change the marginal band intensities for SiR tubulin labeling. The error in fitting (distFit) is evaluated as the average distance of points from the fitted curve. The cutoff for error was set at 0.5µm. The fitting error seems to be independent of the Lmb but for lengths shorter than 5µm, the error estimate is higher. If we consider the marginal band to be homogenously labeled, the summed intensity would correspond to the volume of the marginal band. So, looking at the intensity per length of the marginal band would give us an idea of the area of cross-section or density of polymer. This parameter determines the thickness and eventually the mechanical properties of the band. In a population of resting platelets it is found to be independent of the marginal band length (figure 4.9 (E)). Very low values of OOPness indicate that the resting platelet marginal band is very flat (figure 4.9 (F)).

4.3 Simulation of marginal band coiling driven by membrane associated cytoskeleton

Physiological function of platelets involves them undergoing drastic morphological changes at short time scales. Requisite for such functionality coupled with the role played by cytoskeletal mechanics in the process increases the likelihood that the coiling is a mechanically controlled process. To understand the mechanics of the disc-to-sphere transition and the parameters that could be responsible for it, we

simulated the coiling of platelet marginal band using the software cytosim. The specialized simulation space was designed by Dr. Serge Dmitrieff. The model was set up by Dr.Romain Gibeaux and Dr. Antonio Politi.

The simulation consisted of a three-dimensional space containing microtubules and two kinds of cross-linking motors (figure 4.10 (A)). A specialized simulation space was implemented to mimic a cellular cortex. A surface tension parameter was associated with it in order to implicitly simulate an increase in actin contractility by geometrically minimizing the surface area. The volume was assumed to be constant during such a transition. The number and distribution of MTs were obtained from our electron tomography data. Two kinds of cross-linking motors, one with plus end directed motility (kinesin, red) and other with minus end directed motility (dynein, blue), which are known to be associated with platelet marginal band (Rothwell & Calvert 1997), were implemented. Their numbers were kept arbitrary but equal. These motors held the MTs together and kept their distribution homogenous in the marginal band with their ability to slide MTs apart.

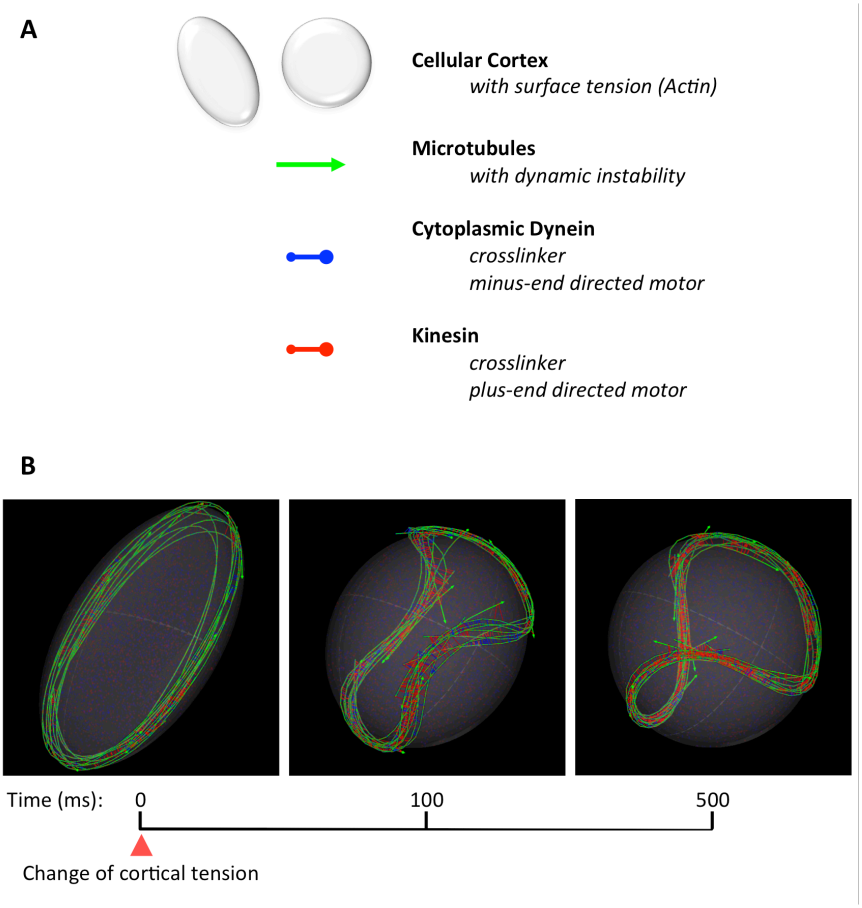

Figure 4.10: Simulation of marginal band coiling with *Cytosim*. (A) Listing of simulation components. **(B)** Effect of increase in cortical tension on marginal band. Tension was increased 16-folds at time t=0.

The simulation was initially set with MTs randomly placed inside a disk shaped simulation space. Upon addition of the motors, MTs were found to readily arrange into a marginal band. The simulation space was then sent to contractile with a low value for contractility (figure 4.10 (B), left panel). This represented a resting platelet with a flat marginal band. The contractility of the space was then increased, which caused the space to minimize its surface area and become spherical. In the process of becoming spherical, the actin cortex also pushed against the marginal band and caused it to coil. After adopting some intermediate states (figure 4.10(B), central panel), the marginal band took up the shape of what is known as the baseball seam curve (figure 4.10 (B), right panel). With the parameter values used, the shape was found to be stable. With this simple simulation, we hypothesized that the marginal band behaves like and elastic ring and actin contractility could be enough to drive its coiling.

4.4 Dynamics of marginal band during platelet activation

The disc-to-sphere transition is the first step of platelets towards activation (Diagouraga et al. 2014). During this process, while the morphology of the platelet changes from the resting disc form to the activated spherical form; the marginal band converts from a flat ring to a coiled shape (figure 4.11). To understand the process of marginal band coiling, we performed live cell fluorescence microscopy and quantitatively analyzed these shape changes over time. The experiments, in part, were performed by Sandra Correia.

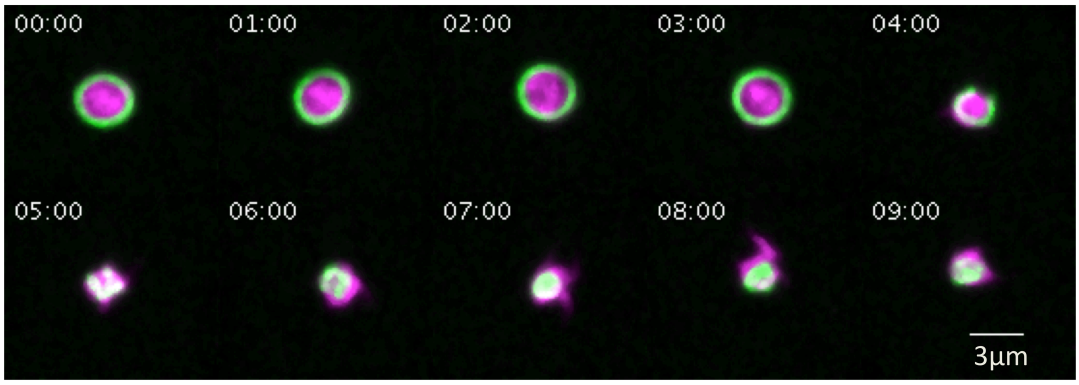

Figure 4.11: Cytoskeleton during platelet activation. Platelet undergoing disc-to-sphere transition in response to ADP (10µM). Green: Microtubules labeled with SIR tubulin (100nM). Magenta: Actin labeled with Lifeact GFP. Images are maximum intensity projections of an axial distance of 2.8µm. Time stamp in minutes.

4.4.1 Visco-elastic behavior of marginal band upon activation with ADP

Platelets have many surface receptors that bind to various agonists, eliciting an activation response. One such chemical ligand is ADP. The images in figure 4.12 show that platelets respond to ADP treatment by inducing marginal band coiling. The top and bottom panels show fluorescence from the SiR and GFP tubulin channels respectively. We observed that the fidelity of marginal band shape recognition with GFP tubulin signal reduces with platelet activation due to higher fluorescence background in a smaller shape. Hence the marginal band measurements were made on SiR tubulin signal.

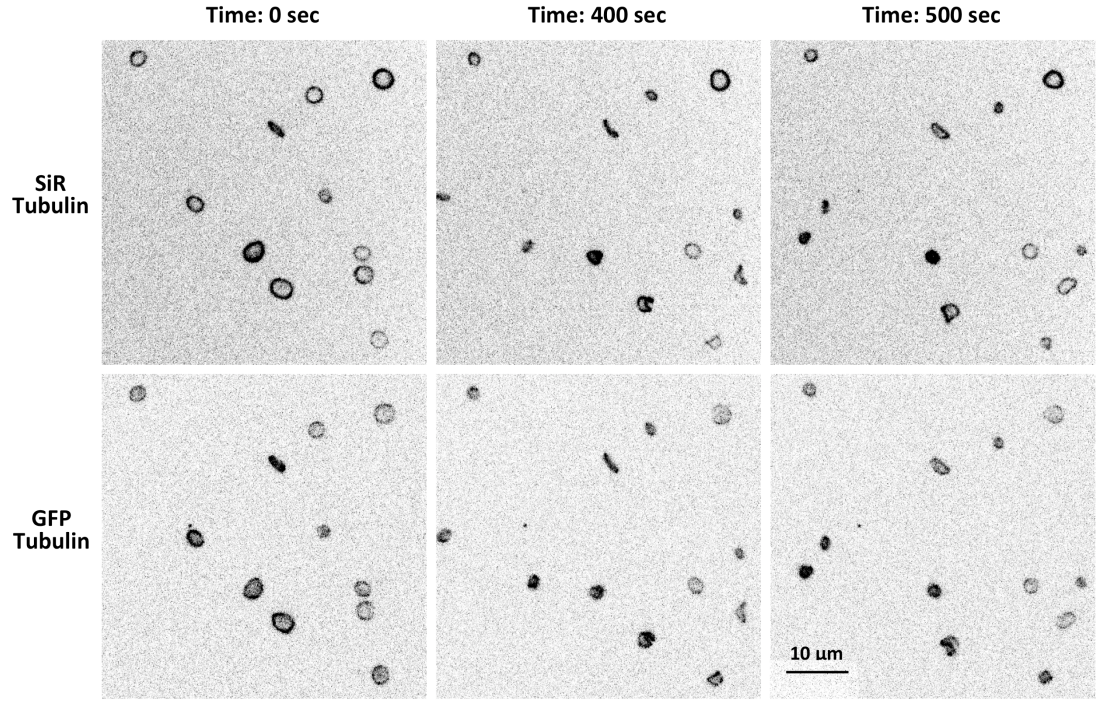

Figure 4.12: Marginal band coiling upon ADP treatment. GFP tubulin platelets labeled with 50nM SiR tubulin were treated with 10µM ADP. Marginal band coiling is observed. Images are maximum intensity projections of an axial distance of 2.8µm.

The live cell experiments were performed using our microfluidics setup (figure 3.1) as described in the methods section. The treatment with agonists in this format works on flow-based introduction of the agonist solution into the central channel of the chip and a subsequent diffusion-based movement of agonist molecules into the imaging channel. The first, flow-based, step is fast while the diffusion through 3µm filter in the rate-limiting step. Time zero in the time-lapse imaging is marked by start of the flow into the chip. As a result, all the recorded videos, where agonist is added, have the initial time points serve as an internal control. This delay in activation is caused not just because of the distance the agonist molecules need to cover to reach the imaging area, but also the time needed by the platelet to respond to this signal.

Therefore, if the activation response is dose dependent, it is hard to interpret the time at which the response becomes visible in our experiments, as it is a superposition of actual time needed for activation and an increasing agonist concentration.

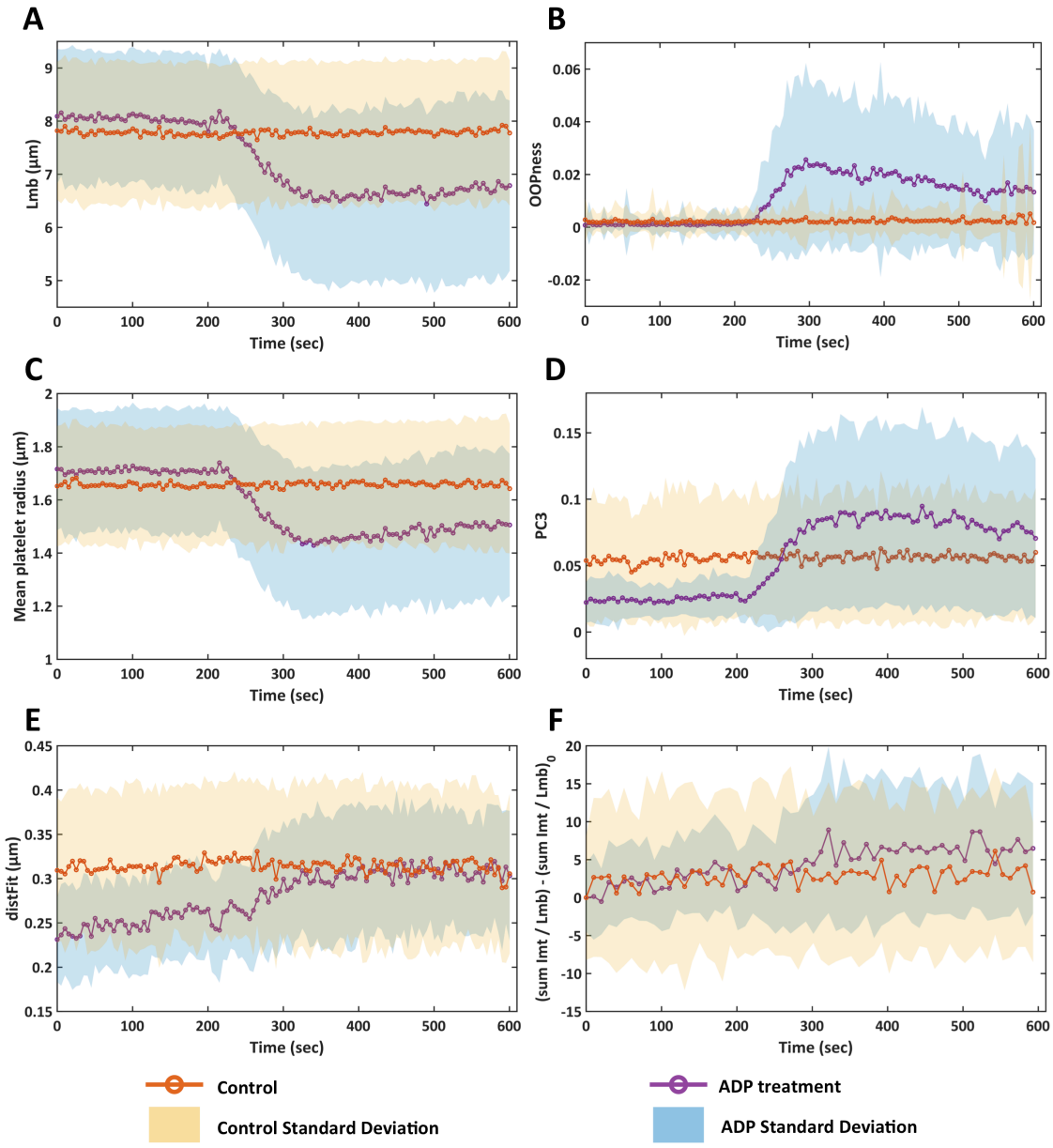

Figure 4.13: Platelet response to ADP activation. Quantification of changes in marginal band morphology in response to 10µM ADP treatment of 50nM SiR tubulin labeled platelets (n between 80 and 120 per time point). Length of marginal band **(A)** and mean platelet radius **(C)** decrease as coiling of the band occurs, as illustrated by increase in OOPness **(B)** and the third principal component **(D)**. Fitting error increases **(E)** as the marginal band slightly increases in thickness **(F)**.

Activation of platelets with ADP induces coiling of the marginal band. It is interesting to note that not all platelets respond to ADP by undergoing coiling. The ones that do coil also show variability in the coiling process, in terms of degree and reversibility of response. The degree of coiling is measured by the OOPness parameter, which starts to increase by around 200 seconds (figure 4.13 (B)), peaks around 300sec and then shows a gradual decrease. While the OOPness is increasing, we see a corresponding decrease in the length of the marginal band (Lmb), which stabilizes after 300 sec (figure 4.13 (A)). Similar trends are observed in parameters for platelet measurement. A decrease in mean platelet radius can be seen around 200sec (figure 4.13 (C)) with a parallel increase in the third principal component (PC3; figure 4.13 (D)). The error in fitting, distFit (figure 4.13 (E)), also increases with time as the platelets become smaller possibly due to decrease in thresholding or fitting accuracy. Since distFit is a measure of average distance of points from the fitted curve, an increase in its value could also imply a loosening or thickening of the marginal band. In figure 4.13 (F), we see that the fluorescence density of the marginal band increases slightly with coiling. As the summed intensity (I_{mt}) is a very noisy measurement, the time discretization for averaging was changed to 10 seconds, as opposed to 5 seconds for the other plots, to see the trend. The values were also normalized to the first data point at time zero because it is an intensity value that has arbitrary units. The fluorescence intensity is a measure of polymerized tubulin content and an increase in fluorescence density of Lmb would imply that the marginal band is becoming thicker over time. Increase in fluorescence density can only be seen around 300sec which is when the decrease in Lmb stabilizes and OOPness starts to lower. These changes in parameter values with time would indicate that the marginal band behaves like a visco-elastic ring, which initially responds elastically to the disc-to-sphere transition by coiling and then undergoes viscous relaxation to fit the new shape.

4.4.2 Marginal band further coils upon activation with Thrombin

ADP is known as a weak platelet agonist as compared to stronger platelet agonists like Thrombin (Brass et al. 2013). The differences in the degree of response these ligands induce arise from the different downstream molecules the ligand receptors they associate with. In our experiments, we observed that platelet activation with ADP caused, what seems to be, only a transient coiling of marginal band. To ascertain that the platelets are capable of a stronger response, we exposed the ADP treated platelet population to thrombin. Upon thrombin treatment, we observed a further coiling of the marginal band. The thrombin response is stronger in the sense that all the platelets respond by coiling and getting reduced to, with MT labels, an indistinguishable mass of tubulin (figure 4.14). Comparing the SiR signal to GFP

tubulin signal at late time points (figure 4.14, right panel), we see that the SiR signal is more confined to a spot while GFP tubulin signal is more diffused and extended. This might suggest that the MTs, labeled with SiR are constrained to platelet centre, while platelet extensions might still contain soluble or newly polymerized tubulin, which would only be visible in the GFP channel.

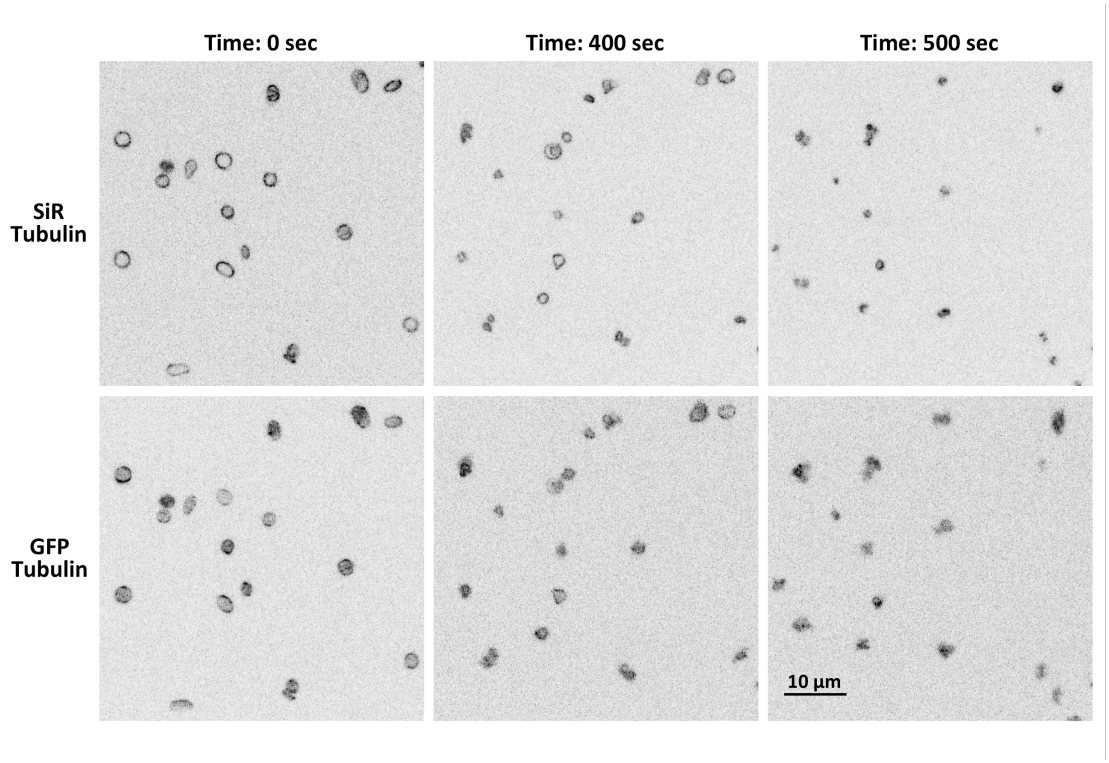

Figure 4.14: Marginal band coiling upon Thrombin treatment. GFP tubulin platelets labeled with 50nM SiR tubulin, post 10µM ADP treatment, were treated with 0.5U/ml of Thrombin. Further marginal band coiling is observed in all platelets till MT structures are reduced to spots. Images are maximum intensity projections of an axial distance of 2.8µm.

Platelet activation with thrombin was followed in time and the recorded images were processed with our data analysis pipeline. Since thrombin elicits a strong response, platelets are lost over time. This could happen during imaging, as platelets either move out of the imaging area of clump, or during analysis, as they become too small for accurate analysis and are filtered out. Combined with time discretization for merging different videos, this results in a highly variable number of platelets per time frame for thrombin treatment. In our data, the platelet numbers per time point vary from 285, down to 26 (mean: 117.5 ±64.9).

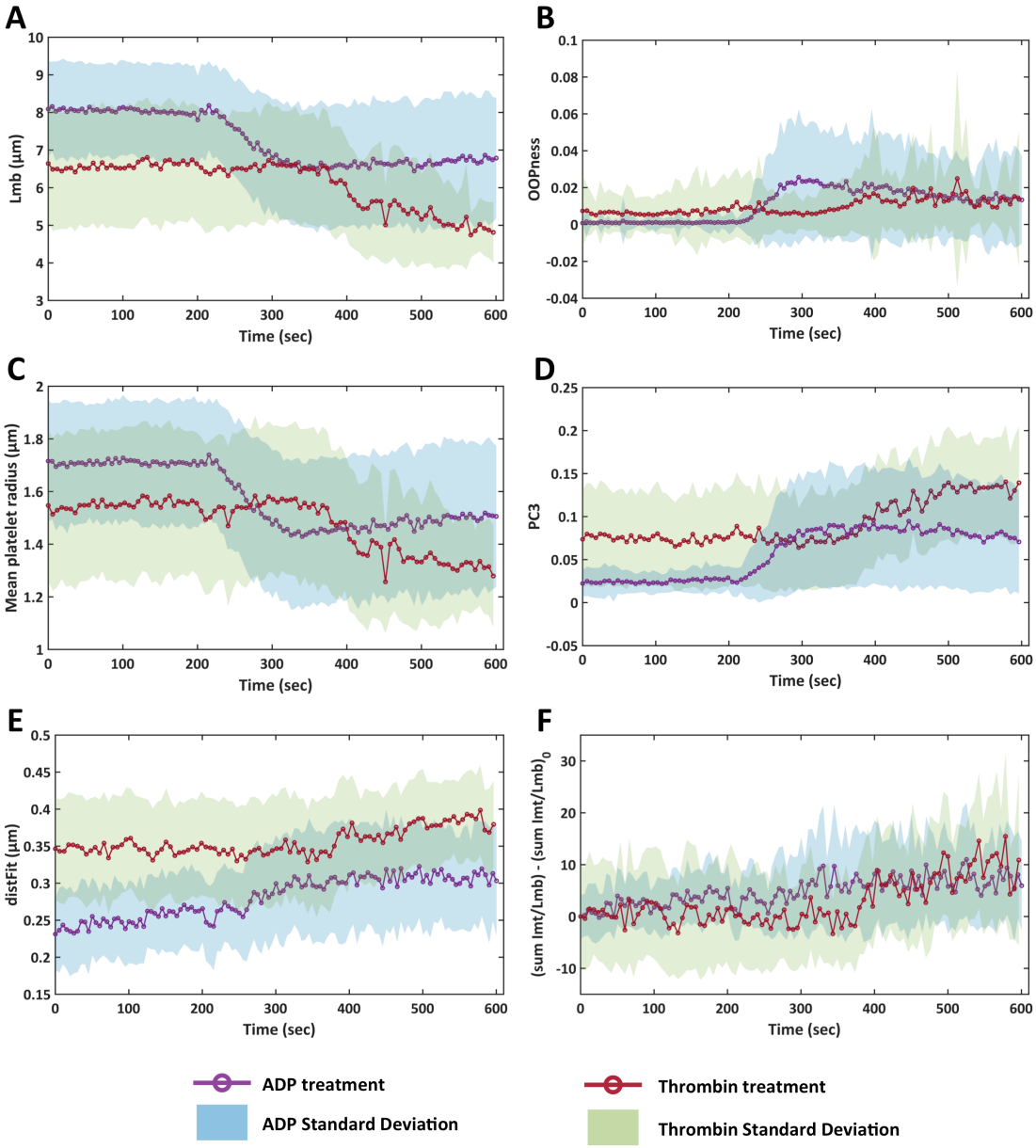

Figure 4.15: Platelet response to thrombin treatment. Quantification of changes in marginal band morphology in response to 0.5U/ml thrombin treatment of 50nM SiR tubulin labeled platelets (n between 26 and 285 per time point) that had been pre-treated with 10µM ADP. Length of marginal band **(A)** and mean platelet radius **(C)** decrease further with respect to ADP treatment. Coiling of the band occurs, as illustrated by an increase in the third principal component **(D)**, while OOPness only marginally increases **(B)**. Fitting error does not increase appreciably (E) while the marginal band slightly increases in thickness **(F)**.

As with ADP treatment, thrombin causes a reduction in Lmb (figure 4.15 (A)) as well as platelet radius (figure 4.15 (C)). Please note that the delay in thrombin response as compared to ADP is arbitrary as timing of response is also a function of agonist concentration, which in our setup is time dependent. What is noteworthy is the initial condition of the population before the treatment. Since thrombin addition

follows the ADP treatment, the initial Lmb for thrombin is already shorter than control (figure 4.15 (A); see ADP at time t=0). Being a strong agonist, thrombin is capable of inducing coiling in marginal bands that are significantly shorter than controls. When we compare degree of coiling (OOPness; figure 4.15 (B)) between the two agonists, we see that thrombin causes only a slight increase in OOPness. The possible explanation could be that the marginal band is shorter and thicker after ADP treatment, which can be expected to cause a change in mechanical properties of the band and make it more resistant to coiling. However, spherical transformation of the platelet or marginal band coiling can be detected with an increase in PC3 (figure 4.15 (D)). Similar trend can be observed for the fluorescence density (figure 4.15 (F)). Fitting error is found not to increase appreciably with marginal band coiling (figure 4.15 (E)). From these results, we can infer that, in our settings, the marginal band response to thrombin treatment is different from ADP treatment. Possible explanations could be the difference in mechanical properties of the marginal band at the beginning of ADP and thrombin treatment, or the presence of different mechanisms of action of either of the agonists owing to different downstream signaling pathways (Bryon et al. 1978).

4.4.3 Actin depolymerization abrogates marginal band coiling upon ADP treatment

One of the hypotheses explaining marginal band coiling during platelet activation implicates increase in actin contractility as the driving force of this process. To verify the role of actin in this process, we added 10µM of cytochalasin D (cytoD), a drug that causes depolymerization of actin, to platelets, incubated them for 45 minutes, and then exposed them to agonists. Upon subsequent addition of 10µM ADP, the platelets showed no sign of marginal band coiling (figure 4.16 (A)). To ensure that the platelets were getting exposed to ADP, we mixed fluorescein with the ADP solution and recorded its fluorescence to track diffusion of molecules over time. The platelets were then treated with 0.5U/ml of thrombin, which still caused platelet activation and marginal band coiling. Quantification of this process shows no effect of ADP treatment on either size of marginal band (Lmb in figure 4.16(B) and platelet radius in figure 4.16 (E)) or its degree of coiling (OOPness in figure 4.16(C) and PC3 in figure 4.16(F)). A decrease in Lmb and platelet radius with a corresponding increase in OOPness and PC3 can be seen with thrombin addition. The number of quantifiable replicates for this treatment was low due to which a higher time discretization of 15 seconds is used for averaging over more platelets. With this experiment, we can conclude that depolymerization of actin completely abolishes marginal band coiling triggered by ADP but not thrombin.

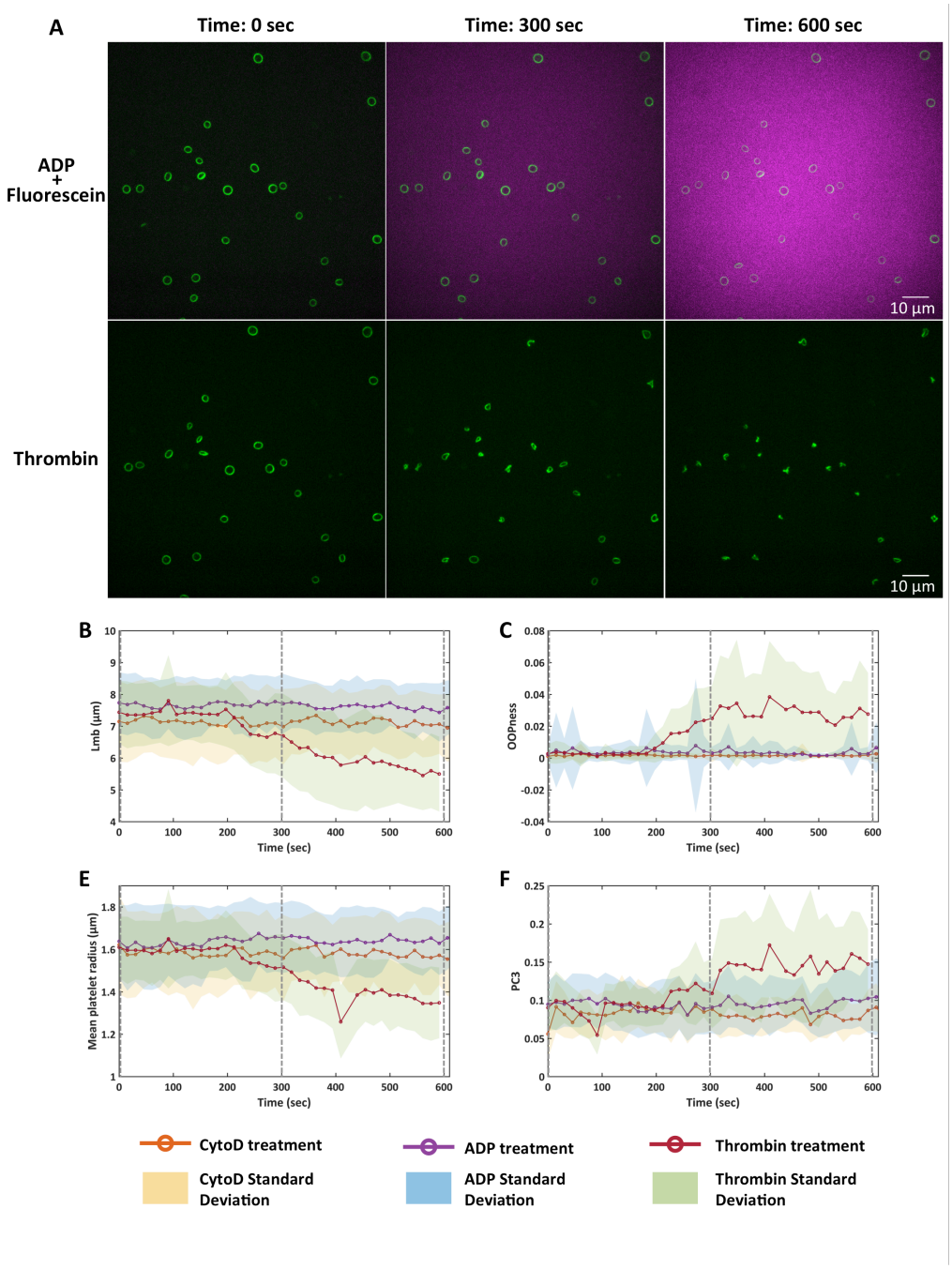

Figure 4.16: Effect of actin depolymerization on platelet activation. Platelets (n between 15 and 50 per time point) labeled with 50nM SiR tubulin were treated with 10µM of Cytochalasin D for 45 mins. Subsequently, 10µM ADP and 1µg/ml fluorescein were added but had no effect. **(A)** Upper panel showing marginal band (green; maximum intensity projection) and fluorescein (magenta; single frame) with ADP treatment. Finally 0.5U/ml of Thrombin was added to the platelets. Lower panel shows marginal band coiling in response to thrombin. Length of marginal band **(B)** and mean platelet radius **(E)** remain unaltered for ADP treatment while decrease with thrombin induced coiling of the band. As illustrated by an increase in OOPness **(C)** and the third principal component **(F)**, marginal band coils with thrombin but not ADP. Gray dashed lines on the plots correspond to the time points visualized in the images above.

4.4.4 Length dependence of marginal band propensity to coil

At a population level, marginal band response to activation due to ADP is a very heterogeneous process, as signified by the large standard deviations (figure 4.13 (A)). Upon monitoring individual tracked platelets, we observed that while some platelets respond to the stimulus strongly by undergoing irreversible coiling, others are either resilient or coil only transiently (figure 4.17). As shown in figure 4.18, the transient coiling, as observed by increase in OOPness, is accompanied by a transient decrease in marginal band length. This points towards a likely elastic response when coiling is temporary. It suggests that the marginal band behaves like an elastic ring with transient deformation and the activation in this case is reversible. It also warrants the requirement of a sustained force to cause reduction in Lmb, which is seen on a population level with ADP activation. This could result from the viscous response of the marginal band. We then speculated, that this difference in response might stem from the variation in initial length of the marginal band (Lmb_0), which while inherent to the population (figure 4.9 (A)), is also an important parameter for determining its mechanical strength.

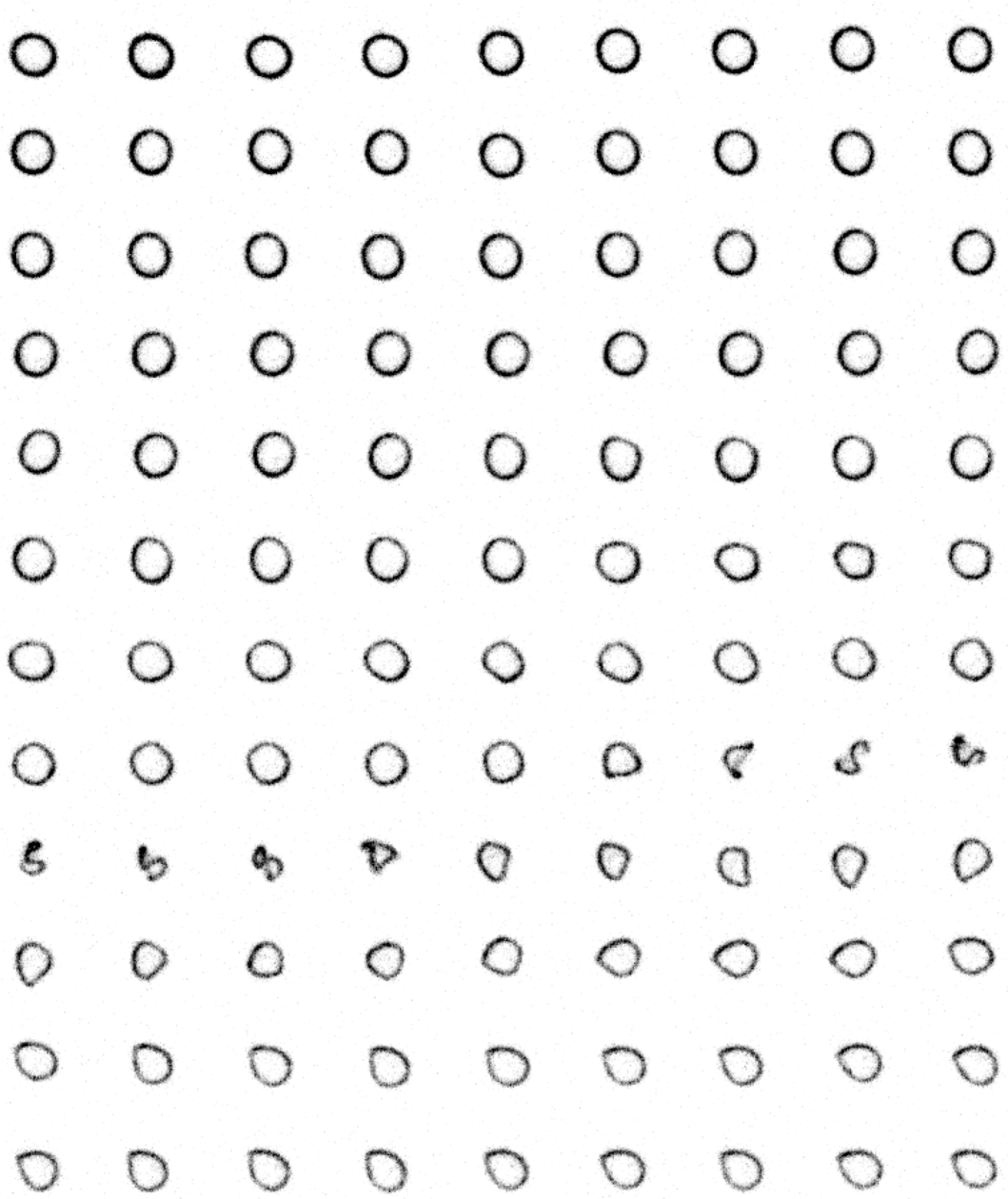

Figure 4.17: Reversible coiling of marginal band. Montage of coiling and uncoiling of a single platelet, labeled with 100nM SiR tubulin, over time. Time lapse between each frame is 5 sec.

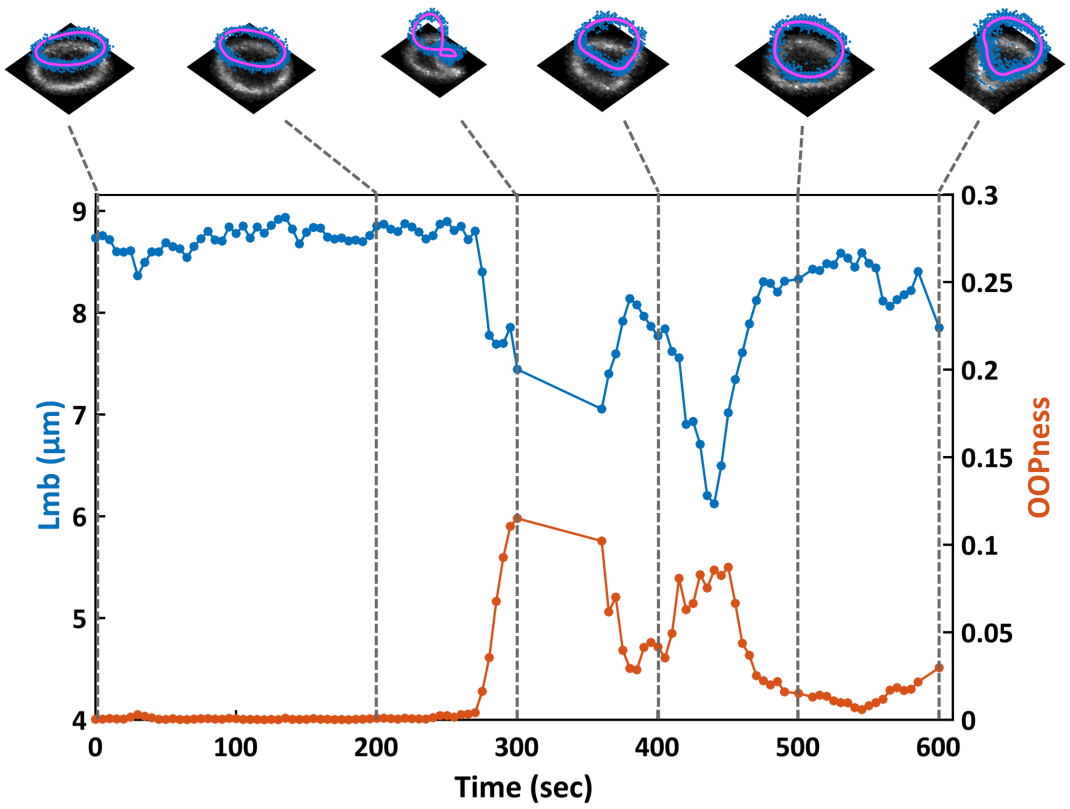

Figure 4.18: Quantification of reversibly coiling marginal band. Changes in marginal band length (Lmb) and degree of coiling (OOPness) for single reversibly coiling platelet. Shapes of the marginal band at the time points marked with gray line are shown above with a maximum intensity projected image at the bottom (grayscale), thresholded marginal band pixels (blue) and corresponding fitted curves (magenta).

To analyze the length dependence, we split the tracks into three time bins from 0 to 200sec, 200 to 400 sec and 400 to 600sec (figure 4.19 (A)). Within these time bins, the platelets were sorted into discretized intervals (0.4µm sized) of Lmb_0 and were averaged for their initial length and the corresponding parameter in question. When we look at the mean Lmb as a function of Lmb_0, we find that the length does not change much initially, but after 200 and 400 seconds, a decrease in Lmb is observed (figure 4.19 (B)). A larger reduction in length is seen for marginal bands that were initially longer. However, the decrease in length does not seem to be linearly dependent on the initial length. Similar trend is found in mean platelet radius (figure 4.19 (C)). Longer marginal bands are also observed to achieve a higher degree of coiling (figure 4.19 (D)). Our data shows that there might be a threshold for the length of marginal band, possibly around 6µm, below which the marginal band does not coil while coiling can be observed for bands that are longer. The fitting error is initially independent of length, but high for small platelets (figure 4.19 (E)). Upon activation, error seems to increase with an increase in coiling. Summed intensity of marginal band (I_{mt}) is dependent on Lmb_0 and does not seem to change over time

with activation (figure 4.19(F)). This shows that the total amount of tubulin is constant over time but scales with the length of the marginal band (as shown before in figure 4.9 (C)). The fluorescence density (I_{mt}/Lmb) of the marginal band, which is independent of Lmb_0 at initial time points, seems to increase as the marginal band coils (figure 4.19 (G)). This, once again, indicates a possible thickening of the marginal band with coiling. It is interesting to observe that the fluorescence density increases irrespective of Lmb_0, while only longer marginal band are found to coil. This might suggest that while the longer marginal bands are capable of initial elastic and subsequent viscous responses, the shorter bands, due to their mechanical properties, only behave as viscous materials. The data for this analysis is limited (94 platelets) as is it restricted to individual platelets tracked all the way through the time course. This is also the reason for high degree of noise.

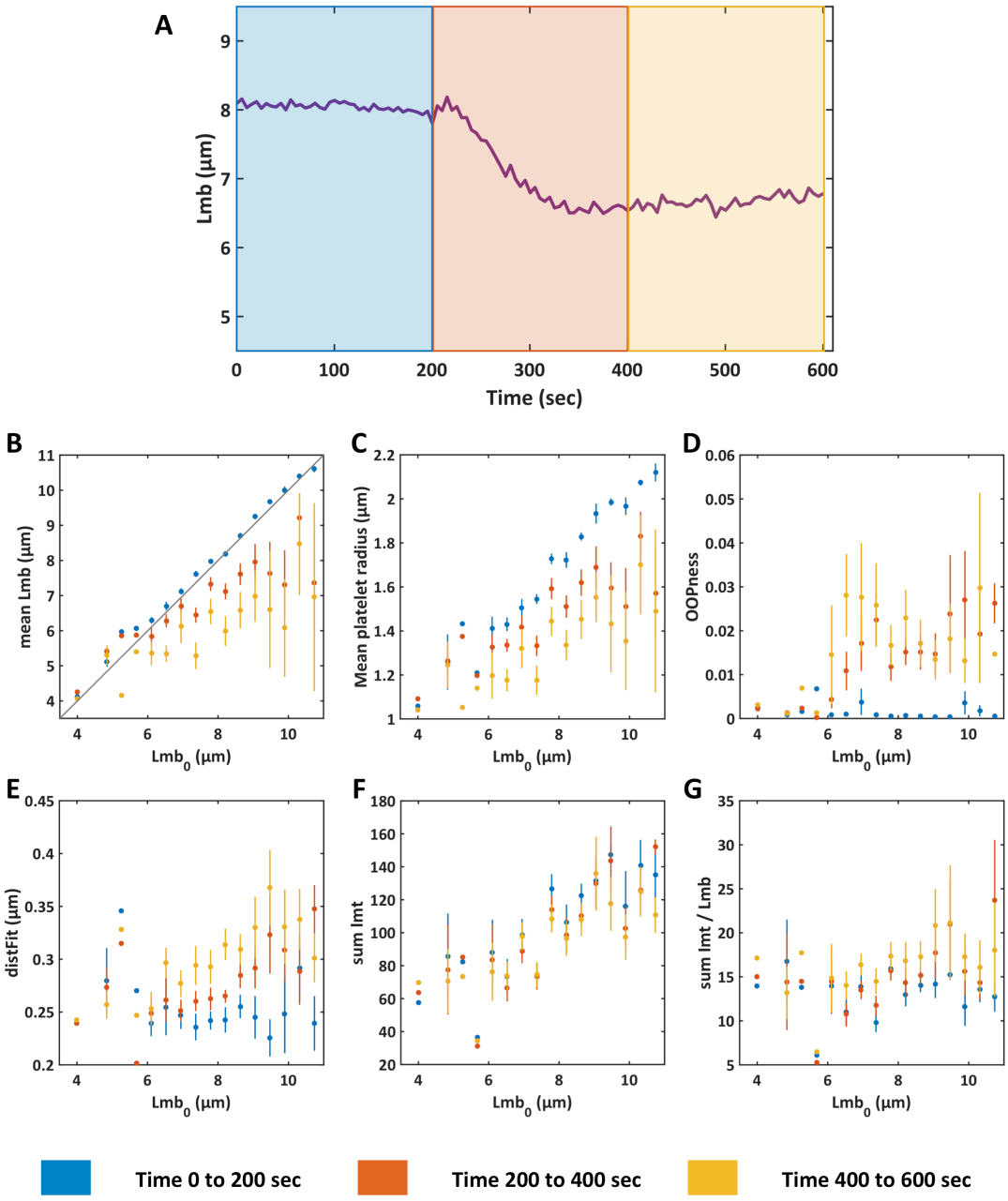

Figure 4.19: Length dependence of marginal band parameters during coiling. Platelets labeled with 50nM SiR tubulin were tracked over time during 10µM ADP treatment (94 tracks). The tracks were binned into three intervals over the time course to ADP action. For each time interval initial platelet length (Lmb_0) was discretized into bins of 0.4µm within which the parameters were averaged. **(A)** Placement of time bins overlaid on plot showing decrease in Lmb over time with ADP treatment. **(B to G)** Changes in marginal band parameters at different times as a function of Lmb_0. Vertical bars show standard error of the mean.

4.5 Measurement of platelet volume

In addition to being a diagnostic measure, platelet volume is a parameter that is suggestive of its state of mechanical equilibrium. The resting morphology of a platelet is a result of balance of forces applied by the marginal band on the membrane cytoskeleton and vice versa. Variations in the magnitude of these forces due to differences in the mechanical properties of the underlying cytoskeleton could be inferred by analyzing their effect on the platelet volume and morphology. The experiments, in part, were performed by Sandra Correia.

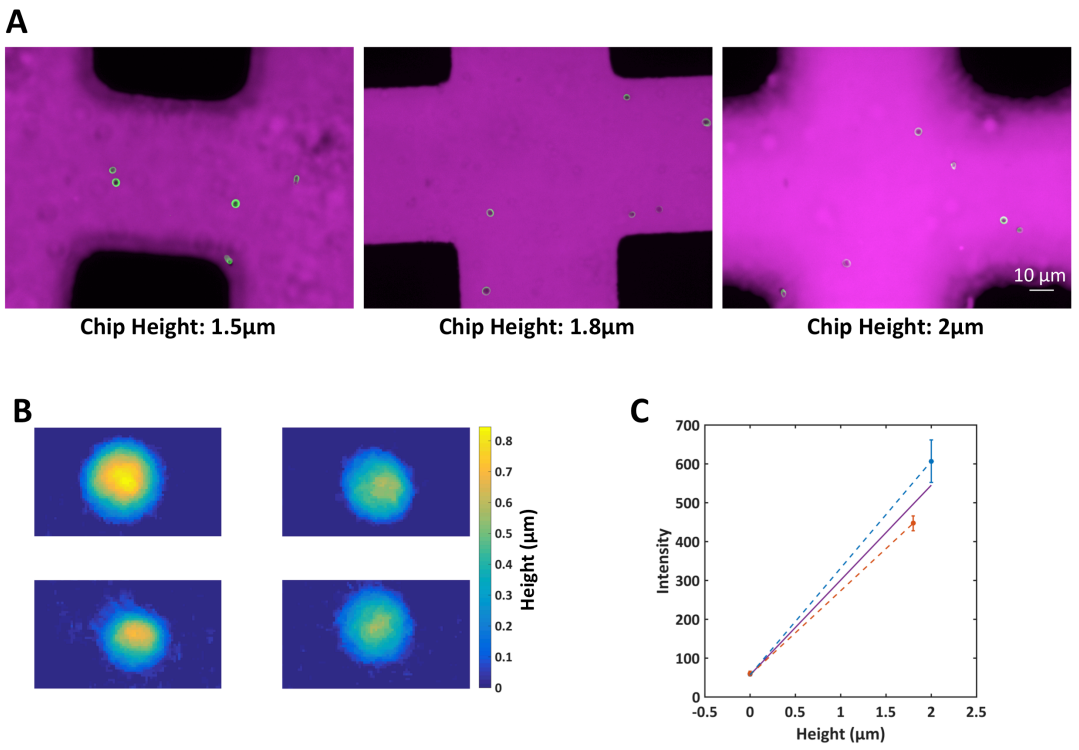

Figure 4.20: Platelet volume measurement by fluorescence exclusion. Platelets from wild-type mice were labeled with 500nM Tubulin-tracker and imaged in medium containing 0.5µg/ml AlexaFluor647. **(A)** Representative images of platelets microfluidic chips of different heights. Green: Maximum intensity projection of marginal band fluorescence. Magenta: Single frame of AlexaFluor647 fluorescence. Dark regions: fluorescence excluded pillars. **(B)** Height encoded images of four platelets from 1.8µm height chip. Fluorescence to height conversion based on only within the chip calibration. **(C)** Calibration plot for correspondence between chip height (1.8µm and 2µm) and fluorescence intensity. Dashed lines: Linear regression in individual chips; Orange: chip height 1.8µm, slope: 216; Blue: chip height: 2µm, slope: 275. Solid purple line: Combined linear regression for both chips, slope: 244.

We used light microscopy to measure volume of a platelet with a method based on fluorescence exclusion (Bottier et al. 2011; Zlotek-Zlotkiewicz et al. 2015). The method works on the principle that the reduction in fluorescence coming from a

homogenous volume of fluorophores, obstructed by a fluorescence excluded transparent object, is proportional to the volume of the object, given the complete volume is imaged simultaneously (figure 3.2). This results in a inverse linear correlation between the height of the object and the recorded fluorescence intensity (Zlotek-Zlotkiewicz et al. 2015).

The experiments were conducted using microfluidic chips fabricated in moulds of known heights. Platelets extracted from wild-type (C57BL/6) mice were labeled with 500nM tubulin-tracker, to mark the marginal band, and imaged in medium containing 0.5µg/ml of AlexaFluor647, which serves as the fluorescent molecule excluded from platelets. Representative images can be seen in figure 4.20 (A) for chips of different heights. In the AlexaFluor647 image, platelets can be seen as shadow in all the chips. The bright background and the dark region (due to pillars) serve as calibration to convert intensity values to height. Figure 4.20 (B) shows an example of four platelets that were imaged in a 1.8µm chip. The colormap corresponds to estimated heights that were calculated using the calibration (orange data points and dashed line) shown in figure 4.20 (C). However, using a chip of 2µm height with the same dye solution gave a calibration curve that was significantly different (blue data points and dashed line). This method is highly sensitive to changes in concentration of the fluorescent molecules and to avoid such differences from one chip to another, an internal calibration system for each chip is desirable. In absence of more than two calibration points per chip, we could not test the robustness for the method for our application. Therefore volume measurements were not performed on the data. Currently the method is being adapted by employing better calibration for increased accuracy.

Chapter 5

Discussion

5 Discussion

A combination of structural and dynamic data acquired during this study provides new insights on the role marginal band mechanics play in platelet activation. Making use of high-resolution techniques, such as electron tomography and super-resolution microscopy, we were able to obtain the structural organization of microtubules (MTs) in the marginal band. Data regarding MT length distribution allows us to propose a dynamic instability model for MT growth dynamics in platelets. Information about the proximity of MTs in the marginal band enabled us to identify the existence of parallel and anti-parallel MT overlaps. These could serve as the site where possible cross-linkers and molecular motors could associate to determine marginal band mechanical properties in the resting state and, as a likely consequence, its propensity to coil. Morphology of the marginal band is also indicative of forces being exerted on it, which in a state of mechanical equilibrium would equate to the force the band applies on platelet cortex. The study of marginal band coiling dynamics with live cell light microscopy reveals the visco-elastic behavior of the structure and its dependence on actin. The difference in marginal band response upon treatment with either ADP or thrombin becomes apparent. Analysis of variation of morphological parameters of the marginal band in a large population enables us to decipher the underlying dependencies and their consequence on the coiling process. The simulation setup provides a framework with which properties of the marginal band can be perturbed to evaluate their effect on the coiling process. In light of previous studies, the current data makes predictions about the involvement of different cytoskeletal elements in the process of marginal band coiling and allows us to identify possible mechanisms of action, some of which are currently under further investigation.

5.1 Implications of platelet marginal band structure

Detailed structural properties of the marginal band were recorded by using electron tomography and super-resolution microscopy. These datasets provide us information about the structure and composition of the marginal band, which, in turn, determines its mechanical properties. The total length of polymerized MTs as measured from our dataset (101.84µm ±12.63) seems in line with the long-standing estimate of approximately 100µm MT per platelet (Kenney & Linck 1985) (Steiner & Ikeda 1979). This is, however, in contrast with a recent study that compares platelets from control versus invasive ovarian cancer patients using cryo electron tomography (Wang et al. 2015). Their analysis estimates the MT length to be 66.1µm ± 14.42 in control resting platelets. The discrepancy between these measurements could be due to difference in the platelet extraction and preparation procedures. It is worthy

to note that in our dataset, the marginal band, whether flat or coiled, is found in close proximity of the membrane; a feature that is also observable in live platelets but seems contrary to the dataset presented by Wang et.al.

Being able to follow individual MTs within the marginal band, we can determine their length distribution in the population. An exponential distribution of MT lengths in a population is a hallmark of dynamic instability (Mitchison & Kirschner 1984) model of MT growth. This model has been previously hypothesized to hold true for platelet marginal band (Patel-Hett et al. 2008). Our data provides evidence in support of dynamic instability model for MT growth. Knowledge of the underlying model could have interesting implications including the possibility to gauge effects of perturbations in parameters that affect MT dynamics, like growth and shrinkage velocities, frequencies of catastrophes etc. The importance of these parameters can be reiterated by the fact that modulators of MT dynamics, like MT stabilizers RanBP10 (Kunert et al. 2009) (Meyer et al. 2012) and mDia1 (Pan et al. 2014), and MT destabilizer stathmin (Iancu-Rubin et al. 2011) are implicated in platelet biogenesis or haemostasis.

Mechanical properties of a marginal band are likely to derive from the structural organization of its constituents, and though they are the most apparent, MTs are definitely not its only component. A very important role in determining the structural integrity and, as a consequence, material properties of the marginal band is played by the cross-linking molecules that hold it together. Even though our data is a direct measure of only MT contours, the pairwise distance between the MTs is an indirect measure of putative cross-linkers. Such analysis has been previously performed on MT bundles in the form of mitotic spindle in *Schizosaccharomyces pombe* (Ward et al. 2014) (Janson et al. 2007) (Ding et al. 1993) or *Diatoma vulgare* (McDonald et al. 1979). These studies show that while a cross-sectional distance of 30nm is found to occur between MTs that run in parallel orientation, a 40nm distance is indicative of anti-parallel MT overlaps. The high proportion of 30nm distances in our dataset indicates the presence of cross-linked parallel overlaps in the MT bundle. This distance also corresponds to the MT cross-linking length of the protein tau which is known to be associated with the marginal band (Sanchez & Cohen 1994). The second peak in distances could indicate presence of other cross-linkers like MAP2 (Tablin & Castro 1991). In addition to passive cross linkers, cross-linking motors could also be associated with the marginal band as previously demonstrated (Rothwell & Calvert 1997) (Diagouraga et al. 2014) (Bender et al. 2015). In presence of anti-parallel overlaps, as demonstrated with our tomography data, the minus end directed motor, cytoplasmic dynein, and plus end directed

kinesin motors, like Eg5 and Kif15, can exert forces to slide MTs with respect to each other. Coupled with varying degrees of cross-linking, the sliding motion could be converted into forces that could result in contraction or extension of the marginal band. The reduction in proportion of 30nm and 60nm distances that we observe with loosening of the MT packing in the marginal band could illustrate loss of certain kind of cross-linkers more than the others which could be instructive of the direction of the force.

An important structural aspect of the platelet marginal band is its cross-section, as it affects the mechanical properties of the band and its propensity to coil (Ward et al. 2014). It has been shown that the thickness of the marginal band in proplatelets is correlated with the final platelet size (Thon et al. 2010); an effect that can be explained by a mechanical model of platelet biogenesis (Thon et al. 2012). In addition, thickness of the marginal band is known to increase in medical conditions where platelets become larger than usual (White & Sauk 1984). Thus being able to measure the marginal band cross-section would be very informative. Our super-resolution microscopy approach provides an assay by which such measurements can be carried out, with high precision and throughput. The cross-section can be measured in alpha tubulin labeled marginal band (figure 4.3 (A)). When challenged with a force acting radially inwards the marginal band could respond in two ways: (i) the MTs could either slide relative to each other causing the band to reduce in length while remaining planar, or (ii) the band could buckle leading to coiling out of plane. The response of the band would depend on the magnitude and rate of application of the force. Magnitude of forces that the band can withstand, in turn, would depend on the number and lengths of MTs in the band and the rate of turnover of cross-linking molecules. These parameters would finally determine whether the band would behave as an elastic or viscous ring.

5.2 Understanding the mechanics of marginal band coiling

Microtubule mechanics play a critical role in platelet biogenesis and maintenance of their resting shape (Schwer et al. 2001). A recent study by Diagouraga et. al. implicates MTs and their associated, plus end directed kinesin and minus end directed dynein, motors in marginal band coiling. Their hypothesis explains the resting marginal band to be a steady state of dynamic MTs fluxing due to opposing but balanced actions of kinesin and dynein motors. An imbalance in these opposing forces during activation is said to cause extension and eventual coiling of the marginal band when treated with ADP. According to this model, coiling is based on an increase in length of marginal band, which they measured in fixed cells by immunostaining.

Our data, measured in live platelets, shows that at a population level, marginal band length decreases as it undergoes coiling. This discrepancy from the previously proposed model might not necessarily be biological, but interpretive. Firstly, the length dependence of coiled state reported by (Diagouraga et al. 2014) is also observed in our data, where longer marginal bands are coiled (figure 4.19 (D)). But since we are able to track the cells from before activation, we can say that those bands were longer to begin with and not necessarily as a consequence of it. This is also supported by the variations in size they observe with coiled state (mean lengths of approximately 9µm for flat and 12.5µm for maximally coiled bands), which are naturally present in our marginal band population in resting state (Lmb_0 from 4µm to 12µm). Furthermore, the live platelet data reported by Diagouraga et. al. shows no increase, and in some cases, slight decrease in marginal band length with coiling. This result is in line with our observations indicating the advantage of live imaging and tracking individual platelets for populations with high intrinsic variability.

We have shown that coiling of the marginal band observed with ADP activation is accompanied by a decrease in its length (figure 4.13 (B and A)) at a population level. The platelet population, however, does not respond homogenously to the stimulus as depicted by the high standard deviation (figure 4.13 (A)). This is a result of variable platelet response where some platelets respond irreversibly while others do so reversibly or not at all. Our data shows, that the first response of the marginal band to ADP treatment is elastic as the band is found to readily coil. It can also be seen, in case of reversible coiling, possibly due to lack of sustained force, that the marginal band comes back to a flat state with length similar to initial state. These results suggest that at short time scales marginal band exhibits an elastic response (figure 5.1 (A); first step of ADP activation). A high degree of cross-linking between MTs, by means of elastic cross-linkers, can explain the elastic response.

At longer time scales, and possibly in presence of sustained force, we observe that the degree of coiling reduces while the length of the marginal band remains short. This indicates, that the marginal band might have adapted to the new platelet state (figure 5.1 (A); second step of ADP activation). Considering that the shortening of the marginal band is unlikely to be due to MT depolymerization, since no significant decrease in summed marginal band intensity is observed, one can expect the band might thicken to accommodate the same amount of polymerized tubulin but in shorter length. This has been indirectly measured by the fluorescence density of tubulin in the marginal band (figure 4.13 (F)) that increases with a slight delay after coiling response. As the marginal band flattens again (figure 4.13 (B); 500sec to

600sec), we observe a corresponding increase in platelet radius (figure 4.13 (C); 500sec to 600sec), which might suggest that the new shape is still possibly determined by marginal band forces as a result of which the platelets might not be spherical. These mechanical changes in marginal band properties indicate that the band might behave as a viscous material as it adapts to the new shape. Such behavior can be facilitated by either sliding or fast binding and unbinding of MT cross-linkers. To understand the reason for this difference in the degree of response, it might be useful to subcategorize the platelets on the basis of how they respond and identify a set of initial parameters that can differentiate between these subcategories. A candidate parameter that affects platelet coiling is the initial marginal band length as platelets with longer marginal bands are found to coil more in response to ADP (figure 4.19).

Thrombin treated platelets shows different activation dynamics as compared to the ADP treatment. With thrombin, all the platelets respond by activating irreversibly, accompanied by a reduction in platelet radius and length of the marginal band. As thrombin is known to cause platelet degranulation, platelets can be expected to reduce in volume while coiling (Bryon et al. 1978). In addition, with our experimental setup, platelets before being treated with thrombin have already been exposed to ADP before. So, even if they have flat and ring like marginal bands, their lengths are already shorter than controls, and even thicker based on fluorescence density. Hence the mechanical response can be expected to be different (figure 5.1 (A); thrombin treatment).

Actin depolymerization by treatment with Cytochalasin D (cytoD) is known to abrogate platelet morphological change in response to activation with ADP but not with thrombin (Casella et al. 1981) (Diagouraga et al. 2014). Our results show similar effect of cytoD treatment where the resting state remained unaffected and ADP did not cause a significant change in marginal band morphology (figure 5.1 (B)). Thus, we can conclude that marginal band lengthening might be an unlikely response to ADP treatment, or that it is a process dependent on polymerized actin. Thrombin treatment, however, did induce coiling of the marginal band even after cytoD treatment, which is contrary to pervious report by Severin et. al. (Séverin et al. 2012). Their experiments include platelet treatment with cytoD followed by activation with thrombin and subsequent fixation, upon which they see no change in marginal band morphology. A possible reason for this discrepancy could be the difference in dose of cytoD, which they set at 10µM as compared to our treatment where dose (starting solution at 10µM) is diffusion limited and is a function of time. Also in our experimental setup, platelets have previously been exposed to ADP,

which might cause some changes in their subsequent response to thrombin. However, it has been previously reported that actin depolymerization, with a different but related compound cytochalasin B, does not abolish signaling that causes platelet activation in response to thrombin (Díaz-Ricart et al. 2002).

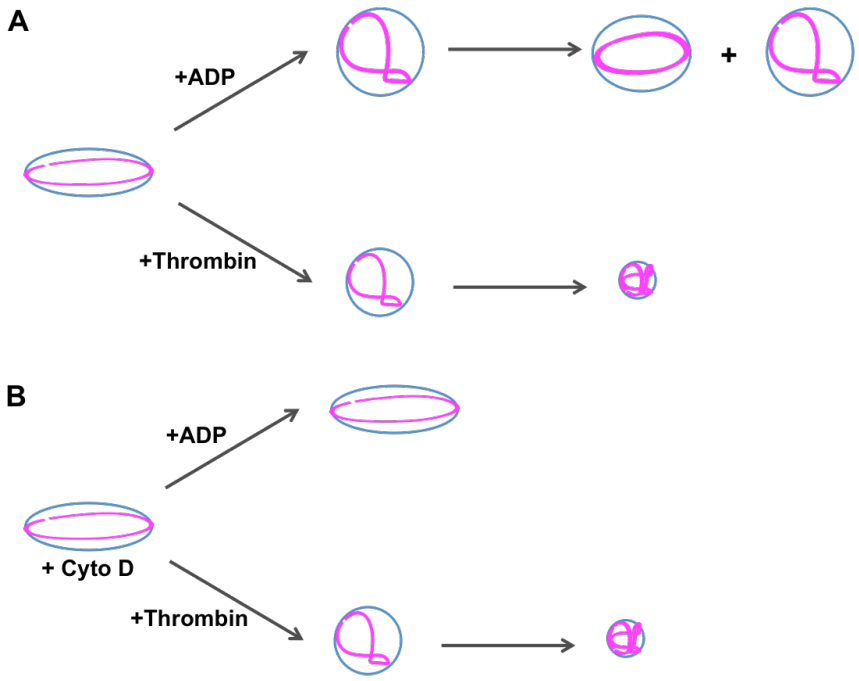

Figure 5.1: Schematic representation of marginal band coiling. (A) Coiling response of marginal band upon ADP and thrombin treatment. **(B)** Marginal band response in platelets pretreated with cytochalasin D. ADP treatment shows no significant effect while thrombin is still able to cause marginal band coiling. **(A, B)** Volume of platelet is assumed to be conserved with ADP while reducing with thrombin treatment.

5.3 Consequences of variations in platelet population

From a medical point of view, the importance of platelet size is well established. In bleeding disorders such as Gray platelet syndrome, May-Hegglin anomaly, Epstein's syndrome, Bernard-Soulier's syndrome, etc., platelets become abnormally large and show modified arrangement of the cytoskeleton (White & Sauk 1984) (White et al. 1984). The changes in cytoskeletal organization could affect their mechanical properties (White et al. 1984) and prevent the morphological changes required for normal platelet activity. Using our live imaging and quantification techniques, we have addressed how natural size variation in platelet population can affect their ability to respond to agonists. With such analysis we get a better understanding of platelet mechanics and can attempt to address the aberrant response of anomalous platelets.

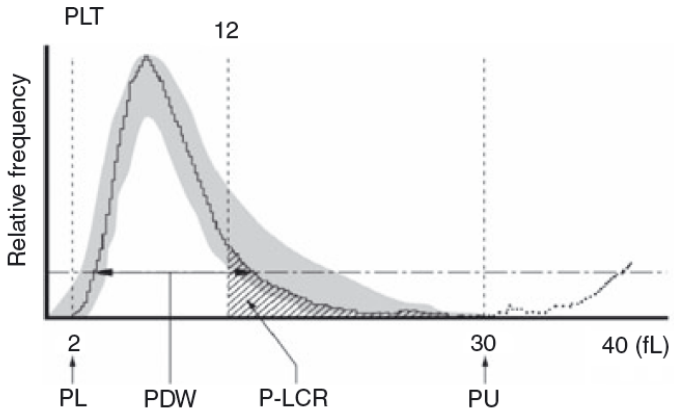

Figure 5.2: Platelet volume distribution. Typical platelet volume distribution generated with an automated haematology analyser. PL, lower discrimination for platelet size distribution. PDW, platelet distribution width. P-LCR, platelets-large cell ratio. PU, upper discrimination for platelet size distribution **(Briggs et al. 2007)**.

An interesting observation we can make about platelet radius from our data (figure 4.7 (A)) is its distribution in the natural population. The process of platelet formation is based on flow shear based fragmentation, binary fission, etc. (Machlus & Italiano 2013). These processes put together result in lognormal distribution platelet volumes (figure 5.2) (Martin & Trowbridge 2012). Such distribution of platelet volumes is shown to be a property of the platelet biogenesis process and shortly after (12hrs) and not a consequence of platelet ageing(Paulus 1975). These observations suggest that there might be an additional mechanism, possibly based on platelet balance of mechanical forces as suggested for platelet biogenesis (Thon et al. 2012), at work to control the platelet radius distribution.

Our data also shows a surprising scaling behavior between tubulin intensity and platelet radius, which suggests that tubulin doesn't partition into platelets depending solely on volume. It means that the platelets might be specifically enriched for polymerized tubulin. Such trends could arise from the MT dependent process by which platelets are formed (Schwer et al. 2001). By virtue of this method, a set of cortical MTs might already be present in platelets and not directly depend on the tubulin content in the platelet itself. It is interesting to note that the fluorescence density, which is a measure of tubulin content per unit length of marginal band, in resting platelet is independent of marginal band length. It indicates that a constant tubulin fluorescence density over varying lengths of the marginal band provides the force required to maintain the discoid shape of a resting platelet, which could be considered as a state of mechanical equilibrium.

We have been able to exploit the natural variation in the marginal band properties in a population of resting platelets to get insight into the mechanics of marginal band coiling. Upon analyzing the dependence of quantitative parameters on initial marginal band length with ADP treatment, we find that larger platelets, harboring longer marginal bands have a higher propensity to coil. This property was also found to be independent of MT fluorescence density of the band, which was constant over the given marginal band lengths but increased with time. This finding might explain why larger platelets have a higher tendency to get activated as observed in many of the giant platelet disorders as well as newly formed platelets.

5.4 Exploring mechanics of marginal band

We have so far done the simulation with parameters that recapitulate time scales at which the marginal band behaves like an elastic band. Interesting insights could be obtained when the band is remodeled in the light of our live cell microscopy data. It would be interesting to see if the marginal band behaves like a viscous material when changes in morphology take place at the time scale similar to those of the experiments. Viscosity of the band would probably be governed by properties of cross-linkers and motors that hold the marginal band together. Simulations would be the method of choice for such an analysis as the marginal band is complex multi-molecular structure with many parameters. Using *Cytosim*, these parameters can be systematically varied and tuned to represent the observed behavior. The model can then be further explored to make prediction about the expected system behavior upon perturbations. These predictions could then be tested by designing suitable experiments. This would help us refine our knowledge of the system mechanics.

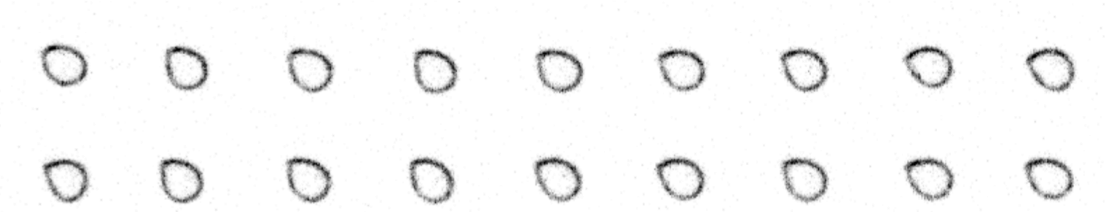

Chapter 6

Conclusion

6 Conclusions

In this study, we have used various experimental and analysis techniques to quantitatively evaluate the role of cytoskeletal mechanics during initiation of platelet activation. During the disc-to-sphere transition, which is the first step of platelet activation, the microtubule marginal band that supports the resting discoid morphology, undergoes coiling as the platelet turns into a sphere. Because of the physiological relevance and mechanical nature of this transition, we wanted to identify the properties and relative contribution of microtubule and actin cytoskeleton in the coiling process. To this end, we have used electron tomography and super-resolution microscopy to study the structural composition of the marginal band, which informs us of its mechanical properties. Dynamics of the coiling response were in turn measured using live cell light microscopy, which enabled us to quantify the morphological changes during coiling. High throughput analysis of resting marginal band shape was done to quantify the variation in the morphological properties that naturally occurs in platelets. The population variation was further explored to determine whether certain properties predisposed platelets to activation.

To understand the mechanical properties of the platelet marginal band, we explored its structure and morphology in a resting state. First, with our ability to follow individual MTs in electron tomography, we estimated the underlying length distribution in a set of four cells, which turns out to be exponential with an average length of 5.18µm. An exponential distribution might indicate that the population is undergoing dynamic instability (Dogterom & Yurke 1997). We also measured the total MT length, which added up to 101.84µm ±12.63 per platelet. This value matches the existing estimates (Kenney et al. 1988). From the histogram of pairwise center-to-center distances between MTs, we found that the tightly packed marginal bands have a distinct peak at 30nm and smaller peak between 50 to 60 nm. The loosely packed bands with smaller radii and shorter MTs do not show preference for these specific distances. This might indicate loss of certain cross-linkers accompanying changes in marginal band morphology. Furthermore from super-resolution microscopy we inferred the composition of the marginal band by labeling gamma-tubulin, which marks the minus ends of MTs. Estimates of MT numbers, revealed that the marginal band length scales as square of the number of MTs in the platelet. This dependence is currently under further investigation by double labeling with other MT minus-end markers.

By analyzing the coiling dynamics of marginal band in response to ADP, we inferred that the marginal band behaves like a visco-elastic ring as it coils in response to the stimulus.
This response was dependent on the presence of polymerized actin. The coiling response elicited by thrombin followed a different mechanism, as it was independent of actin.

Although platelets are formed by a combination of processes that yield fragments of various sizes, we find that the distribution of platelet radius in a population is narrow. This might indicate presence of mechanisms, possibly based on cytoskeletal mechanics, keeping it in check. The scaling behavior observed between platelet intensity and radius, which is a power of approximately five, is also surprising. It might indicate specific enrichment of tubulin in platelets. Based on natural variation in platelet sizes, we observed that platelets with longer marginal bands have a higher tendency to coil.

Overall our study shed light on the mechanical properties of the cytoskeleton which matter for the shape transition from resting to activated state. Further elucidation of the mechanisms involved in activation will be important for understanding of this complex physiological change. Most importantly, what leads to the rapid change of marginal band structure is still to be uncovered. Nonetheless, this study has made headway in bringing platelets under experimental investigation with state of the art imaging techniques and quantitative analysis.

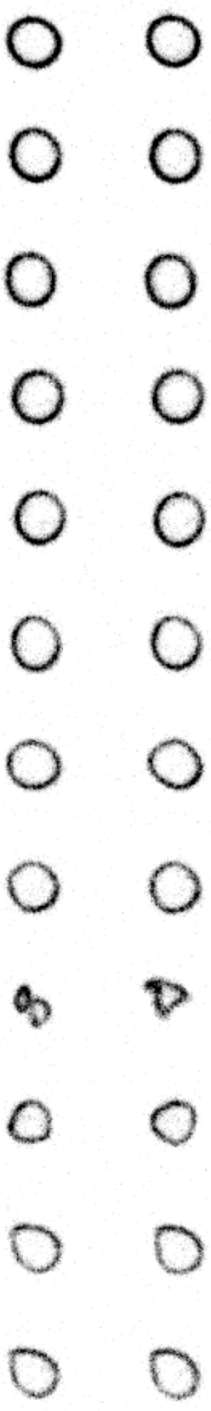

Chapter 7

References

7 References

Aarts, P.A. et al., 1988. Blood platelets are concentrated near the wall and red blood cells, in the center in flowing blood. *Arteriosclerosis (Dallas, Tex.)*, 8(6), pp.819–824.

Abe, T. et al., 2011. Establishment of conditional reporter mouse lines at ROSA26 locus for live cell imaging. *Genesis (New York, N.Y. : 2000)*, 49(7), pp.579–590.

AMOS, L.A. & Klug, A., 1974. Arrangement of subunits in flagellar microtubules. *Journal of cell science*.

Bearer, E.L., Prakash, J.M. & Li, Z., 2002. Actin dynamics in platelets. *International review of cytology*, 217, pp.137–182.

Behnke, O., 1965. Further studies on microtubules. A marginal bundle in human and rat thrombocytes. *Journal of ultrastructure research*, 13(5), pp.469–477.

Behnke, O., 1967. Incomplete microtubules observed in mammalian blood platelets during microtubule polymerization. *The Journal of cell biology*, 34(2), pp.697–701.

Behnke, O. & Zelander, T., 1966. Substructure in negatively stained microtubules of mammalian blood platelets. *Experimental cell research*, 43(1), pp.236–239.

Bender, M. et al., 2010. ADF/n-cofilin-dependent actin turnover determines platelet formation and sizing. *Blood*, 116(10), pp.1767–1775.

Bender, M. et al., 2014. Megakaryocyte-specific Profilin1-deficiency alters microtubule stability and causes a Wiskott-Aldrich syndrome-like platelet defect. *Nature communications*, 5, p.4746.

Bender, M. et al., 2015. Microtubule sliding drives proplatelet elongation and is dependent on cytoplasmic dynein. *Blood*, 125(5), pp.860–868.

Bizzozero, J., 1882. Ueber einen neuen Formbestandtheil des Blutes und dessen Rolle bei der Thrombose und der Blutgerinnung. *Archiv für Pathologische Anatomie und Physiologie und für Klinische Medicin*, 90(2), pp.261–332.

Bottier, C. et al., 2011. Dynamic measurement of the height and volume of migrating cells by a novel fluorescence microscopy technique. *Lab Chip*, 11(22), pp.3855–3863.

Boyles, J. et al., 1985. Organization of the cytoskeleton in resting, discoid platelets: preservation of actin filaments by a modified fixation that prevents osmium damage. *The Journal of cell biology*, 101(4), pp.1463–1472.

Brass, L.F. et al., 2013. Chapter 19 - Signal Transduction During Platelet Plug Formation. In A. D. Michelson, ed. *Platelets (Third Edition)*. Platelets (Third Edition). Academic Press CY -, pp. 367–398.

Briggs, C., Harrison, P. & Machin, S.J., 2007. Continuing developments with the automated platelet count. *International journal of laboratory hematology*, 29(2), pp.77–91.

Bryon, P.A., Lagarde, M. & Dechavanne, M., 1978. [Sterologic evaluation on in vitro thrombin-induced platelet degranulation and contraction (author's transl)]. *Nouvelle revue française d'hématologie*, 20(2), pp.173–178.

Burkhart, J.M. et al., 2012. The first comprehensive and quantitative analysis of human platelet protein composition allows the comparative analysis of structural and functional pathways. *Blood*, 120(15), pp.e73–82.

Burkhart, J.M. et al., 2014. What can proteomics tell us about platelets? *Circulation research*, 114(7), pp.1204–1219.

CALAMINUS, S.D.J. et al., 2007. MyosinIIa contractility is required for maintenance of platelet structure during spreading on collagen and contributes to thrombus stability. *Journal of*

thrombosis and haemostasis : JTH, 5(10), pp.2136–2145.

Casella, J.F., Flanagan, M.D. & Lin, S., 1981. Cytochalasin D inhibits actin polymerization and induces depolymerization of actin filaments formed during platelet shape change. *Nature*, 293(5830), pp.302–305.

Cazenave, J.-P. et al., 2004. Preparation of washed platelet suspensions from human and rodent blood. *Methods in molecular biology (Clifton, N.J.)*, 272, pp.13–28.

Chen, J. et al., 1992. Projection domains of MAP2 and tau determine spacings between microtubules in dendrites and axons. *Nature*, 360(6405), pp.674–677.

Choi, E.S. et al., 1995. Platelets generated in vitro from proplatelet-displaying human megakaryocytes are functional. *Blood*, 85(2), pp.402–413.

Coller, B.S., 2013. Foreword - A Brief History of Ideas About Platelets in Health and Disease. In A. D. Michelson, ed. *Platelets (Third Edition)*. Platelets (Third Edition). Academic Press CY -, pp. xix–xliv.

Conrad, M. et al., 2004. Cytoskeletal organization of limulus amebocytes pre- and post-activation: comparative aspects. *The Biological bulletin*, 207(1), pp.56–66.

Cooper, J., 1987. Effects of cytochalasin and phalloidin on actin. *The Journal of cell biology*, 105(4), p.1473.

Davies, T.A. et al., 1989. Cytoplasmic Ca2+ is necessary for thrombin-induced platelet activation. *Journal of Biological Chemistry*.

Desai, A. & Mitchison, T.J., 1997. Microtubule polymerization dynamics. *Annual review of cell and developmental biology*, 13, pp.83–117.

Diagouraga, B. et al., 2014. Motor-driven marginal band coiling promotes cell shape change during platelet activation. *The Journal of cell biology*. Available at: http://jcb.rupress.org/content/early/2014/01/06/jcb.201306085.

Ding, R., McDonald, K.L. & McIntosh, J.R., 1993. Three-dimensional reconstruction and analysis of mitotic spindles from the yeast, Schizosaccharomyces pombe. *The Journal of cell biology*, 120(1), pp.141–151.

Díaz-Ricart, M. et al., 2002. Inhibition of cytoskeletal assembly by cytochalasin B prevents signaling through tyrosine phosphorylation and secretion triggered by collagen but not by thrombin. *The American journal of pathology*, 160(1), pp.329–337.

Dogterom, M. & Leibler, S., 1993. Physical aspects of the growth and regulation of microtubule structures. *Physical review letters*, 70(9), pp.1347–1350.

Dogterom, M. & Yurke, B., 1997. Measurement of the force-velocity relation for growing microtubules. *Science (New York, N.Y.)*, 278(5339), pp.856–860.

Foster, P.J. et al., 2015. Active contraction of microtubule networks. *eLife*, 4.

Fox, J.E., 1988. Identification of a membrane skeleton in platelets. *The Journal of cell biology*, 106(5), pp.1525–1538.

Fox, J.E., 1993. The platelet cytoskeleton. *Thrombosis and haemostasis*, 70(6), pp.884–893.

Fox, J.E. & Phillips, D.R., 1981. Inhibition of actin polymerization in blood platelets by cytochalasins. *Nature*, 292(5824), pp.650–652.

Fox, J.E. et al., 1987. Spectrin is associated with membrane-bound actin filaments in platelets and is hydrolyzed by the Ca2+-dependent protease during platelet activation. *Blood*, 69(2), pp.537–545.

Galambos, P. & Forster, F.K., 1998. Micro-Fluidic Diffusion Coefficient Measurement. In Dordrecht: Springer Netherlands, pp. 189–192.

Geddis, A.E. et al., 2007. Endomitotic megakaryocytes that form a bipolar spindle exhibit cleavage furrow ingression followed by furrow regression. *Cell cycle (Georgetown, Tex.)*, 6(4), pp.455–460.

Gibeaux, R. et al., 2012. Electron tomography of the microtubule cytoskeleton in multinucleated hyphae of Ashbya gossypii. *Journal of cell science*, 125(Pt 23), pp.5830–5839.

Goodwin, S.S. & Vale, R.D., 2010. Patronin regulates the microtubule network by protecting microtubule minus ends. *Cell*, 143(2), pp.263–274.

Gouveia, S.M. & Akhmanova, A., 2010. Cell and molecular biology of microtubule plus end tracking proteins: end binding proteins and their partners. *International review of cell and molecular biology*, 285, pp.1–74.

Hartwig, J.H., 2013. Chapter 8 - The Platelet Cytoskeleton. In A. D. Michelson, ed. *Platelets (Third Edition)*. Platelets (Third Edition). Academic Press CY -, pp. 145–168.

Hartwig, J.H. & Italiano, J.E., 2006. Cytoskeletal mechanisms for platelet production. *Blood cells, molecules & diseases*, 36(2), pp.99–103.

Heuser, J.A. & Pollard, T.D., 1998. The interaction of Arp2/3 complex with actin: nucleation, high affinity pointed end capping, and formation of branching networks of filaments. In Proceedings of the ….

Holmes, K.C. et al., 1990. Atomic model of the actin filament. *Nature*.

Höög, J.L. et al., 2011. Electron tomography reveals a flared morphology on growing microtubule ends. *Journal of cell science*, 124(Pt 5), pp.693–698.

Huxley, A.F. & Niedergerke, R., 1954. *Structural changes in muscle during contraction; interference microscopy of living muscle fibres*, Nature.

HUXLEY, H. & HANSON, J., 1954. Changes in the cross-striations of muscle during contraction and stretch and their structural interpretation. *Nature*, 173(4412), pp.973–976.

Iancu-Rubin, C. et al., 2011. Down-regulation of stathmin expression is required for megakaryocyte maturation and platelet production. *Blood*, 117(17), pp.4580–4589.

Italiano, J.E. et al., 1999. Blood platelets are assembled principally at the ends of proplatelet processes produced by differentiated megakaryocytes. *The Journal of cell biology*, 147(6), pp.1299–1312.

Italiano, J.E. et al., 2003. Mechanisms and implications of platelet discoid shape. *Blood*, 101(12), pp.4789–4796.

Italiano, J.E., Jr & Hartwig, J.H., 2013. Chapter 2 - Megakaryocyte Development and Platelet Formation. In A. D. Michelson, ed. *Platelets (Third Edition)*. Platelets (Third Edition). Academic Press CY -, pp. 27–49.

Janson, M.E. et al., 2007. Crosslinkers and motors organize dynamic microtubules to form stable bipolar arrays in fission yeast. *Cell*, 128(2), pp.357–368.

Jolly, A.L. et al., 2010. Kinesin-1 heavy chain mediates microtubule sliding to drive changes in cell shape. *Proceedings of the …*.

Jones, T.W., 1851. *Jones: On the state of the blood and blood vessels... - Google Scholar*, Guy's Hosp. Rep.

Jurak Begonja, A. et al., 2011. FlnA-null megakaryocytes prematurely release large and fragile platelets that circulate poorly. *Blood*, 118(8), pp.2285–2295.

Kabsch, W. et al., 1990. Atomic structure of the actin:DNase I complex. *Nature*, 347(6288), pp.37–44.

Kapitein, L.C. et al., 2008. Microtubule cross-linking triggers the directional motility of kinesin-5. *The Journal of cell biology*, 182(3), pp.421–428.

Kapitein, L.C. et al., 2005. The bipolar mitotic kinesin Eg5 moves on both microtubules that it crosslinks. *Nature*, 435(7038), pp.114–118.

Karsenti, E., Nedelec, F. & Surrey, T., 2006. Modelling microtubule patterns. *Nature cell biology*, 8(11), pp.1204–1211.

Kelley, M.J. et al., 2000. Mutation of MYH9, encoding non-muscle myosin heavy chain A, in May-Hegglin anomaly. *Nature genetics*, 26(1), pp.106–108.

Kenney, D.M. & Linck, R.W., 1985. The cystoskeleton of unstimulated blood platelets: structure and composition of the isolated marginal microtubular band. *Journal of cell science*, 78, pp.1–22.

Kenney, D.M., Weiss, L.D. & Linck, R.W., 1988. A novel microtubule protein in the marginal band of human blood platelets. *The Journal of biological chemistry*, 263(3), pp.1432–1438.

Knoll, M. & Ruska, E., 1932. Das Elektronenmikroskop. *Zeitschrift für Physik*, 78(5-6), pp.318–339.

Kollman, J.M. et al., 2011. Microtubule nucleation by γ-tubulin complexes. *Nature Reviews Molecular Cell Biology*, 12(11), pp.709–721.

Kremer, J.R., Mastronarde, D.N. & McIntosh, J.R., 1996. Computer visualization of three-dimensional image data using IMOD. *Journal of structural biology*, 116(1), pp.71–76.

Kunert, S. et al., 2009. The microtubule modulator RanBP10 plays a critical role in regulation of platelet discoid shape and degranulation. *Blood*, 114(27), pp.5532–5540.

Kuwahara, M. et al., 2002. Platelet shape changes and adhesion under high shear flow. *Arteriosclerosis, thrombosis, and vascular biology*, 22(2), pp.329–334.

Levin, J., 2013. Chapter 1 - The Evolution of Mammalian Platelets. In A. D. Michelson, ed. *Platelets (Third Edition)*. Platelets (Third Edition). Academic Press CY -, pp. 3–25.

Léon, C. et al., 2007. Megakaryocyte-restricted MYH9 inactivation dramatically affects hemostasis while preserving platelet aggregation and secretion. *Blood*, 110(9), pp.3183–3191.

Li, Z., Kim, E.S. & Bearer, E.L., 2002. Arp2/3 complex is required for actin polymerization during platelet shape change. *Blood*, 99(12), pp.4466–4474.

Lukinavičius, G. et al., 2014. Fluorogenic probes for live-cell imaging of the cytoskeleton. *Nature methods*, 11(7), pp.731–733.

Machlus, K.R. & Italiano, J.E., 2013. The incredible journey: From megakaryocyte development to platelet formation. *The Journal of cell biology*, 201(6), pp.785–796.

MacRae, T.H., 1992. Microtubule organization by cross-linking and bundling proteins. *Biochimica et biophysica acta*, 1160(2), pp.145–155.

Martin, J. & Trowbridge, A., 2012. *Platelet heterogeneity: biology and pathology*,

Mazzarello, P., Calligaro, A.L. & Calligaro, A., 2001. *Giulio Bizzozero: a pioneer of cell biology*,

McDonald, K.L., Edwards, M.K. & McIntosh, J.R., 1979. Cross-sectional structure of the central mitotic spindle of Diatoma vulgare. Evidence for specific interactions between antiparallel microtubules. *The Journal of cell biology*, 83(2 Pt 1), pp.443–461.

Meseguer, J., Esteban, M.N. & Rodr guez, A., 2002. Are thrombocytes and platelets true phagocytes? *Microscopy research and technique*, 57(6), pp.491–497.

Meyer, I. et al., 2012. Altered microtubule equilibrium and impaired thrombus stability in mice lacking RanBP10. *Blood*.

Mickey, B. & Howard, J., 1995. Rigidity of microtubules is increased by stabilizing agents. *The Journal of cell biology*, 130(4), pp.909–917.

Mitchison, T. & Kirschner, M., 1984. Dynamic instability of microtubule growth. *Nature*, 312(5991), pp.237–242.

Monnier, S. et al., 2015. Effect of an osmotic stress on multicellular aggregates. *Methods (San Diego, Calif.)*.

Morano, I. et al., 2000. Smooth-muscle contraction without smooth-muscle myosin. *Nature cell …*.

Murrell, M. et al., 2015. Forcing cells into shape: the mechanics of actomyosin contractility. *Nature Reviews Molecular Cell Biology*, 16(8), pp.486–498.

Nachmias, V.T., 1980. Cytoskeleton of human platelets at rest and after spreading. *The Journal of cell biology*, 86(3), pp.795–802.

Nakata, T., 1987. Cytoskeletal reorganization of human platelets after stimulation revealed by the quick-freeze deep-etch technique. *The Journal of cell biology*, 105(4), pp.1771–1780.

O'Toole, E.T. et al., 2003. Morphologically distinct microtubule ends in the mitotic centrosome of Caenorhabditis elegans. *The Journal of cell biology*, 163(3), pp.451–456.

Offermanns, S., 2006. Activation of platelet function through G protein–coupled receptors. *Circulation research*.

Osler, W., 1873. An account of certain organisms occurring in the liquor sanguinis. In Proceedings of the Royal Society of ….

Oury, C. et al., 2004. ATP augments von Willebrand factor-dependent shear-induced platelet aggregation through Ca2+-calmodulin and myosin light chain kinase activation. *The Journal of biological chemistry*, 279(25), pp.26266–26273.

P Holly, S., Chen, X. & V Parise, L., 2011. Abundance- and Activity-Based Proteomics in Platelet Biology. *Current proteomics*, 8(3), pp.216–228.

Pan, J. et al., 2014. The formin DIAPH1 (mDia1) regulates megakaryocyte proplatelet formation by remodeling the actin and microtubule cytoskeletons. *Blood*, 124(26), pp.3967–3977.

Pantaloni, D. & Carlier, M.F., 1993. How profilin promotes actin filament assembly in the presence of thymosin β4. *Cell*.

Patel, S.R. et al., 2005. Differential roles of microtubule assembly and sliding in proplatelet formation by megakaryocytes. *Blood*, 106(13), pp.4076–4085.

Patel-Hett, S. et al., 2011. The spectrin-based membrane skeleton stabilizes mouse megakaryocyte membrane systems and is essential for proplatelet and platelet formation. *Blood*, 118(6), pp.1641–1652.

Patel-Hett, S. et al., 2008. Visualization of microtubule growth in living platelets reveals a dynamic marginal band with multiple microtubules. *Blood*, 111(9), pp.4605–4616.

Paulus, J.M., 1975. Platelet size in man. *Blood*, 46(3), pp.321–336.

Pollard, T.D., 1986. Rate constants for the reactions of ATP-and ADP-actin with the ends of actin filaments. *The Journal of cell biology*.

Pollard, T.D. & Cooper, J.A., 1986. Actin and actin-binding proteins. A critical evaluation of mechanisms and functions. *Annual review of biochemistry*, 55, pp.987–1035.

Pruyne, D., 2002. Role of Formins in Actin Assembly: Nucleation and Barbed-End Association. *Science (New York, N.Y.)*, 297(5581), pp.612–615.

Radley, J.M. & Hartshorn, M.A., 1987. Megakaryocyte fragments and the microtubule coil. *Blood cells*, 12(3), pp.603–614.

Ratcliffe, N.A. & Millar, D.A., 1988. *Ratcliffe: Comparative aspects and possible phylogenetic... - Google Scholar*,

Richardson, J.L. et al., 2005. Mechanisms of organelle transport and capture along proplatelets during platelet production. *Blood*, 106(13), pp.4066–4075.

Ries, J. et al., 2012. A simple, versatile method for GFP-based super-resolution microscopy via nanobodies. *Nature methods*, 9(6), pp.582–584.

Rothwell, S.W. & Calvert, V.S., 1997. Activation of human platelets causes post-translational modifications to cytoplasmic dynein. *Thrombosis and haemostasis*, 78(2), pp.910–918.

Sakurai, Y. et al., 2015. Platelet geometry sensing spatially regulates α-granule secretion to enable matrix self-deposition. *Blood*, 126(4), pp.531–538.

Sanchez, I. & Cohen, W.D., 1994. Localization of tau and other proteins of isolated marginal bands.

Cell motility and the cytoskeleton, 27(4), pp.350–360.

Schiff, P.B. & Horwitz, S.B., 1980. Taxol stabilizes microtubules in mouse fibroblast cells. *Proceedings of the National Academy of Sciences of the United States of America*, 77(3), pp.1561–1565.

Schmaier, A.A. et al., 2011. Occlusive thrombi arise in mammals but not birds in response to arterial injury: evolutionary insight into human cardiovascular disease. *Blood*, 118(13), pp.3661–3669.

Schmitt, A. et al., 2001. Of mice and men. *Experimental Hematology*, 29(11), pp.1295–1302.

Schulze, H. et al., 2006. Characterization of the megakaryocyte demarcation membrane system and its role in thrombopoiesis. *Blood*, 107(10), pp.3868–3875.

Schwarz Henriques, S. et al., 2012. Force field evolution during human blood platelet activation. *Journal of cell science*, 125(Pt 16), pp.3914–3920.

Schwer, H.D. et al., 2001. A lineage-restricted and divergent beta-tubulin isoform is essential for the biogenesis, structure and function of blood platelets. *Current biology : CB*, 11(8), pp.579–586.

Seri, M. et al., 2000. Mutations in MYH9 result in the May-Hegglin anomaly, and Fechtner and Sebastian syndromes. The May-Hegglin/Fechtner Syndrome Consortium. *Nature genetics*, 26(1), pp.103–105.

Séverin, S. et al., 2012. A confocal-based morphometric analysis shows a functional crosstalk between the actin filament system and microtubules in thrombin-stimulated platelets. *Journal of thrombosis and haemostasis : JTH*.

Skoufias, D.A. & Scholey, J.M., 1993. Cytoplasmic microtubule-based motor proteins. *Current opinion in cell biology*.

Spinler, K.R. et al., 2015. Myosin-II repression favors pre/proplatelets but shear activation generates platelets and fails in macrothrombocytopenia. *Blood*, 125(3), pp.525–533.

Steiner, M. & Ikeda, Y., 1979. Quantitative assessment of polymerized and depolymerized platelet microtubules. Changes caused by aggregating agents. *The Journal of clinical investigation*, 63(3), pp.443–448.

Steinmetz, M.O. et al., 2000. Op18/stathmin caps a kinked protofilament-like tubulin tetramer. *The EMBO Journal*, 19(4), pp.572–580.

Stenberg, P.E. & Levin, J., 1989. Ultrastructural analysis of acute immune thrombocytopenia in mice: dissociation between alterations in megakaryocytes and platelets. *Journal of cellular physiology*.

Stewart, M.P. et al., 2011. Hydrostatic pressure and the actomyosin cortex drive mitotic cell rounding. *Nature*, 469(7329), pp.226–230.

Strassel, C. et al., 2009. Intrinsic impaired proplatelet formation and microtubule coil assembly of megakaryocytes in a mouse model of Bernard-Soulier syndrome. *Haematologica*, 94(6), pp.800–810.

Swaminathan, V. et al., 2011. Mechanical stiffness grades metastatic potential in patient tumor cells and in cancer cell lines. *Cancer research*, 71(15), pp.5075–5080.

Tablin, F. & Castro, M.D., 1991. Bovine platelets contain a 280 kDa microtubule-associated protein antigenically related to brain MAP 2. *European journal of cell biology*, 56(2), pp.415–421.

TABLIN, F. & Levin, J., 1988. The fine structure of the amebocyte in the blood of Limulus polyphemus. II. The amebocyte cytoskeleton: a morphological analysis of native, activated, and endotoxin- ….

Tablin, F., Reeber, M.J. & Nachmias, V.T., 1988. Platelets contain a 210K microtubule-associated protein related to a similar protein in HeLa cells. *Journal of cell science*, 90 (Pt 2), pp.317–324.

Tanenbaum, M.E., Vale, R.D. & McKenney, R.J., 2013. Cytoplasmic dynein crosslinks and slides anti-parallel microtubules using its two motor domains. *eLife*, 2, p.e00943.

Thon, J.N. & Italiano, J.E., 2012. Does size matter in platelet production? *Blood*, 120(8), pp.1552–1561.

Thon, J.N. et al., 2010. Cytoskeletal mechanics of proplatelet maturation and platelet release. *The Journal of cell biology*, 191(4), pp.861–874.

Thon, J.N. et al., 2012. Microtubule and cortical forces determine platelet size during vascular platelet production. *Nature communications*, 3, p.852.

van Mameren, J. et al., 2009. Leveraging single protein polymers to measure flexural rigidity. *The journal of physical chemistry. B*, 113(12), pp.3837–3844.

Venier, P. et al., 1994. Analysis of microtubule rigidity using hydrodynamic flow and thermal fluctuations. *The Journal of biological chemistry*, 269(18), pp.13353–13360.

Vitrat, N. et al., 1998. Endomitosis of human megakaryocytes are due to abortive mitosis. *Blood*, 91(10), pp.3711–3723.

Wakatsuki, T., Schwab, B. & Thompson, N.C., 2001. Effects of cytochalasin D and latrunculin B on mechanical properties of cells. *Journal of cell …*.

Wang, R. et al., 2015. Electron cryotomography reveals ultrastructure alterations in platelets from patients with ovarian cancer. *Proceedings of the National Academy of Sciences of the United States of America*, 112(46), pp.14266–14271.

Ward, J.J. et al., 2014. Mechanical design principles of a mitotic spindle. *eLife*, 3, p.e03398.

Wegner, A., 1976. Head to tail polymerization of actin. *Journal of molecular biology*.

Wettschureck, N., 2005. Mammalian G Proteins and Their Cell Type Specific Functions. *Physiological reviews*, 85(4), pp.1159–1204.

White, J.G., 2013. Chapter 7 - Platelet Structure. In A. D. Michelson, ed. *Platelets (Third Edition)*. Platelets (Third Edition). Academic Press CY -, pp. 117–144.

White, J.G. & Burris, S.M., 1984. Morphometry of platelet internal contraction. *The American journal of pathology*, 115(3), pp.412–417.

White, J.G. & Rao, G.H., 1998. Microtubule coils versus the surface membrane cytoskeleton in maintenance and restoration of platelet discoid shape. *The American journal of pathology*, 152(2), pp.597–609.

White, J.G. & Sauk, J.J., 1984. The organization of microtubules and microtubule coils in giant platelet disorders. *The American journal of pathology*, 116(3), pp.514–522.

White, J.G. et al., 1984. Micropipette aspiration of human blood platelets: a defect in Bernard-Soulier's syndrome. *Blood*, 63(5), pp.1249–1252.

Woolley, R. et al., 2013. A rapid, topographical platelet activation assay. *The Analyst*, 138(16), pp.4512–4518.

Woulfe, D., Yang, J. & Brass, L., 2001. ADP and platelets: the end of the beginning. *The Journal of clinical investigation*, 107(12), pp.1503–1505.

Yau, K.W. et al., 2014. Microtubule minus-end binding protein CAMSAP2 controls axon specification and dendrite development. *Neuron*, 82(5), pp.1058–1073.

Zander, D.M.W. & Klinger, M., 2009. The blood platelets contribution to innate host defense - What they have learned from their big brothers. *Biotechnology journal*, 4(6), pp.914–926.

Zheng, Y. et al., 1995. Nucleation of microtubule assembly by a gamma-tubulin-containing ring complex. *Nature*, 378(6557), pp.578–583.

Zlotek-Zlotkiewicz, E. et al., 2015. Optical volume and mass measurements show that mammalian cells swell during mitosis. *The Journal of cell biology*, 211(4), pp.765–774.

Zucker-Franklin, D., 1969. Microfibrils of blood platelets: their relationship TO MICROTUBULES AND THE CONTRACTILE PROTEIN. *The Journal of clinical investigation*, 48(1), pp.165–175.